Aus dem Fachbereich Medizin
der Johann Wolfgang Goethe-Universität
Frankfurt am Main

betreut am
Zentrum der Biochemie
Institut für Biochemie II (Kardiovaskuläre Biochemie)
Direktor: Prof. Dr. Ivan Đikić

Interaction proteomics display the spatio-temporal complexity of mitochondrial RNA granules

Dissertation
zur Erlangung des Doktorgrades der theoretischen Medizin
des Fachbereichs Medizin
der Johann Wolfgang Goethe-Universität
Frankfurt am Main

vorgelegt von
Melinda Elaine Brunstein
Master of Science

aus Nürnberg

Frankfurt am Main, 2023

Dekan:	Prof. Dr. Stefan Zeuzem
Referent:	Prof. Dr. Christian Münch
Korreferent:	Prof. Dr. Georg Auburger
Tag der mündlichen Prüfung:	13.06.2024

Table of contents

I List of abbreviations

°C	Degree Celsius
%	Percent
α	Anti
Ψ	Pseudouridine
τm5U	5-taurinomethyluridine
µg	Microgram
µM	Micrometer
µm	Micromolar
aaRSs	Aminoacyl-tRNA sythetases
ACN	Acetonitrile
ActD	Actinomycin D
ADP	Adenosine diphosphate
ATP	Adenosine triphosphate
BCA	Bicinchoninic acid protein
BF	Biological function
BrU	5’-bromouridine
BSA	Bovine serum albumin
c18	Octadecylsilane (18 carbons atoms)
CCCP	Carbonyl cyanide m-chlorophenyl hydrazone
cDNA	Coding deoxyribonucleic acid
circRNA	Circular RNA
CM	Cristae membrane
CO_2	Carbon dioxide
Cryo-EM	Cryogenic electron microscopy
$CsCl_2$	Calcium chloride
CSB	Conserved sequence block
C-terminus	Carboxyl-terminus
CTFI	Corrected total fluorescence intensity
CTRL	Control
D	Dihydrouridine

DAPI	4',6-diamidino-2-phenylindole
DAVID	Database for annotation, visualization and integrated discovery
D-foci	Degradosome foci
D-loop	Displacement loop
DMEM	Dulbecco's modified eagle medium
DMSO	Dimethyl sulfoxide
DNA	Deoxyribonucleic acid
Dox	Doxycycline
dsRNA	Double-stranded RNA
DTT	Dithiothreitol
E. coli	*Escherichia coli*
EDTA	Ethylenediaminetetraacetic acid
EGFP	Enhanced green fluorescent protein
EtBr	Ethidium bromide
ETC	Electron transport chain
FASTA	FAST-All
FA	Formic acid
FBS	Fetal bovine serum
FDR	False discovery rate
FI	Functional interaction
Flp-In T-Rex	Flippase-in tetracycline regulatory expression system
g	Gravity
G4	G-quadruplex
GO	Gene ontology
GTPase	Guanosine triphosphate hydrolase
h	Hour
HCl	Hydrogen chloride
HeLa	Henrietta Lacks
HSP	Heavy strand promoter
H-strand	Heavy strand
IBM	Inner boundary membrane

iCLIP	Individual-nucleotide resolution crosslinking and immunoprecipitation
IMM	Inner mitochondrial membrane
IMS	Intermembrane space
kb	Kilobase
KD	Knockdown
kDa	Kilodalton
kV	Kilovolt
LC-MS/MS	Liquid chromatography-tandem mass spectrometry
LLPS	Liquid-liquid phase separation
lncRNA	Long non-coding RNA
LB	Lysogeny broth
LSP	Light strand promoter
L-strand	Light strand
LSU	Large subunit
Lys C	Lysyl endopeptidase
M	Molar
m/z	Mass/charge
m^1A	N^1-methyladenosine
m^6A	N^6-methyladenosine
MF	Molecular function
min	Minute
ml	Milliliter
MRG	Mitochondrial RNA granule
mRNA	Messenger RNA
MS	Mass spectrometry
ms	Millisecond
mt	Mitochondrial
MTase	Methyltransferase
mtDNA	Mitochondrial deoxyribonucleic acid
mtEXO	Mitochondrial degradosome
mtRNA	Mitochondrial ribonucleic acid

MTS	Mitochondrial targeting sequence
NCR	Non-coding region
ncRNA	Non-coding RNA
nm	Nanometer
nM	Nanomolar
NTC	Non-targeting control
O/N	Over/night
O_H	Origin of heavy strand replication
O_L	Origin of light strand replication
OMM	Outer mitochondrial membrane
OXPHOS	Oxidative phosphorylation system
PBLMM	Peptide-based linear mixed model
PBS	Phosphate-buffered saline
PBST	PBS supplemented with 0.01% Tween 20
PCR	Polymerase chain reaction
PD	Proteome discoverer
PEI	Polyethylenimine
piRNA	PIWI interacting RNA
pH	Potential of hydrogen
Pi	Phosphate ions
PPI	Protein-protein interaction
pre	Precursor
Q	Queuosine
qPCR	Quantitative real-time PCR
RBP	RNA binding protein
RNA	Ribonucleic acid
RNAi	RNA interference
ROS	Reactive oxygen species
RPMI	Roswell Park Memorial Institute
rRNA	Ribosomal RNA
RT	Room temperature

s	Second
SDS	Sodium dodecyl sulfate
SDS-PAGE	SDS-polyacrylamide gel electrophoresis
siRNA	Small interfering RNA
sncRNA	Small non-coding RNA
SSU	Small subunit
STRING	Search tool for the retrieval of interacting genes/proteins
TAE	Tris-acetate-EDTA
TAS	Termination-associated sequence
TCA	Trifluoroacetic acid
TCEP	Tris(2-chloroethyl) phosphate
TFA	Trifluoroacetic Acid
Th	Thomson
TMT	Tandem mass tag
tRNA	Transfer RNA
UPR^{mt}	Unfolded protein response
v	Version
v/v	Volume/volume
w/v	Weight/volume

II List of Figures

III Summary

Mitochondrial RNA granules (MRGs) are membraneless, highly specialized compartments that play an essential role in the post-transcriptional regulation of mitochondrial gene expression. This regulation is crucial for maintaining energy production, controlling metabolic functions and ensuring homeostasis in cells. Dysregulation of mitochondrial genes has been linked to various human diseases, including neurodegenerative and metabolic disorders as well as certain types of cancer.

MRGs are composed of different RNA species, including mitochondrial precursor RNA (pre-RNA), mature tRNAs, rRNAs and mRNAs complexed with multiple proteins involved in RNA processing and mitoribosome assembly. However, despite the significance of MRGs, their protein composition, structural organization, stability and dynamics during stress conditions remain elusive. In the study reported here, I adopted a three-step approach to address the aforementioned fundamental issues.

First and foremost, I identified the protein composition of MRGs and unveiled their architectural complexity. To characterize the MRG proteome, I applied the cutting-edge TurboID-based proximity labeling approach combined with quantitative mass spectrometry. Proximity labeling was conducted on 20 distinct MRG-associated human proteins, resulting in the identification of more than 1,700 protein-protein interactions. This expansive dataset enabled me to create a comprehensive network, providing valuable insights into both the (sub)architecture as well as the core structure of MRGs in-depth.

Secondly, I investigated the spatio-temporal dynamics of MRGs under various mitochondrial stress conditions. To monitor the morphological alterations and compositional changes of MRGs, I utilized time-resolved confocal fluorescence microscopy and proteomics, respectively. In this analysis, I applied IMT1, the first specific inhibitor that selectively targets mitochondrial transcription. Using this methodology, I pinpointed precise conditions that triggered MRGs' disassembly during stress, followed by their reassembly when nascent RNA production was restored. The results of this examination elucidate that MRGs are highly dynamic and stress adaptive

structures, capable of rapid dissolution and reassembly, a process closely connected to mitochondrial transcription.

Thirdly, I aimed to explore the impact of RNA turnover on MRGs' integrity during stress, employing confocal fluorescence microscopy and quantitative real-time PCR. I observed that depletion of MRG proteins associated with RNA degradation counteracts MRGs' disassembly under stress conditions, a phenomenon attributed to the accumulation of double-stranded RNA (dsRNA). These results emphasize the critical role of pre-RNA turnover in maintaining MRG integrity and reveal that MRGs can be stabilized by dsRNA.

Taken together, the comprehensive investigation reported in this thesis has substantially broadened and deepened our understanding of MRGs' complexity. By identifying their molecular structure and dynamics, I have gained significant insights into the fundamental characteristics and biological functions of MRGs in cellular processes. This knowledge contributes to the identification of disease-related pathways linked to mitochondrial gene expression and may inspire future studies to develop novel therapeutic approaches.

IV Zusammenfassung

Mitochondriale RNA Granulate (MRGs) sind membranlose, hochspezialisierte Kompartimente, die eine wesentlich Rolle bei der post-transkriptionellen Regulierung der mitochondrialen Genexpression spielen. Diese Regulierung ist entscheidend für die Aufrechterhaltung der Energieproduktion, die Kontrolle der Stoffwechselfunktionen und die Gewährleistung der Homöostase in Zellen. Eine Fehlregulation mitochondrialer Gene wird in Verbindung mit verschiedenen menschlichen Krankheiten gebracht, darunter neurodegenerative und metabolische Störungen sowie bestimmte Krebsarten.

MRGs bestehen aus verschiedenen Arten von RNA, einschließlich mitochondrialer Vorläufer-RNA (prä-RNA), reifer tRNAs, rRNAs und mRNAs, die mit zahlreichen Proteinen verbunden sind, die an der RNA-Verarbeitung und dem Zusammenbau der Mitoribosomen beteiligt sind. Obwohl MRGs von großer Bedeutung sind, bleibt ihre Proteinzusammensetzung, strukturelle Organisation, Stabilität und Dynamiken unter Stressbedingungen nach wie vor unbekannt. In der hier vorgestellten Studie habe ich einen dreistufigen Ansatz gewählt, um die oben genannten grundlegenden Fragen zu klären.

Zuallererst habe ich die Proteinzusammensetzung der MRGs identifiziert und ihre architektonische Komplexität aufgeklärt. Zur Charakterisierung des MRG-Proteoms wendete ich den fortschrittlichen TurboID-basierten *proximity-labeling*-Ansatz in Kombination mit quantitativer Massenspektrometrie an. Ich führte dieses *proximity labeling* an 20 verschiedenen MRG-assoziierten menschlichen Proteinen durch und identifizierte dabei mehr als 1.700 Protein-Protein-Interaktionen. Dieser umfangreiche Datensatz ermöglichte mir die Erstellung eines umfassenden Netzwerkes, das wertvolle Einblicke sowohl in die (Teil-)Architektur als auch in die Kernstruktur der MRGs in großer Tiefe bietet.

Zweitens untersuchte ich die raumzeitlichen Dynamiken der MRGs unter verschiedenen mitochondrialen Stressbedingungen. Um sowohl die morphologischen Veränderungen als auch die Veränderungen in der Zusammensetzung der MRGs zu beobachten, nutzte ich zeitaufgelöste konfokale Fluoreszenzmikroskopie und Proteomik. Für diese Analysen setzte ich IMT1, den ersten spezifischen Inhibitor für die mitochondriale Transkription

ein. Mithilfe dieser Methodik konnte ich die genauen Bedingungen ermittelt, unter denen sich MRGs während Stress auflösen und nach Wiederherstellung der RNA Transkription erneut zusammensetzen. Die Ergebnisse dieser Untersuchung verdeutlichen, dass es sich bei den MRGs um hochdynamische und stressangepasste Strukturen handelt, die in der Lage sind, sich schnell aufzulösen und wieder zusammensetzen, ein Vorgang der eng mit der mitochondrialen Transkription verbunden ist.

Drittens hatte ich das Ziel, die Auswirkungen des RNA-Umsatzes auf die Integrität der MRGs unter Stressbedingungen mithilfe von Fluoreszenzmikroskopie und quantitativer Echtzeit-PCR zu untersuchen. Dabei beobachtete ich, dass die Depletion von MRG-Proteinen, die mit dem RNA-Abbau verbunden sind, der Auflösung von MRGs unter Stressbedingungen entgegenwirkt. Dieses Phänomen ging mit einer Anhäufung von doppelsträngiger RNA (dsRNA) einher. Die Ergebnisse unterstreichen die kritische Rolle des prä-RNA-Umsatzes für die Aufrechterhaltung der MRG-Integrität und zeigen, dass MRGs durch dsRNA stabilisiert werden können.

Insgesamt hat die umfassende Untersuchung, die im Rahmen dieser Dissertationsschrift berichtet wird, unser Verständnis für die Komplexität von MRGs erheblich erweitert und vertieft. Durch die Identifizierung ihrer molekularen Struktur und Dynamiken habe ich bedeutende Einblicke in die grundlegenden Eigenschaften und biologischen Funktionen der MRGs in zellulären Prozessen gewonnen. Dieses Wissen trägt zur Identifizierung von krankheitsbezogenen Signalwegen bei, die mit der mitochondrialen Genexpression verbunden sind und kann künftige Studien zur Entwicklung neuer therapeutischer Ansätze inspirieren.

1 Introduction

1.1 Mitochondrial origin

Mitochondria are essential energy-producing organelles present in most eukaryotic cells. The endosymbiotic theory postulates that mitochondria descended from an α-proteobacterium engulfed by an archaebacterium more than 1 billion years ago.[1,2]

The earliest reports of mitochondria date back to the mid-19th century wherein mitochondria were initially referred to as "bioplasts" by Richard Altman.[3] In 1898 Carl Benda coined the term mitochondria from the Greek words "mitos" (thread) and "chondros" (granules).[4]

Emerging from this pioneering work, our understanding of the mitochondrial structure, physiology and their diverse functions has grown significantly in the past century.

1.2 Mitochondrial structure and function

Mitochondria are highly dynamic structures and their shape varies from filamentous to rod-like to granular phenotypes.[5] They are surrounded by a double-membrane and the inner membrane forms curved ridges defining a number of different compartments within the mitochondria. The outer membrane (OMM) serves as a first barrier, followed by the intermembrane space (IMS) and the inner membrane (IMM), which encloses the matrix (Figure 1).[5–7]

Each compartment is composed of different protein complexes and plays a distinct role in many essential processes spanning from cell survival to programmed cell death.[8] The protein-rich matrix forms the center for a subset of metabolic pathways, such as tricarboxylic acid cycle (TCA), synthesis of fatty acids and amino acids, iron-sulfur clusters and production of ROS.[8,9]

However, the most prominent role of mitochondria is energy-production in form of ATP through the oxidative phosphorylation system (OXPHOS).[10] The human mitochondrial OXPHOS is predominantly embedded in the IMM and composed of the electron transport chain (ETC). The ETC is formed by four complexes (I-IV), transporting electrons to the fifth complex, an ATP synthase that produces ATP by phosphorylation of ADP.[10] A special characteristic of mitochondrial protein complexes is their dual regulation by

two genetic systems: the mitochondrial genome and the nuclear genome.[11] Besides complex II, all complexes of the ETC are assembled by protein subunits encoded in both the mitochondria and the nucleus. While the majority of proteins are nuclear-encoded, translated within the cytosol, imported into mitochondria via an N-terminal specific mitochondrial targeting sequence (MTS) through the outer- (TOM) and inner-membrane (TIM) translocase and integrated into the membrane by the OXA1 insertase, only a small set of proteins is encoded by the mitochondrial genome hosted within the matrix.[11]

Thus, the precise regulation of mitochondrial gene expression is a complex process and essential for a functional oxidative phosphorylation.[12] Moreover, defects in mitochondrial energy production due to impaired OXPHOS proteins cause mitochondrial dysfunction, leading to various neurodegenerative diseases, such as the Leigh syndrome, in humans.[10]

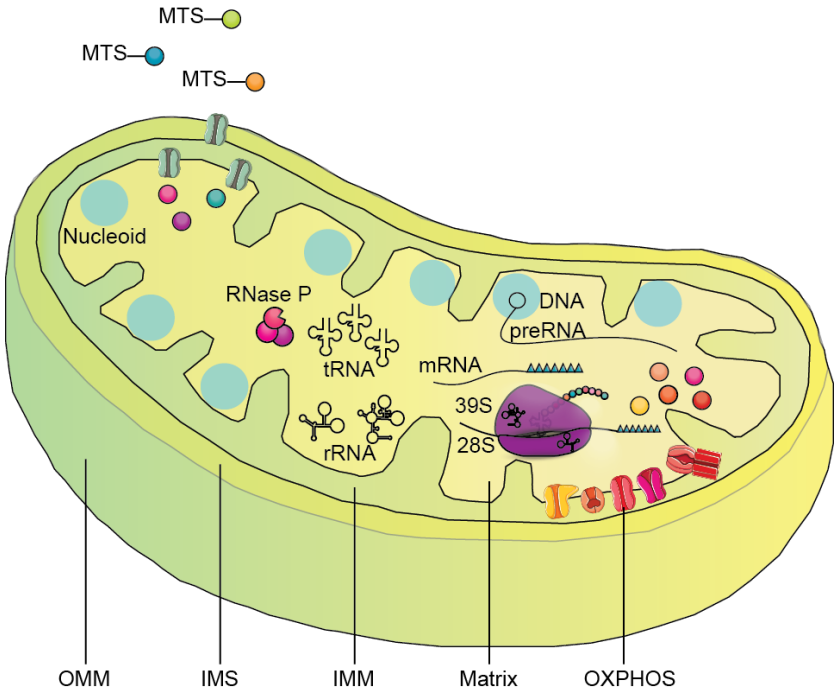

Figure 1: Gene expression in human mitochondria. Mitochondria (mt) contain several copies of the genome packed into nucleoids. Each nucleoid contains a single copy of the mitochondrial DNA (mtDNA). Transcription leads to long polycistronic precursor RNA transcripts (pre-RNA) that are further processed into individual transfer RNAs (tRNAs), ribosomal RNAs (rRNAs) and messenger RNAs (mRNAs), were the latter ones are translated into proteins in the mitochondrial matrix. The mtDNA encodes for 37 genes including 13 OXPHOS proteins, two rRNAs (16S and 12S) that form the mitochondrial ribosome and 22 tRNAs. The tRNAs are processed by RNase P that consists of three different proteins MRPP1, MRPP2 MRPP3. MRPP3 cleaves the 5' end of pre-tRNAs to generate functional tRNAs. However, the majority of mitochondrial proteins are encoded in the nucleus and imported across different compartments, guided by the N-terminal targeting sequence (MTS): first the outer membrane (OMM), followed by the intermembrane space (IMS) and finally, the inner membrane (IMM).

1.3 Mitochondrial gene expression

Mitochondria are direct descendants of bacteria and thus the only organelles in human cells that harbor multiple copies of their own genome.[13] The human mitochondrial DNA (mtDNA) is a 16.6 kb small circular molecule and contains information for 37 genes including the two ribosomal RNAs (rRNA), 12S rRNA and 16S rRNA, 22 transfer RNAs (tRNA) and 13 proteins essential for the OXPHOS system (Figure 1).[13,14] Moreover, it has recently emerged that the mitochondrial genome encodes non-coding RNAs such as long non-coding RNAs (lncRNA), circular RNAs (circRNAs) and double-stranded RNAs (dsRNAs).[15–18]

Mitochondria are not fully autonomous entities and mtDNA gene expression requires an enormous repertoire of nuclear-encoded proteins.[19] Proteins encoded by the mitochondrial genome represent only 1% of the human mitochondrial proteome, which comprises in total more than 1,000 proteins. The majority of those proteins are involved in metabolism (29.1%) and mitochondrial gene expression (18.8%), including DNA- and RNA-related processes as well as ribosome assembly and translation.[19]

1.3.1 Mitochondrial genome

The double-stranded mtDNA lacks histones, however, it becomes compacted by the replication and transcription machinery, forming dense aggregates within the mitochondrial matrix.[20] These aggregates were discovered as foci by Satoh and Kuroiwa[21] and referred to as nucleoids in 1990. One human cell contains hundreds of nucleoids with a mean size of 100 nm and each comprises a single mtDNA copy.[22] The two strands of the mtDNA can be separated by density centrifugation in alkaline $CsCl_2$ gradients and thus are defined according to their different content of guanines, in heavy (H) and light (L) strand.[14] While the H-strand encodes for the majority of genes, the L-strand contains only the genetic information for NADH-ubiquinone oxidoreductase chain 6 (ND6), eight t-RNAs and three lncRNAs (lncND5, lncND6, and lncCYTB).[13] Furthermore, the mitochondrial genome contains a major non-coding region (NCR), frequently forming the so-called displacement loop (D-loop).[23] This control region encompasses the regulatory segments, heavy strand promoter (HSP) and light strand promoter (LSP) for transcription of both strands, the H-strand origin for replication (O_H)

initiation, as well as the conserved sequence blocks (CSB1-3). The origin for L-strand replication (O_L) is located outside of the NCR (Figure 2).[23]

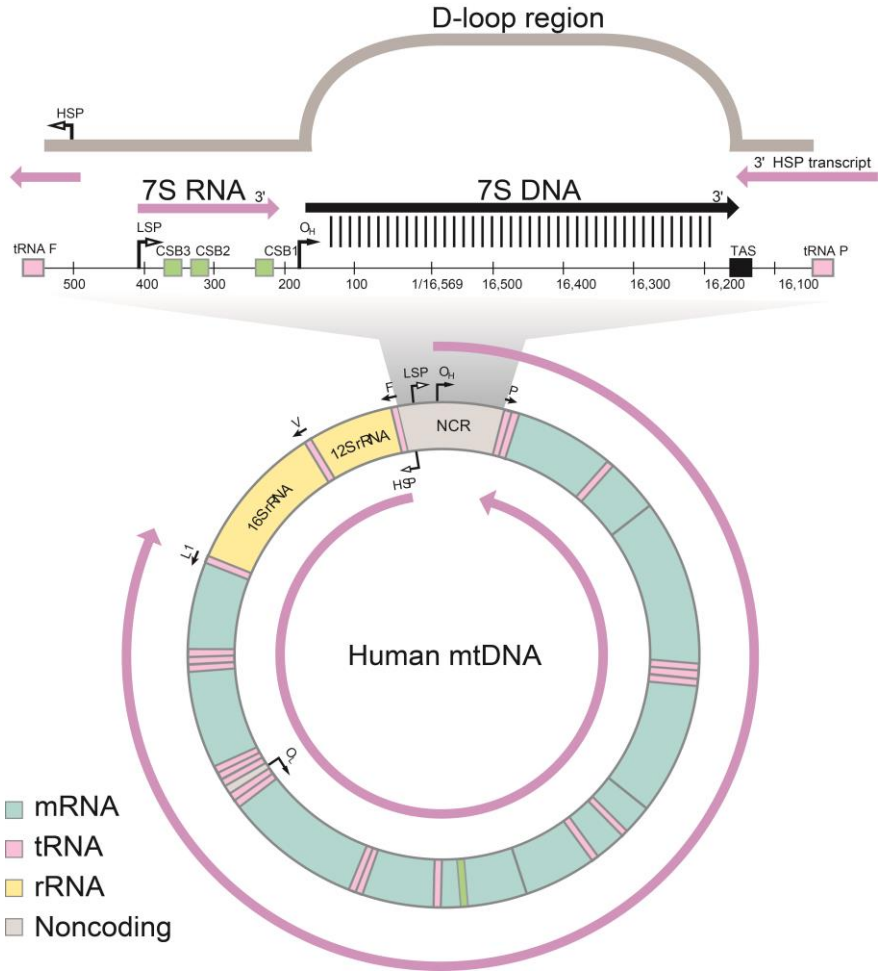

Figure 2: Genome of human mitochondria. The mitochondrial genome consists of two strands, the heavy (H) and light (L) strand that encode for 13 mRNAs (cyan), 22 tRNAs (pink) and 2 rRNAs (yellow). The major non-coding region (NCR) contains the two transcription promoters, light strand promoter (LSP) and heavy strand promoter (HSP), the H-strand origin of replication (O_H), three conserved sequence boxes (CSB1-3, green), and the termination-associated sequence (TAS, black). The 7S DNA is synthesized during premature termination of the H-strand replication. In association with the mtDNA, 7S DNA forms the triple stranded displacement loop (D-loop). In addition to the full-length transcript from the LSP, premature transcription termination at CSB1 generates the 7S RNA. The second non-coding region downstream of O_H contains the L-strand origin of replication (O_L). Figure modified from Gustafsson et al.[23]

1.3.2 Mitochondrial DNA replication

The model of mtDNA replication still remains elusive despite being examined for decades.[24] According to the prevailing strand displacement model (SDM), replication of both strands proceeds unidirectional and continuously.[23,25] Initiation of replication requires RNA-primers generated by the DNA dependent RNA polymerase POLRMT

during transcription from the LSP.[24] The DNA polymerase-γ (Polγ) recognizes these primers and initiates synthesis of the H-strand at the O_H by forming a triple-stranded region (D-loop).[26] During replication, the Twinkle mtDNA helicase (TWNK) unwinds the DNA at the replication fork while the single-stranded DNA-binding protein (SSBP1) coats and protects the single H-strand.[27] When the replication fork has moved and the replication machinery passes the O_L, a single stranded stem loop is formed and initiation of light-strand replication proceeds in the opposite direction.[27,28] Once replication of both strands is completed, primers are removed by RNase H1 and DNA ends are ligated by DNA ligase III (Figure 3).[27]

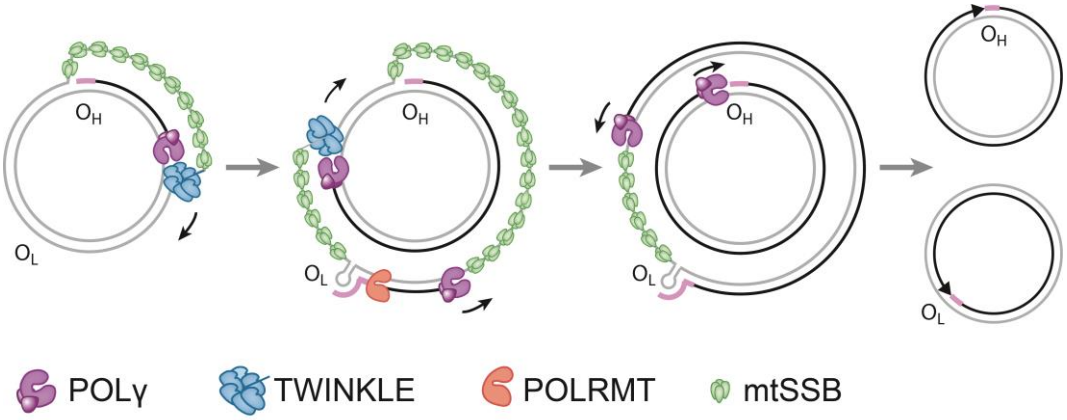

Figure 3: Replication of the mitochondrial genome in humans. Mitochondrial replication is initiated at heavy-strand origin (O_H) and proceeds unidirectionally to synthesize the full-length H-strand. The replisome consists of the DNA polymerase gamma (POLγ, violet), Twinkle DNA helicase (TWINKLE, blue), and mitochondrial single-stranded DNA-binding protein (mtSSB, green). While TWINKLE unwinds the double-stranded DNA, mtSSB binds and stabilizes the displaced H-strand during replication. When the replisome passes the light-strand origin (O_L), a stem loop is formed that blocks mtSSB binding. The DNA-directed RNA polymerase (POLRMT, orange) recognizes this structure and generates primers. POLγ replaces POLRMT and initiates full-length L-strand synthesis in the opposite direction. Figure modified from Gustafsson et al.[23]

1.3.3 Mitochondrial DNA transcription

The NCR of the mitochondrial genomes is the control center to launch replication and transcription.[23] Both processes have to be closely coordinated to avoid collision of the replication machinery and the transcription machinery. The key regulator POLRMT, in cooperation with the transcription elongation factor TEFM, mediates the switch between replication and transcription, keeping the balance between both processes.[29,30]

As aforementioned, both mtDNA strands have a dedicated promoter (HSP & LSP).[31] Transcription initiation is facilitated by two essential transcription factors, A (TFAM) and B2 (TFB2M), in association with POLRMT.[32,33] TFAM is a crucial factor in the packaging and organization of mtDNA into condensed nucleoids.[32] Within the transcription complex, TFAM induces bending of the mtDNA into a U-shape and recruits the RNA polymerase, POLRMT to the promoter region.[34] Afterwards, TFB2M modulates the structure of POLRMT and unwinds the double-stranded mtDNA to disclose the promoter.[32,33,34] During elongation phase, transcription initiation factors are released and replaced by TEFM to promote synthesis of near genome-length transcripts. TEFM was found to stimulate the processivity of POLRMT by preventing the formation of G-quadruplexes in nascent RNAs.[35,36,37] Formation of such a G-quadruplex causes a premature stopping of L-strand transcription at the NCR and results in short RNA snippets that might favor mtDNA replication (Figure 4).[38]

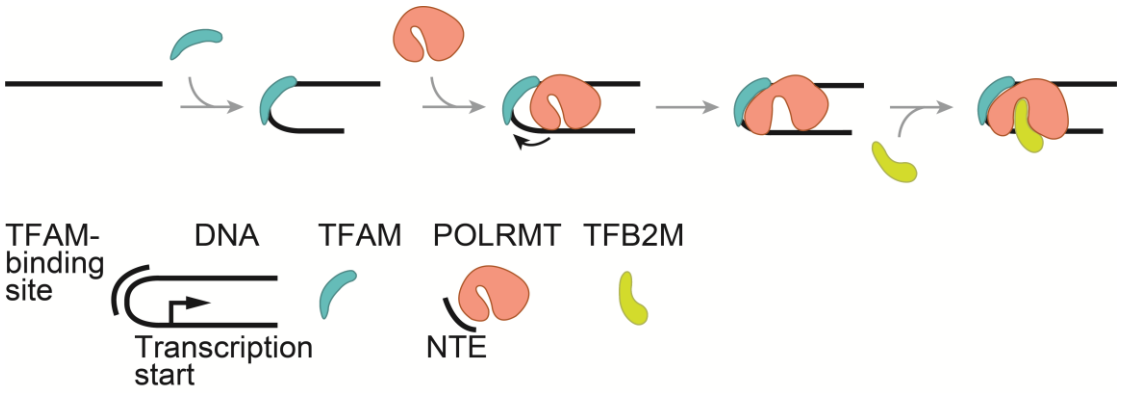

Figure 4: Transcription of the mitochondrial genome in humans. The transcription factor A (TFAM) induces bending of the mtDNA into a U-shape and recruits the mitochondrial RNA polymerase, POLRMT to the promoter region. POLRMT contains an N-terminal extension (NTE) that enhances promoter specificity. POLRMT undergoes a conformational change and the second transcription factor, TFB2M is recruited. TFB2M modulates the structure of POLRMT and melts the double-stranded mtDNA to disclose the promoter. Figure modified from Gustafsson et al.[23]

Although the first transcription termination factor MTERF1 was identified in the 1980s, the mechanism of transcription termination is still not fully understood.[39] It is assumed that MTERF1 blocks the transcription machinery by inducing base flipping, thereby leading to termination of L-strand transcription, while H-strand transcription is only partially completed.[39,40]

1.3.4 Mitochondrial RNA processing

Mitochondrial transcription from HLP and LSP generates long polycistronic precursor transcripts that are subsequently processed to create functional tRNAs, mRNAs and rRNAs.[41] According to the "tRNA punctuation model", tRNAs flank most of the mitochondrial primary transcripts and constitute a recognition signal for precise endonucleolytic cleavage.[42] This processing mechanism of the precursor RNA releases individual tRNAs, mRNAs and rRNAs that undergo a number of extensive maturation steps mediated by a variety of RNA binding proteins (RBPs).[43]

The 5' end of precursor tRNAs is cleaved by RNase P, a nuclease composed of three subunits, the mitochondrial RNase P proteins 1-3 (MRPP1/TRMT10C, MRPP2/HSD17B10 and MRPP3/KIAA0391), while the 3' end is processed by the RNase Z enzyme, ELAC2.[41,44,45] The RNase P components MRPP1 and MRPP2 form a sub-complex that enhances the binding affinity of MRPP3 for tRNAs to promote 3' end processing by ELAC2.[46,44] MRPP3 is the catalytic site of RNase P and is associated with the mitochondrial unfolded protein response (UPR^{mt}).[47] The UPR^{mt} is a protective mechanism activated in response to stress to cope with misfolded proteins accumulating in the mitochondrial matrix. One downstream effect of this stress response is the internal shutdown of mitochondrial translation by downregulating the MRPP3 protein levels.[48] The reduced processing of precursor RNAs by RNase P causes a decrease in the protein folding load and enhances mitochondrial proteostasis.[47,48] This mechanism is highly critical in preventing the abnormal aggregation of proteins, such as β-amyloid, α-synuclein, or tau, which are characteristic hallmarks of neurodegenerative disorders like Alzheimer's disease or Parkinson's disease.[49]

However, some precursor transcripts are not punctuated by tRNAs and are thus described as non-canonical junctions, including the mRNAs CO1, ATP8/6, CO3, ND5, CYB and ND6.[50] Recently, it was discovered that members of the Fas-activated serine/threonine kinase (FASTK) protein family play a key role in non-canonical processing of mitochondrial RNA.[50] In total, five different homologs of FASTK, known as FAST kinase domain-containing proteins 1-5 (FASTKD1-5), have been identified. All family members are localized to the mitochondrial matrix but have different mechanisms of action, ranging from RNA processing to mitoribosome maturation and

translation. For Instance, FASTK stabilizes and protects the ND6 transcript from degradation, whereas FASTKD1 has the opposite effect and decreases mRNA levels of ND3 by destabilization.[50,51] Depletion of FASTKD2 affects RNA processing, causing loss of 16S rRNA (RNR2) and resulting in impaired mitoribosome assembly.[52] Strong interactions of FASTKD2 with the ND6 mRNA and the 16S rRNA were confirmed by CLIP-seq. data, suggesting a role of FASTKD2 in ribosome assembly and mRNA translation.[52] Furthermore, FASTKD2 is associated with a subset of RNA modifying proteins (*e.g.,* RPUSD4) required for pseudouridylation of 16S rRNA to increase its stability and binding to the mitoribosome.[53] FASTKD3 interacts with factors involved in RNA processing and is essential for an efficient translation of CO1, which is necessary for ETC complex IV.[51] The two members FASTKD4 and FASTKD5 are crucial for non-canonical processing and may cooperate to ensure efficient maturation of precursors that lack the flanking tRNAs.[50]

Once the processing of the polycistronic transcript is completed, various types of mitochondrial RNAs undergo a diverse range of post-transcriptional modifications. Further, more than 170 different regulatory modifications have been discovered to play a fundamental role in RNA structure, stability and interactions with proteins, in particular with the mitoribosome.[54]

1.3.5 Mitochondrial post-transcriptional RNA maturation

One essential RNA modification is polyadenylation of mRNAs that adds a poly(A) tail at the 3' end of all mRNAs, except for ND6.[55] This reaction is catalyzed by the mitochondrial poly(A) RNA polymerase (MTPAP) that creates a functional stop codon for half of all mitochondrial transcripts.[56] Interestingly, polyadenylation in mitochondria plays an ambivalent role, stabilizing some transcripts while targeting others for degradation.[57] In addition to polyadenylation, mRNA stability is regulated by a multifunctional leucine-rich PPR motif containing protein (LRPPRC).[58] LRPPRC forms a chaperone complex with the stem-loop interacting RNA binding protein (SLIRP) that stabilizes and protects RNA in both mitochondria and the nucleus. Loss of LRPPRC results in reduced steady-state levels of several mRNAs, aberrant polyadenylation and misregulated translation.[58] Furthermore, LRPPRC mutations lead to complex IV deficiency and cause severe neurological disorders such as the French-Canadian type of Leigh syndrome.[59]

Methylation is the most prevalent post-transcriptional modifications found in mitochondria, affecting mRNAs, tRNAs, rRNAs[54] as well as lncRNAs.[60] Among these modifications, N^6-methyladenosine (m^6A)[54] is highly abundant, while N^1-methyladenosine (m^1A)[60] has been discovered at distinct positions across all types of mitochondrial RNAs, catalyzed by the two methyltransferases (MTases) TRMT61B and TRMT10C.[54,60] The site-specific methylation of the two rRNAs, 12S and 16S, is of primary importance in assembly of the mitoribosome that in turn is essential for mRNA translation.[54] Furthermore, it is important to note that members of the rRNA methyltransferase (MTase) family, specifically MRM1, MRM2, and MRM3 (also known as RNMTL1), are responsible for catalyzing the methylation of 2'-O-ribose sites at the peptidyl transferase center of rRNAs.[61] This modification play a significant role in facilitating tRNA binding to the mitochondrial ribosome.[61]

Another highly prevalent modification of mRNAs, rRNAs, and particularly tRNAs, involves the conversion of uridines to pseudouridines (Ψ) through the activity of specific pseudouridine synthases.[62] These synthases, including PUS1, TRUB2, RPUSD3 and RPUSD4, play a crucial role in catalyzing the pseudouridylation process.[62] Extensive research,[63] has led to the identification of the Pentatricopeptide Repeat-Containing Protein 1 (PTCD1) as a key factor in stabilizing the 16S rRNA during the modification process facilitated by RPUSD4. This stabilization mechanism ensures proper biogenesis of the 16S rRNA.[63] Besides, pseudouridine, tRNAs undergo a wide range of diverse base modifications such as dihydrouridine (D), queuosine (Q) or 5-taurinomethyluridine (τm^5U), just to mention a few (Figure 5).[64,65] These precisely modified nucleotides are crucial in mediating the recognition of tRNAs by aminoacyl-tRNA sythetases (aaRSs). In mitochondria, 17 different aaRSs exist to couple each tRNA to its cognate amino acid by esterification, before it is transferred to the mitoribosome.[66,67]

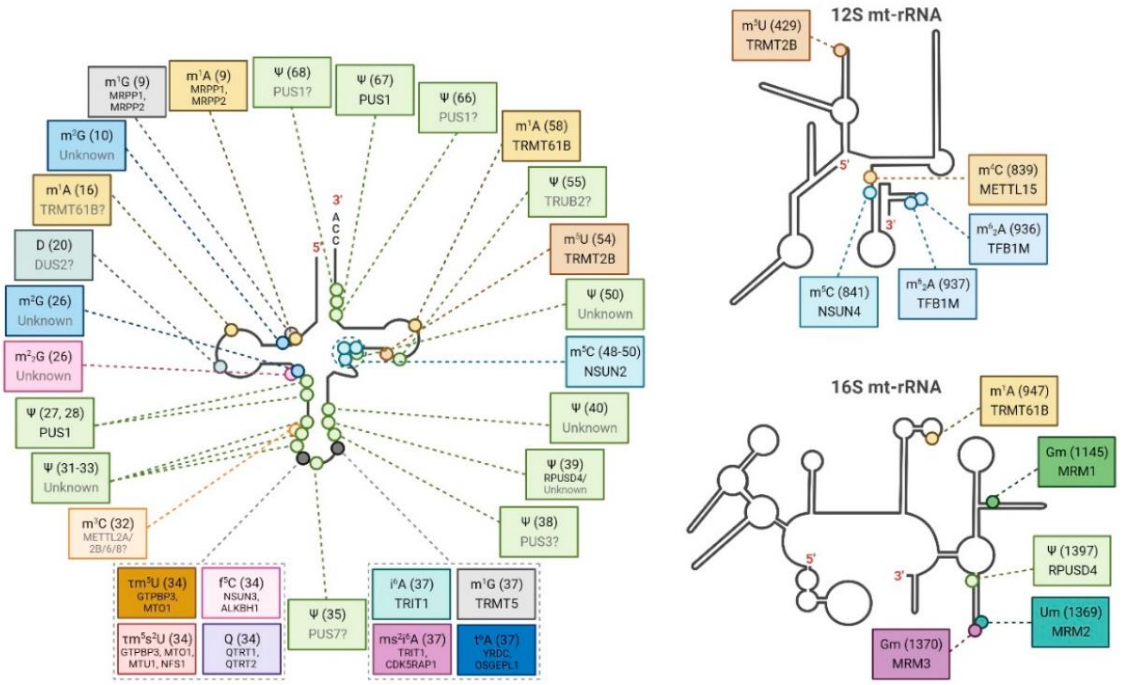

Figure 5: Post-transcriptional modifications of mitochondrial tRNAs and rRNAs in humans. In particular, tRNAs and rRNA undergo intensive base modifications. The boxes display chemical modifications along with the base position number in brackets and the corresponding enzyme. Modifying enzymes that are predicted but not confirmed for the indicated modifications are represented in gray, followed by a question mark. One of the most prevalent modification of tRNAs, is the conversion of uridines to pseudouridines (Ψ) through the activity of specific pseudouridine synthases. Further modifications are: 1-methyladenosine (m^1A), 1-methyl-guanosine (m^1G), N^2-methylguanosine (m^2G), dihydrouridine (D), N^2,N^2-dimethylguanosine (m^2_2G), pseudouridine (Ψ), 3-methylcytidine (m^3C), 5-taurinomethyluridine (τm^5U), 5-taurinomethyl-2-thiouridine (τm^5s^2U), 5-formylcytidine (f^5C), Queuosine (Q), N^6-isopentenyl-adenosine (i^6A), 2-methylthio- N^6-isopentenyladenosine (ms^2i^6A), N^6-threonylcarbamoyl-adenosine (t^6A), 5-methylcytidine (m^5C), 5-methyluridine (m^5U), N^4-methylcytidine (m^4C), N^6,N^6-dimethyladenosine (m^6_2A), 2´-O-methylguanosine (Gm), and 2´-O-methyluridine (Um). Figure from Jedynak-Slyvka et al. [62]

The mitochondrial ribosome has a sedimentation coefficient of 55S and consists of two subunits, the 28S small subunit (SSU) and the 39S large subunit (LSU).[68] The SSU is composed of the 12S rRNA and nearly 30 small ribosomal subunit proteins (MRPS), whereas the LSU is formed by the 16S rRNA and approximately 50 large ribosomal subunit proteins (MRPL).[69] The maturation of the 55S ribosome in mitochondria involves a complex interplay between the transcription of mitochondrial encoded rRNAs and the import of nuclear encoded mitoribosomal protein subunits.[69] This mechanism, which coordinates the assembly of these components into a functional ribosome, has not been fully understood. However, it was reported[70] that MRPL12, a subunit of the LSU, binds to POLRMT and thereby stimulates mitochondrial transcription according to the import

rate of mitoribosomal proteins. In 2016, it was shown[71] that loss of tRNA 5' end processing by knockout of MRPP3 leads to defects in SSU assembly and an impaired protein synthesis. These findings indicate a direct crosstalk between RNA transcription and protein translation via ribosome assembly.

The stepwise formation of the mitoribosome is mainly carried out by ATP-dependent RNA helicases and guanosine triphosphate hydrolases (GTPases; Figure 6).[45] The RNA helicases DExH-Box Helicase 30 (DHX30) and the DEAD-Box Helicase 28 (DDX28) are characterized by a conserved amino acid motif (Asp-Glu-Ala-Asp/His) and have been recently discovered to facilitate LSU biogenesis.[72] Depletion of DHX30 leads to decreased translation and loss of the 55S monosomes. DDX28 is crucial for the early stage assembly and binds the 16S rRNA in complex with FASTKD2.[73] It is thought that DDX28 might function as a RNA chaperone stabilizing mitoribosome intermediates, whereas the precise function of DHX30 hasn't been identified yet.[73]

The GTPase family constitutes the largest collection of assembly factors and is in the spotlight of current research[74–78]: two GTPases, Era like 12S mitochondrial RRNA chaperone 1 (ERAL1)[74] and nitric oxide associated 1 (NO1)[79] can be clearly allocated to SSU assembly. ERAL1 binds close to the 3' terminus of the 12S rRNA and acts as a RNA chaperone before methylation.[74] LSU biogenesis is regulated by at least four different GTP-binding proteins (GTPBPs): GTPBP5,[75] GTPBP6,[78] GTPBP7[80] and GTPBP10.[76,77] GTPBP5 and GTPBP10 are homologs of the bacterial GTPase ObgE and their key functions during LSU assembly in humans were recently identified.[75-77] The proximity interactome of GTPBP5 identified the rRNA methyltransferase MRM2 as a top interaction.[75] This specific interaction has led to the assumption that GTPBP5 could act as a quality checkpoint for the 16S rRNA methylation status to facilitate late-stage assembly, similar to its bacterial counterpart.

The second Obg homolog, GTPBP10, coordinates the maturation of the 39S large subunit at late stages. GTPBP10 was found to associate with LSU assembly factors such as DDX28 and the mitochondrial assembly of ribosomal large subunit protein 1 (MALSU1). In addition, GTPBP10 interacts with several RNA modification factors including TRMT61B and RPUSD4.[76,77] In an analogous manner to GTPBP5, GTPBP10 engages with 16S rRNA and represents a checkpoint for quality control to ensure proper ribosome

biogenesis.[75-77] Furthermore, GTPBP10 is proposed to play a role in processing of the rRNA precursor. Depletion of GTPBP10 causes accumulation of the unprocessed 12S-16S rRNA transcript and seems to affect indirectly also SSU formation.[76,77]

Latest research[78] on ribosome biogenesis in human mitochondria, uncovered the new assembly factor GTPBP6, the bacterial homolog of HflX, fulfilling a dual function in recycling and assembly of the mitoribosome. HflX is known as ribosome splitting factor, rescuing arrested ribosomes upon heat shock.[78] The human equivalent, GTPBP6, has been suggested to have a similar function and facilitate ribosome dissociation.[78] Moreover, stalled LSU maturation and accumulation of assembly factors including GTPBP5, GTPBP10 and MALSU1 could be observed during loss of GTPBP6. However, the biological function of ribosome recycling by GTPBP6 remains obscured and needs to be further investigated.[78]

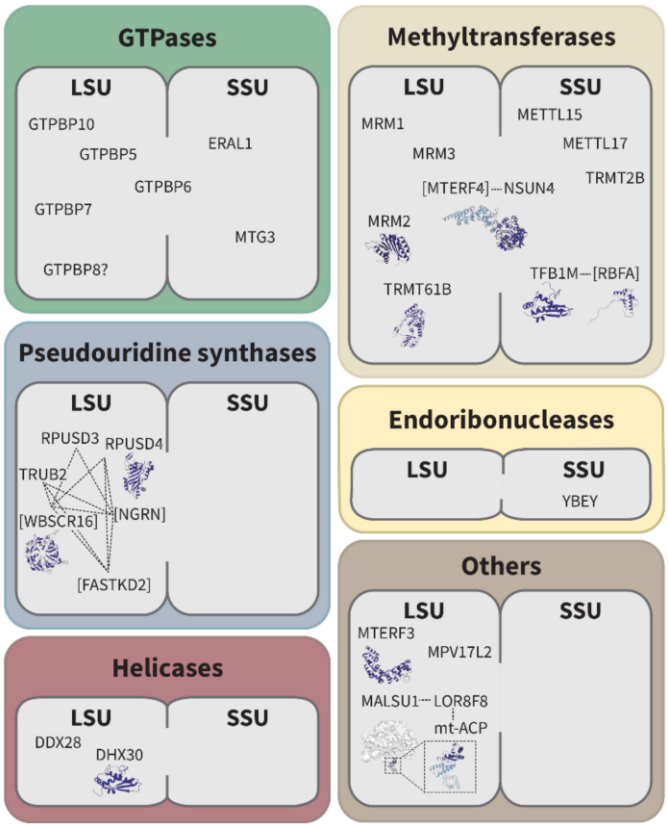

Figure 6: Mitochondrial ribosome assembly factors in humans. Mitoribosome maturation is facilitated by several nuclear encoded enzymes classified in six categories: guanosine triphosphate hydrolases (GTPases, green), methyltransferases (beige), pseudouridine synthases (blue), endoribonucleases (yellow), helicases (red) and factors without known enzymatic activity (others, brown). Protein modules lacking the corresponding enzymatic activity are denoted within squared brackets as non-active factors. Specific functions within protein modules are visually represented together, connected by dashed lines. Protein structures (if available) are shown and derived from the protein data bank PDB. Figure from Lopez Sanchez et al.[45]

1.4 Mitochondrial RNA Granules (MRGs)

The mitochondrial gene expression is a highly specialized and complex process built on a dual genetic system.[11] Mitochondria comprise nucleoids as dedicated domains for mitochondrial DNA replication and transcription.[21] Adjacent to nucleoids another membraneless, RNA-rich entity was discovered, in 2004 (Figure 7).[81] Iborra et al.[81] visualized nascent RNA using 5-bromouridine (BrU) labeling and initially observed punctate structures besides nucleoids in mitochondria. These newly transcribed RNA containing foci were scattered along the mitochondrion, clearly separate from DNA foci. Moreover, the BrU labeling was used for pulse-chase experiments and determined the half-life of nascent RNA to about 45 min.[81]

In 2013, the pioneering research conducted by the groups of Jean-Claude Martinou[82] and Eric Shoubridge[83] provided new insights into the field of RNA processing by identifying a novel key regulator known as G-rich sequence factor 1 (GRSF1). Isoform 1 of GRSF1 was found[82,83] to accumulate close to nucleoids in distinct foci within mitochondria, while isoform 2 showed[82] a diffuse staining in the cytosol. GRSF1 is an RBP known for its selective affinity towards G-rich sequences, critical for its functional interaction with RNA molecules.[84] The specific interaction between GRSF1 and the light strand transcripts ND6, lncND5, and lncCYTB demonstrates the functional significance of GRSF1 in the processing and modulation of these mitochondrial RNA molecules.[82,83] Through its binding, GRSF1 likely influences various aspects of their maturation and stability, contributing to the finely tuned gene expression machinery within mitochondria.

Further, immunofluorescence staining of GRSF1 combined with nascent RNA demonstrated[82,83] a striking co-localization of GRSF1 with BrU-labeled punctae and indicated a direct association between GRSF1 and newly transcribed regions of RNA within mitochondria. Furthermore, the interaction of GRSF1 with subunits of RNase P, gave rise to the idea that newly transcribed RNA is processed in a separate structure within the mitochondrial matrix. Therefore, this compartmentalized ribonucleoprotein complex was termed mitochondrial RNA granule (MRG; Figure 7).[82]

These discoveries highlighting GRSF1 as a key player in post-transcriptional processes and raises many fundamental questions about the spatio-temporal organization of the mitochondrial gene expression. Hence, MRGs' composition, function and relation to other mitochondrial foci are subject of current research.

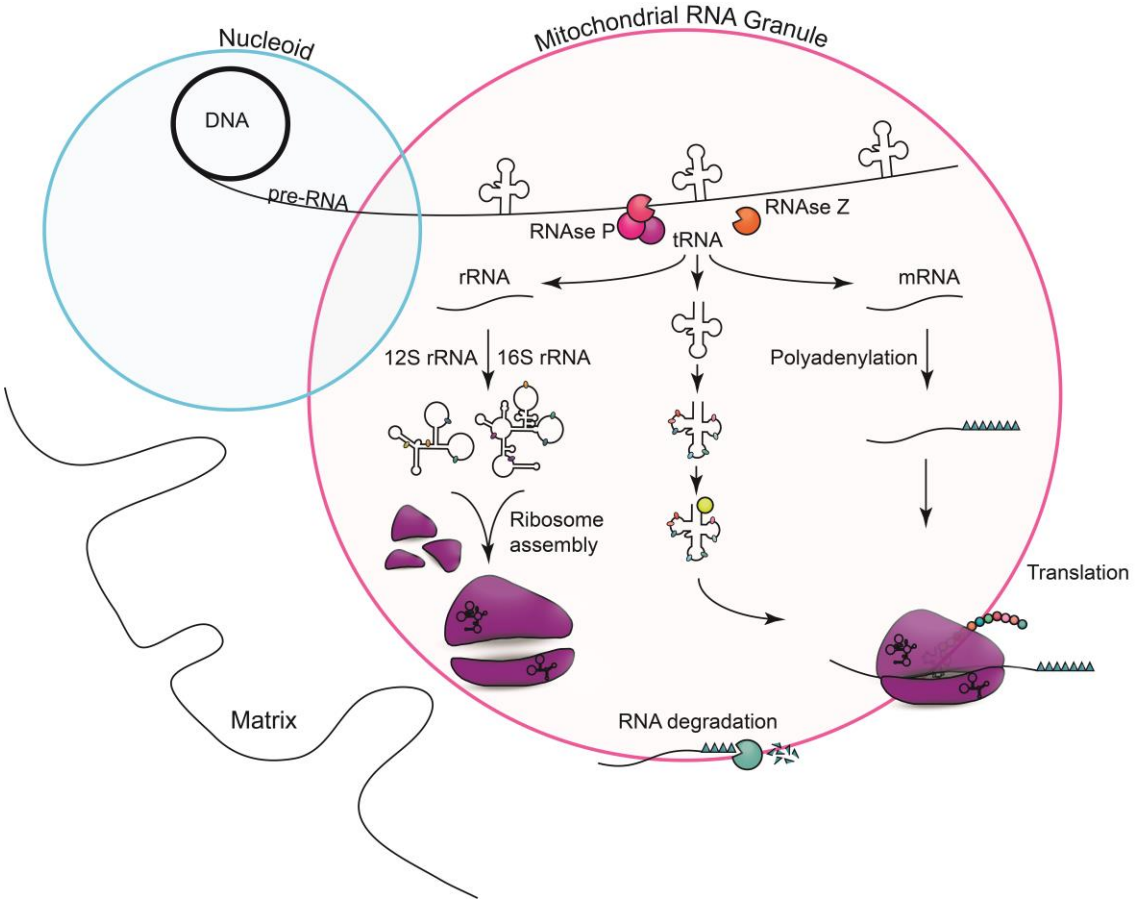

Figure 7: Model of mitochondrial RNA granules (MRGs) in humans. MRGs are specialized and discrete structures adjacent to nucleoids within the mitochondrial matrix. The primary function of MRGs is to regulate gene expression of mitochondrial RNAs. Transcription of the mitochondrial genome produces long polycistronic precursor RNAs (preRNAs) that undergo various maturing steps. Enzymes involved in tRNA processing are the endoribonucleases RNase P and Z, that create functional mRNAs, tRNAs, and rRNAs. MRGs are involved in various pathways, ranging from RNA processing and RNA modification to RNA degradation. Additionally, MRGs are implicated in mitoribosome maturation and the subsequent release of assembled ribosomes. However, it is still not entirely clear whether the assembly of mitoribosomes occurs within the MRGs or in a neighboring entity.

1.4.1 MRG composition

GRSF1 was the first protein discovered in MRGs and is considered as gold standard for microscopic visualization.[82,83] Shortly after the discovery of GRSF1, it was reported[61] that members of the 16S rRNA methyltransferase family, MRM1, MRM2 and RNMTL1, form distinct foci in close proximity to mtDNA, as well. Immunoprecipitation experiments disclosed the association of RNMTL1 with a dozen of RBPs such as GRSF1, LRRPRC, RPUSD4 and DDX28 that were later defined as MRG components.[61] Additional factors involved in polyadenylation (MTPAP) and RNA degradation (SUPV3L1 and PNPT1) were found to co-localize with MRGs.[85,86] It became evident that MRGs are the centers for mitochondrial RNA processing and maturation.[51,87] Proteins of the FASTK family were identified as crucial part of MRGs and essential regulators of gene expression in mitochondria.[51,87-89] In particular, the proteins FASTK,[88] FASTKD1,[89] FASTKD2[87] and FASTKD5[87] have already been identified as integral components of the MRGs.

In addition, the ribosome-assembly factors DDX28 and DHX30 were found to be part of the MRGs as well.[87] This finding turned into the idea that MRGs might be more than sites of post-transcriptional RNA processing and provide likewise a center for mitoribosome maturation. Further interactome[53] and co-localization-analysis[90] of FASTKD2 identified novel MRG-related proteins involved in RNA processing (*e.g.,* PTCD1 and PTCD2[90]), RNA modification (*e.g.,* TRUB2, RPUSD3 and RPUSD4[53,90]), mitoribosome assembly (ERAL1 and NOA1[90]) and several structural components of the mitoribosome (*e.g.,* MRPL19,[53] MRPS6,[53] MRPL47[90] and MRPS9[90]).

These results imply that MRGs are involved in multiple activities and probably provide a comprehensive platform for RNA metabolism including RNA processing, modification, polyadenylation and degradation on one hand and ribosome maturation including ribosome assembly and its release for translation on the other hand.

1.4.2 MRG compartmentalization

As mentioned before, MRGs host a variety of complex and precise processes that need to be closely coordinated, not only with one another but also with the nucleoids to ensure an efficient gene expression. It has been suggested that MRGs are highly organized and likely subdivided into specialized entities.[91] Nevertheless, how exactly they are separated from nucleoids and sub-compartmentalized is poorly understood and has to be further investigated.

The BioID proximity-labeling assay of the well-known nucleoid protein TEFM revealed interactions with several RNA processing factors like GRSF1, MRPP1-3 or FASTKD5 as well as the RNA degradation complex (SUPV3L1 and PNPT1).[38] Notably, loss of TFEM affected RNA processing and led to accumulation of unprocessed transcripts in mitochondria.[38] Moreover, both GRSF1 and the nucleoid component SSBP1 were found to be involved in the degradation of double-stranded RNA and RNA:DNA hybrids. This suggests a dual function of both proteins in maintaining the integrity of mitochondrial RNA by participating in the clearance of aberrant RNA species.[92]

Based on immunolabeling experiments of mitochondrial DNA and RNA, nucleoids and MRGs were previously described as distinct structures with autonomous protein machineries.[81] However, most likely there is a link between transcription and RNA processing to ensure accurate and coordinated gene expression. Recent studies[38,93] confirmed a strong interplay and dependency of RNA granules and DNA nucleoids. Furthermore, the identification of an RNA degradosome foci (D-foci) in mitochondria added an additional layer of complexity to the spatial properties of MRGs.[85] The RNA degradation complex (mtEXO) formed by the RNA helicase SUPV3L1 and the ribonuclease PNPT1 appears as distinct foci that are partially associated with GRSF1.[94,95] Interestingly, the co-localization between GRSF1 and the D-foci was shown[95] to be dependent on the catalytic activity of the degradation complex. The presence of GRSF1 positive D-foci was significantly increased when the SUPV3L1-PNPT1 complex was inactive. Hence, the hypothesis was proposed that GRSF1 regulates the degradosome activity when mtEXO is compromised.[95] A contrary regulation of the mtEXO has been described for the LRPPRC-SLIRP complex, that prevents mRNA from degradation and facilitates polyadenylation by MTPAP.[96]

GRSF1 is known to preferentially bind Guanine- (G-) rich non-coding RNAs derived from L-strand transcription.[95] These G-rich ncRNAs are predicted to form stable secondary structures, also referred to as four-stranded G-quadruplexes (G4). Accumulation of these G4 RNAs could be observed when both GRSF1 and the degradosome were impaired. In conclusion, a model was considered in which GRSF1 melts the secondary structures of G4 RNAs, mediating RNA decay by the SUV3L1-PNPT1 complex.[95] Both studies conducted by Pietras et al.[95] and Hensen et al.[93] emphasize the major role of GRSF1 in degradation of dsRNA and links MRGs to the RNA decay pathway. However, it could not yet be proved whether D-foci are part of the MRGs or a separate domain.

In 2018,[18] dsRNA granules were discovered in mitochondria utilizing the anti-ds RNA J2 antibody. It was shown that 99% of the detectable dsRNA descended from the mitochondrial genome.[18] Mitochondria have the special property of bidirectional transcription of their circular genome, resulting in the formation of complementary H- and L-strands.[97] Under basal conditions, the SUPV3L1-PNPT1 complex efficiently degrades L-strand transcripts, thereby preventing formation of RNA:RNA hybrids in mitochondria (Figure 8).[18] The study by Dhir et al.[18] unveiled that mitochondrial dsRNA plays an important role in mediating the innate immune response, particularly during microbial and viral attacks. In such scenarios, mitochondrial dsRNA is released into the cytosol and activates the interferon response. Interestingly, depletion of GRSF1,[93] SSBP1,[93] SUPV3L1,[18] or PNPT1[18] results in impaired RNA degradation, leading to accumulation of dsRNA. Although dsRNA granules are regulated by MRG proteins their spatial arrangement and relationship to each other remain completely unknown.[18,93] These dsRNA punctae could either represent a separate reservoir or form a unit with D-foci in association to MRGs.[98]

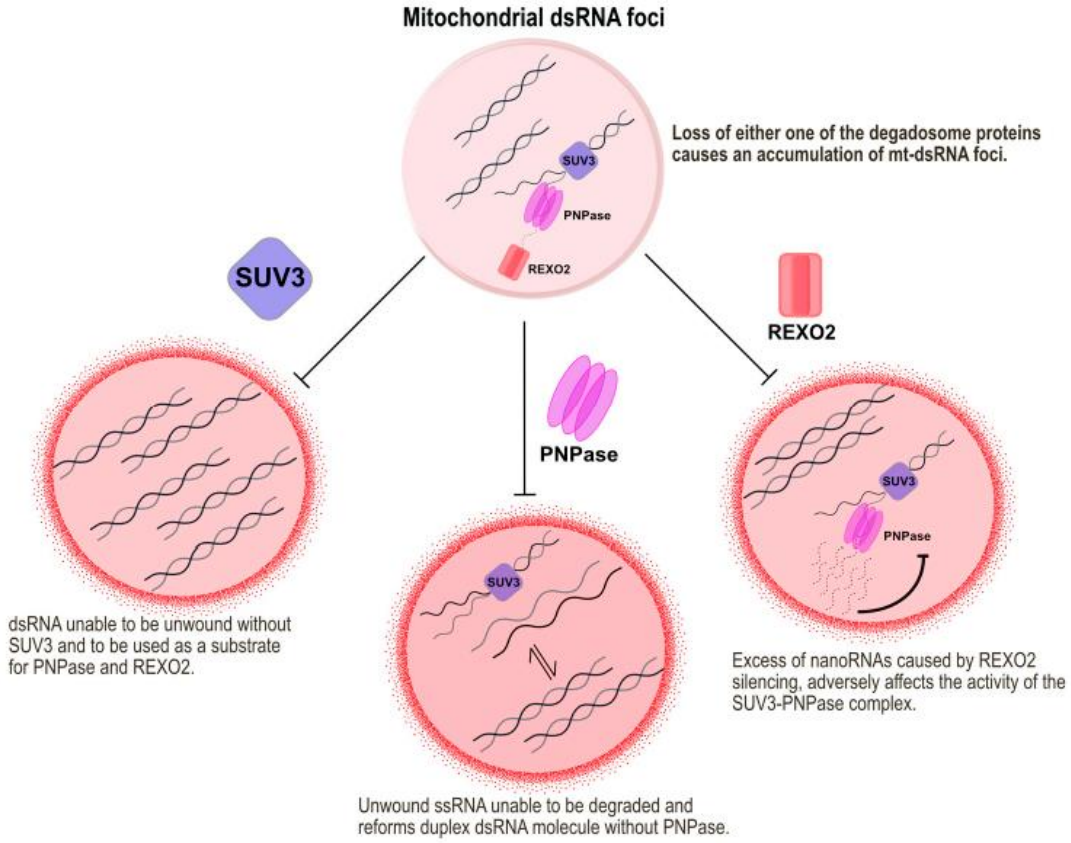

Figure 8: Dysregulation of MRG proteins causes accumulation of dsRNA in human mitochondria. Double-stranded RNA (dsRNA) is formed by complementary H- and L-strands transcripts in mitochondria. Loss of RNA degradation proteins SUV3, PNPase or REXO2 leads to different pathways resulting in dsRNA accumulation. It has been suggested that MRGs probably participate in processing or sequestration of dsRNA to prevent accumulation in mitochondria. However, the exact mechanisms and functions of this interplay are still an active area of research, and further studies are needed to fully understand the relationship between MRGs and dsRNA in mitochondria. Figure from Xavier and Martinou.[98]

A recent publication from 2022,[99] has reported that the mtEXO complex modulates non-coding 7S RNA levels by degradation in mitochondria. Depletion of SUPV3L1 and PNPT1 led to a strong increase in 7S RNA and impaired transcription initiation. Cryo-EM experiments[99] elucidated enhanced dimerization of the RNA polymerase PORLMT when interacting with 7S RNA. Thus, 7S RNA functions as a negative regulator of transcription by preventing PORLMT from recognizing the promoter. To conclude, these findings demonstrate the key role of the degradosome in controlling the mitochondrial gene expression.[99]

1.4.3 Physical properties of MRGs

MRGs are not surrounded by a membrane, yet they appear clearly delimited within the mitochondrial matrix.[87] It was shown[100] that MRGs are fluid condensates formed by liquid-liquid phase separation (LLPS). The application of super-resolution microscopy enabled novel insights into the nanostructure of MRGs, revealing their dimensions with an overall diameter of about 130 nm, wherein RNA constitutes the predominant proportion with 92 nm. In this study,[100] differences in size and shape were identified between RNA, GRSF1 and FASTKD2 foci suggesting that the mitochondrial RNA, similar to the DNA within nucleoids, is compacted and surrounded by proteins.[100] Moreover, MRGs were found to associate with the inner mitochondrial membrane and their fusion is influenced by membrane dynamics.[100] Major questions in the field of MRGs revolve around their assembly, preservation of integrity and potential disruption of their formation.

In particular, the mechanism of their formation by LLPS and the precise factors influencing their integrity are not fully understood.[100] Notably, cells lacking mtDNA (referred to as Rho-0 cells) show reduced levels of the MRG components GRSF1,[87,83] DHX30,[87] DDX28,[87] FASTKD2[87] and FASTKD5,[87] consequently leading to diminished MRG foci.[87,83] These Rho-0 cells have been extensively studied and are commonly generated by exposing cells to low doses of the intercalating reagent ethidium bromide (EtBr) over a span of several weeks.[101] However, cells that contain mtDNA and form discrete MRGs did not show disruption even when GRSF1 or other related MRG components (*e.g.*, FASTKD2, FASTKD5) where impaired.[87] Remarkably, two studies observed[82,83] complete disassembly of MRGs when cells were treated with the transcription inhibitors ActinomycinD (ActD) or EtBr. This supports the notion that RNA may serve as a scaffold for MRG formation. Considering this hypothesis, there arises a compelling need to investigate and identify the precise RNA species responsible for MRGs' integrity.

1.5 Research questions, aims and objectives

Despite the fact that MRGs have emerged as key regulators of mitochondrial gene expression,[82,83] little is known about their (sub)architecture and their characteristics, especially under stress conditions. Impaired mitochondrial RNA metabolism has been associated with various human diseases, yet the underlying molecular details remain elusive. Deciphering the proteins carrying out the required processes within MRGs is crucial for a better understanding of their physiological relevance.

Since their discovery in 2013,[82] MRGs have not yet been extensively investigated and fundamental questions about their composition, structure and regulation remain unanswered. Moreover, MRGs are supposed to be dynamic structures, however our knowledge about the mechanism leading to their formation and their physical properties upon stress conditions is rudimentary. Hence, it is tempting to explore diverse questions, such as what causes changes in MRGs' morphology, their potential ability to reassemble during recovery from stress, and the factors compromising their structural integrity.

Therefore, the primary objectives of this work are as follows: firstly, to comprehensively define the MRG proteome and identifying essential components in-depth; secondly, to investigate the spatio-temporal effects under stress conditions; and thirdly, to identify factors that contribute to maintaining their integrity. These goals aim to provide extensive insights into the biology of MRGs.

Firstly, establishment of the MRG network and identification of essential components:

I employed the cutting-edge proximity labeling technique TurboID, combined with quantitative mass spectrometry, to characterize both the overall protein composition and individual protein-protein interactions within the MRGs. To achieve this, I induced the expression of well-known MRG marker proteins such as GRSF1 and RNase P subunits in human Flp-In T-Rex HeLa cells at near-endogenous levels. These markers were C-terminally fused to the biotin ligase (TurboID) tag, enabling the biotinylation of their interacting proteins in close proximity and subsequent isolation using a streptavidin pull-down. This innovative approach allows capturing of even weak and transient interactions under biological conditions in a time-resolved manner. Building upon the

initial proteome data, I expanded the set of MRG candidates to create a comprehensive and accurate MRG protein network at high-depth. The cross-validating proximity data set allowed me to determine essential hub proteins that define the core of MRGs.

Secondly, determine the spatio-temporal dynamics of mitochondrial stress on MRGs:

Previously, changes in the morphology and protein compositions of MRGs have not been monitored under stress conditions in a time dependent manner. To address this gap, I studied MRGs upon different mitochondrial stressors and identified conditions upon which MRGs disassemble during stress and then recover. In this study, I impaired mitochondrial transcription utilizing IMT1, the first specific inhibitor for the mitochondrial RNA polymerase. To study MRGs' appearance during these stress conditions, I employed inducible HeLa Flp-In T-Rex cells expressing GRSF1 fused to EGFP and confocal fluorescence microscopy. Furthermore, changes in protein compositions were monitored using TurboID proximity labeling of a novel MRG protein.

Thirdly, elucidate the effect of mitochondrial RNA on MRGs' integrity:

Building upon the hypothesis that mitochondrial RNA potentially serves as a scaffold for MRGs assembly, I sought to demonstrate that MRGs are not only formed by RNA but are also stabilized by RNA, making them more resistant to stress conditions. Therefore, I conducted siRNA-mediated knockdowns targeting MRG-related proteins involved in RNA turnover to increase endogenous RNA levels in mitochondria. These knockdowns were combined with IMT1-induced stress and MRGs' morphology was monitored with aforementioned confocal fluorescence microscopy. Simultaneously, I detected mitochondrial nascent RNA as well as dsRNA with immunolabeling and measured RNA transcript levels using quantitative polymerase chain reaction (RT-qPCR).

2 Materials and methods

In this thesis, the company name "Thermo Fisher Scientific" will be abbreviated to "Thermo Fisher" for ease of reference.

2.1 Antibodies

Reagent or resource	Source	Identifier
Mouse anti-dsRNA (J2)	Scicons	Cat# 10010200
Mouse anti-FLAG M2	Sigma-Aldrich	Cat# F1804
Mouse anti-Bromodeoxyuridine	Roche	Cat# 11170376001
Rabbit anti-GRSF1	Abcam	Cat# ab194358
Rabbit anti-ATP5A1 antibody	Proteintech	Cat# 14676-1-AP
Streptavidin, Alexa Fluor 568	Thermo Fisher	Cat# S11226
Goat anti-Mouse Alexa Fluor Plus 594	Thermo Fisher	Cat# A32742
Goat anti-Mouse Alexa Fluor Plus 488	Thermo Fisher	Cat# A32723
Goat anti-Rabbit Alexa Fluor Plus 405	Thermo Fisher	Cat# A48254
IRDye 800CW Streptavidin	Licor	Cat# 925-32230

2.2 Chemicals, peptides and recombinant proteins

Reagent or resource	Source	Identifier
20x Bolt MES SDS Running Buffer	Thermo Fisher	Cat# B0002
2x qPCR SYBR Green Master Mix, no ROX	Steinbrenner	Cat# SL-9902
5-Bromouridine	Sigma-Aldrich	Cat# 850187
Acetone, LC-MS grade	Sigma-Aldrich	Cat# 34850M
Acetonitrile LC-MS grade	VWR	Cat# AE70.0
Actinomycin D (ActD)	Sigma	Cat# A1410
Agarose peqGOLD	VWR	Cat# D00049
Ammonia solution (25%), LC-MS grade	Sigma-Aldrich	Cat# 5330030050
*Bam*HI-HF	NEB	Cat# R3136S
Biotin	Sigma-Aldrich	Cat# B4639
Blasticidin	Thermo Fisher	Cat# ant-bl-1
Bolt 4-12 % Bis-Tris Plus Gels, 15-well	Thermo Fisher	Cat# NW04125
Bolt 4-12% Bis-Tris Plus Gels, 10-well	Thermo Fisher	Cat# NW04120
Bolt 4-12% Bis-Tris Plus Gels, 12-well	Thermo Fisher	Cat# NW04122

Bovine Serum Albumin (BSA)	Sigma-Aldrich	Cat# A7906
Carbenicillin	AppliChem	Cat# A1490
Carbonyl cyanide m-chlorophenyl hydrazone (CCCP)	MedChem Express	Cat# HY-100941
Chameleon Duo Pre-stained Protein Ladder	Li-Cor	Cat# 928-60000
Chloroacetamide	Sigma-Aldrich	Cat# C0267
cOmplete, mini, EDTA-free Protease Inhibitor Cocktail	Sigma-Aldrich	Cat# 11836170001
Cordycepin	Sigma-Aldrich	Cat# C3394
Cover glasses, round 18 mm	VWR	Cat# 631-0153
Dimethyl sulfoxide (DMSO)	AppliChem	Cat# A3672,0100
Doxycycline	Sigma-Aldrich	Cat# D9891-10G
Dithiothreitol (DTT) ≥99 %	ROTH	Cat# 6908.2
Dulbecco's Phosphate-Buffered Saline (PBS)	Thermo Fisher	Cat# 14190-169
Dulbecco's Modified Eagle Medium (DMEM)	Thermo Fisher	Cat# 41966-029
Empore C-18 Disk, 47 mm	Sigma-Aldrich	Cat# 66883U
Empore SDB-RPS Disk, 47 mm,	Sigma-Aldrich	Cat# 66886U
EPPS ≥99.5%	Sigma-Aldrich	Cat# E9502
Erythromycin	Sigma-Aldrich	Cat# E5389
Ethanol	Sigma-Aldrich	Cat# 32205
Ethidium Bromide (EtBr)	Sigma-Aldrich	Cat# E1385
Fetal Bovine Serum (FBS)	Thermo Fisher	Cat# 10270-106
GeneRuler 100 bp DNA-Ladder	Thermo Fisher	Cat# SM0241
Glycerol	Sigma-Aldrich	Cat# G6279
Hydroxylamine	Sigma-Aldrich	Cat# 438227
Hygromycin B Gold	Invivogen	Cat# ant-hg-2
IMT1	Biozol	Cat# HY-134539
LightCycler 480 Multiwell Plate 384	Roche	Cat# 4729749001
Lipofectamine RNAiMAX	Thermo Fisher	Cat# 13778150
Lysyl endopeptidase (LysC)	Wako Chemicals	Cat# 129-02541

Menadione (Vitamin K3)	Sigma-Aldrich	Cat# M5625
Midori Green Direct	Nippon Genetics	Cat# MG06
MitoTracker Deep Red FM	Thermo Fisher	Cat# M22426
NotI-HF	NEB	Cat# R3189S
Opti-MEM Reduced Serum Medium	Thermo Fisher	Cat# 31985047
Paraformaldehyde solution (4%)	Santa Cruz	Cat# sc-281692
pH-Fix 0–14, test sticks	Macherey-Nagel	Cat# 92110
Pierce BCA Protein Assay	Thermo Fisher	Cat# 23228
Pierce Streptavidin Magnetic Beads	Thermo Fisher	Cat# 88816
Polyethylenimine (PEI), linear	Polysciences	Cat# 23966-1
ProLong Diamond Antifade Mountant DAPI	Thermo Fisher	Cat# P36962
Protein LoBind Tubes, 1.5 mL	VWR	Cat# 525-0133
Protein LoBind Tubes, 2.0 mL	VWR	Cat# 525-0134
Q5 Hot Start High-Fidelity DNA polymerase	NEB	Cat# M0493L
Rifampicin	Sigma-Aldrich	Cat# R3501
Gibco RPMI 1640 Medium (+L-Glutamine)	Thermo Fisher	Cat# 21875-034
TCEP 0.5 M pH 7	Sigma-Aldrich	Cat# 646547
TMT10plex Label Reagent	Thermo Fisher	Cat# 90111
TMT11-131C Label Reagent	Thermo Fisher	Cat# A37724
TMTpro 16plex Label Reagent	Thermo Fisher	Cat# A44520
TMTsixplex Label Reagent	Thermo Fisher	Cat# 90061
Trichloroacetic acid solution (TCA)	Sigma-Aldrich	Cat# T0699
Triton X100	VWR	Cat# 28817
Trypsin-EDTA (0.25%), phenol red	Thermo Fisher	Cat# 25200-056
Trypsin LC-MS grade	Promega	Cat# V5280
Trypton	ROTH	Cat# 8952.1
Tween 20	Sigma-Aldrich	Cat# P1379
Ultrapure water, DNAse/RNAse-free	Thermo Fisher	Cat# 10977

Water HiPerSolv Chromanorm LC-MS grade	VWR	Cat# 83645290
Yeast extract	ROTH	Cat# 2363.2
Zeocin	Invivogen	Cat# ant-zn-1

2.3 Commercial assays

Reagent or resource	Source	Identifier
GeneJET Gel Extraction Kit	Thermo Fisher	Cat# K0692
GeneJET Plasmid Miniprep Kit	Thermo Fisher	Cat# K0503
High-Capacity cDNA Reverse Transcription Kit	Thermo Fisher	Cat# 4368814
NucleoSpin RNA Kit	Macherey-Nagel	Cat# 740955.250
QIAquick PCR Purification Kit	Quiagen	Cat# 28106
Trans-Blot Turbo RTA Mini 0.2 µm Nitrocellulose Transfer Kit	Bio-Rad	Cat# 1704270

2.4 Experimental models: cell lines

Reagent or resource	Source	Identifier
HeLa Flp-In T-REx	Ullmann et al.[102]	N/A
HeLa Flp-In T-Rex DDX28 TurboID	This study	N/A
HeLa Flp-In T-Rex ELAC2 TurboID	This study	N/A
HeLa Flp-In T-Rex ERAL1 TurboID	This study	N/A
HeLa Flp-In T-Rex FASTK TurboID	This study	N/A
HeLa Flp-In T-Rex FASTKD2 TurboID	This study	N/A
HeLa Flp-In T-Rex FASTKD5 TurboID	This study	N/A
HeLa Flp-In T-Rex GFM1 TurboID	This study	N/A
HeLa Flp-In T-Rex GRSF1 EGFP	This study	N/A
HeLa Flp-In T-Rex GRSF1 TurboID	This study	N/A
HeLa Flp-In T-Rex GTPBP6 TurboID	This study	N/A
HeLa Flp-In T-Rex GTPBP10 TurboID	This study	N/A
HeLa Flp-In T-Rex IARS TurboID	This study	N/A
HeLa Flp-In T-Rex MRPP1 TurboID	This study	N/A

HeLa Flp-In T-Rex MRPP3 TurboID	This study	N/A
HeLa Flp-In T-Rex MRPS7 TurboID	This study	N/A
HeLa Flp-In T-Rex MTPAP TurboID	This study	N/A
HeLa Flp-In T-Rex MTS TurboID	This study	N/A
HeLa Flp-In T-Rex NOA1 TurboID	This study	N/A
HeLa Flp-In T-Rex POLDIP2 TurboID	This study	N/A
HeLa Flp-In T-Rex PUS1 TurboID	This study	N/A
HeLa Flp-In T-Rex RNMTL1 TurboID	This study	N/A
HeLa Flp-In T-Rex SSBP1 TurboID	This study	N/A
HeLa Flp-In T-Rex TUFM TurboID	This study	N/A

2.5 siRNAs

Reagent or resource	Source	Identifier
Firefly luciferase GL2 siRNA: 5' CGUACGCGGAAUACUUCG 3'	Dharmacon	N/A
FASTKD2 siRNA	Thermo Fisher	Cat# HSS176985
MTPAP siRNA	Thermo Fisher	Cat# HSS123986
PNPT1 siRNA	Thermo Fisher	Cat# HSS131758
SUPV3L1 siRNA	Thermo Fisher	Cat# HSS110378

2.6 Primer

Gibson cloning

Primer name	Primer sequence
Turbo_rev	ttaaacgggccctctagactcgagcttacttatcgtcgtcatccttgtagtcgctag ccttttcggcagaccgcag
DDX28_fwd	aaacttaagcttggtaccgagctcgaccatggctctaacgcggccg
DDX28_rev	gccgctactgcctccggttgcttggggcaaagg
DDX28_Turbo_fwd	gccccaagcaaccggaggcagtagcggcgggtcgagcaaagacaatactgtgc ctctgaag
ERAL1_fwd	aaacttaagcttggtaccgagctcgaccatggctgcccccagctgg
ERAL1_rev	gccgctactgcctcccttgaggagcttcacagagaggcg
ERAL1_Turbo_fwd	gaagctcctcaagggaggcagtagcggcgggtcgagcaaagacaatactgtgcc tctgaag

FASTK_fwd	aaacttaagcttggtaccgagctcgaccatgaggaggccgcgggg
FASTK_rev	gccgctactgcctccgccccttcaggcccccagc
FASTK_Turbo_fwd	gcctgaaggggcggaggcagtagcggcgggtcgagcaaagacaatactgtgcctctgaag
FASTKD2_fwd	aaacttaagcttggtaccgagctcgaccatgttgacaactttgaagc
FASTKD2_rev	gccgctactgcctccttgtgtgctttgcacatttac
FASTKD2_Turbo_fwd	gcaaagcacacaaggaggcagtagcggcgggtcgagcaaagacaatactgtgcctctgaag
FASTKD5_fwd	aaacttaagcttggtaccgagctcgaccatggcagctactctcaag
FASTKD5_rev	gccgctactgcctccgagagcagaggtgaatac
FASTKD5_Turbo_fwd	cacctctgctctcggaggcagtagcggcgggtcgagcaaagacaatactgtgcctctgaag
GFM1_fwd	aaacttaagcttggtaccgagctcgaccatgagactcctgggagctg
GFM1_rev	gccgctactgcctccgttcttggcttttccttttttaacag
GFM1_Turbo_fwd	aaaagccaagaacggaggcagtagcggcgggtcgagcaaagacaatactgtgcctctgaag
GRSF1_fwd	aaacttaagcttggtaccgagctcgaccatggccggcacgcgctgg
GRSF1_rev	gccgctactgcctccttttccttttggacatgaattcaggaacagttcaatatacctatgatgaacgtg
GRSF1_Turbo_fwd	tccaaaaggaaaaggaggcagtagcggcgggtcgagcaaagacaatactgtgcctctgaag
GTPBP10_fwd	aaacttaagcttggtaccgagctcgaccatggtgcattgcagttg
GTPBP10_rev	gccgctactgcctccaattatatccattttggaagtagtaacagc
GTPBP10_Turbo_fwd	aatggatataattggaggcagtagcggcgggtcgagcaaagacaatactgtgcctctgaag
GTPBP6_fwd	aaacttaagcttggtaccgagctcgaccatgtgggccctgcgggcc
GTPBP6_rev	gccgctactgcctcctcctggaaagagcttccggaatttgccg
GTPBP6_Turbo_fwd	gctctttccaggaggaggcagtagcggcgggtcgagcaaagacaatactgtgcctctgaag
IARS2_fwd	aaacttaagcttggtaccgagctcgaccatgcgttgggggctg
IARS2_rev	gccgctactgcctccttttccactgacaacttctgcacatc
IAR2_Turbo_fwd	tgtcagtggaaaaggaggcagtagcggcgggtcgagcaaagacaatactgtgcctctgaag
MRPP1_fwd	aaacttaagcttggtaccgagctcgaccatggctgctttcctcaaaatg
MRPP1_rev	gccgctactgcctccagtctttgccttctttagtc
MRPP1_Turbo_fwd	gaaggcaaagactggaggcagtagcggcgggtcgagcaaagacaatactgtgcctctgaag
MRPP3_fwd	aaacttaagcttggtaccgagctcgaccatgactttctatttgtttggtattcg
MRPP3_rev	gccgctactgcctcctgtcttttggtggaggcaaag
MRPP3_Turbo_fwd	ccaccaaaagacaggaggcagtagcggcgggtcgagcaaagacaatactgtgcctctgaag

MRPS7_fwd	aaacttaagcttggtaccgagctcgaccatggctgcccccgcagtg
MRPS7_rev	gccgctactgcctccccaccagcggtagtgggc
MRPS7_Turbo_fwd	ctaccgctggtggggaggcagtagcggcgggtcgagcaaagacaatactgtgcctctgaag
MTPAP_fwd	aaacttaagcttggtaccgagctcgaccatggcggttcccggcgtg
MTPAP_rev	gccgctactgcctcctgtctgagtactaattgttctcttcccactgg
MTPAP_Turbo_fwd	tagtactcagacaggaggcagtagcggcgggtcgagcaaagacaatactgtgcctctgaag
NOA1_fwd	aaacttaagcttggtaccgagctcgaccatgctgcccgctcgccta
NOA1_rev	gccgctactgcctcctacatttatctttcctttcttcttcctcacgttgtac
NOA1_Turbo_fwd	aaagataaatgtaggaggcagtagcggcgggtcgagcaaagacaatactgtgcctctgaag
POLDIP2_fwd	aaacttaagcttggtaccgagctcgaccatggcagcctgtacagcc
POLDIP2_rev	gccgctactgcctccccagtgaaggcctgaggg
POLDIP2_Turbo_fwd	aggccttcactggggaggcagtagcggcgggtcgagcaaagacaatactgtgcctctgaag
PUS1_fwd	aaacttaagcttggtaccgagctcgaccatgggcctccagcttcgc
PUS1_rev	gccgctactgcctccgtcagtgtctccgtcccc
PUS1_Turbo_fwd	cggagacactgacggaggcagtagcggcgggtcgagcaaagacaatactgtgcctctgaag
RNMTL1_fwd	aaacttaagcttggtaccgagctcgaccatggcggcgctggtgaga
RNMTL1_rev	gccgctactgcctccgtggtaactcctgtccctgctc
RNMTL1_Turbo_fwd	caggagttaccacggaggcagtagcggcgggtcgagcaaagacaatactgtgcctctgaag
SSBP1_fwd	aaacttaagcttggtaccgagctcgaccatgtttcgaagacctgtattac
SSBP1_rev	gccgctactgcctccctccttctctttcgtctg
SSBP1_Turbo_fwd	gaaagagaaggagggaggcagtagcggcgggtcgagcaaagacaatactgtgcctctgaag
TUFM_fwd	aaacttaagcttggtaccgagctcgaccatgaccacaatggcggcc
TUFM_rev	gccgctactgcctccaccccatttgatattcttctcctcc
TUFM_Turbo_fwd	tatcaaatggggtggaggcagtagcggcgggtcgagcaaagacaatactgtgcctctgaag

Sequencing

Primer name	Primer sequence
DDX28_seq._1	ggcaagactctcagctacct
DDX28_seq._2	tgcacagacatagcctctcg
ERAL1_seq._1	tgttgtggttcttgtggatgt
ERAL1_seq._2	actgtgcctctgaagctgat

FASTK_seq._1	gttttctgcggtatccacgg
FASTK_seq._2	gggaacgctggcatttctg
FASTKD2_seq._1	acagttcgtggaagttatggc
FASTKD2_seq._2	ctcttcctgttgctgctgta
FASTKD5_seq._1	gccagctgagtgtgaagaag
FASTKD5_seq._2	gccacccaatgcagaagaat
GFM1_seq._1	ccctgcagcaaatgaggtc
GFM1_seq._2	caacagcggcctttctatgg
GFM1_seq._3	aggtcatgcacagagggaaa
GRSF1_seq._1	ttgcaggtcaaatcttcgcc
GTPBP10_seq._1	agtagctgatcttccgggtt
GTPBP10_seq._2	tcgactccaccaatcagtacc
GTPBP6_seq._1	cccgaccaagaaagaactgg
GTPBP6_seq._2	atgcggcggttttgaagg
IARS2_seq._1	cgttggggaataatggcaga
IARS2_seq._2	tggttattcgtgccagcaag
IARS2_seq._3	cagattccatccctgtaaacga
IARS2_seq._4	acagcggagtcttcagataca
MRPP1_seq._1	cccagcttttagaaagtgaagga
MRPP3_seq._1	tacagtcttctcatccgggg
MRPP3_seq._2	agtggagtcgggatgagatg
MRPS7_seq._1	gcaacccctacaccatcttc
MTPAP_seq._1	cgcgtattttccagactgca
MTPAP_seq._2	ccgagaaagtgcctggattt
NOA1_seq._ 1	ctacctgccccgagagaag
NOA1_seq._ 2	tcgtaggaagagttggaagga
NOA1_seq._ 3	agcctccttcccttatgtaca
pcDNA5_seq._1	aggaaaggacagtgggagtg
POLDIP2_seq._1	ctccactgatcaggttccca
POLDIP2_seq._2	tccaccaatcagtacctgct
PUS1_seq._1	cagatgtgatgccaggacct

PUS1_seq._2	cagggccgctatcaacaag
RNMTL1_seq._1	ttttgccaagcctgaccatg
RNMTL1_seq._2	cacattcagactctgcgcg
TUFM_seq._1	tatgtgaacaaggctgacgc
TUFM_seq._2	ggactattggcaccggtcta

qPCR

Primer name	Primer sequence
Mitochondrial mature and precursor RNAs	Fleck et al.[103]
Non-coding 7S RNA	Zhu et al.[99]

2.7 Recombinant DNA

Reagent or resource	Source	Identifier
pcDNA 5/FRT/TO Vector	Thermo Fisher	Cat# V652020
pOG44 Flp-Recombinase Expression Vector	Thermo Fisher	Cat# V600520
V5-TurboID-NES_pCDNA3	Addgene	Cat# 107169

2.8 Software and algorithms

Program	Source	Identifier
Circos	Krzywinski et al.[104]	http://mkweb.bcgsc.ca/tableviewer/
Cytoscape v3.5.1	Shannon et al.[105]	https://cytoscape.org/
Excel 2016	Microsoft	Cat# KB4011684
Illustrator CS6	Adobe	Illustrator-CS6-Win-GM
ImageJ v2.3.0	Schneider et al.[106]	https://doi.org/10.1038/nmeth.2089
MaxQuant v1.6.17	Cox & Mann[107]	https://doi.org/10.1038/nbt.1511
PBLMM-v2.2.0	Klann & Münch[108]	https://onlinelibrary.wiley.com/doi/10.1002/jcb.30225

Phython v3.9	Python Consortium	https://www.python.org/
Prism 6	GraphPad	https://graphpad-prism.software.informer.com/6.0
ProHits-viz	Knight et al.[109]	https://prohits-viz.org/
Proteome Discoverer v2.4	Themo Fisher	Cat# OPTON-30957
R studio v3.6.2	RStudio Team	http://www.rstudio.com/
Random Image labeler package	This study	https://github.com/science64/Random-Image-Labeler
Xcalibur v4.0	Thermo Fisher	Cat# OPTON-30965

2.9 Human cell culture methods

Cells were cultured in Roswell Park Memorial Institute (RPMI) 1640 medium supplemented with 10% FBS, 5 µg/ml balsticidin and 150 µg/ml zeocin at 37°C and maintained in a humidified incubator at 37°C with a controlled atmosphere of 5% CO_2 and 95% air. Cells were cultured in an antibiotic-free cell medium prior to the experiments. The culture medium was changed frequency to provide cells with fresh nutrients. Sterile techniques were strictly followed during the entire cell culture process, including the use of a flow hood, autoclaved tools, and sterile culture dishes.

2.9.1 Stable cell line generation

The Flp-In T-Rex cell system was used to generate stable human epithelial cervix-adenocarcinoma (HeLa) cells. One day before transfection, cells were seeded into 10 cm dishes (Sarstedt) and cultured without antibiotics. Transfection was performed when cells were 60-70% confluent by using PEI in the ratio 1:3 (µg DNA/ µl PEI). The plasmid pcDNA5/FRT/TO containing the protein of interest C-terminally fused to TurboID was co-transfected with pOG44 Flp-Recombinase Expression Vector in a ratio of 1:9. On the next day, growth medium was supplemented with 5 µg/ml balsticidin. 48 h post-transfection the growth medium was changed to 5 µg/ml balsticidin and 50 µg/ml hygromycin B to select positive cells.

2.9.2 Freezing and thawing cells

Selected cell lines were cultured in medium without any antibiotics 24 h before freezing. Cells were washed with PBS and detached by 0.25% Trypsin-EDTA solution. Cells were transferred to sterile centrifuge tubes and centrifuged at 800 × g and room temperature (RT) for 3 min. Cell pellets were resuspended in medium supplemented with 10% DMSO and transferred to cryo tubes. Tubes were placed in a Mr. Frosty container (Thermo Fisher), gently cooled down to - 80°C over night (O/N) and later transferred to a -150°C freezer for long term storage.

Frozen cells were rapidly thawed, resuspended in pre-warmed medium and transferred into a sterile centrifuge tube. Cells were centrifuged at 800 × g and RT for 3 min. The supernatant was aspirated to remove the DMSO. Cell pellets were reseuspended in fresh RPMI medium without antibiotics and plated on a 10 cm cell culture dish (Sarstedt). On the next day, growth medium was supplemented with 5 µg/ml balsticidin and 50 µg/ml hygromycin B.

2.9.3 RNA interference

Knockdown was induced by transient transfection of small interfering RNAs (siRNAs) in HeLa Flp-In T-Rex cells. One day before transfection, 2.5×10^6 cells were seeded into 6-well plates (Sarstedt). Cells were transfected with 40 nM of stealth siRNAs targeting PNPT1, SUPV3L1, MTPAP and FASTKD2 or a pooled non-targeting control (NTC) siRNA against firefly luciferase GL2 as a control (see section 2.5). Transfection was conducted by Lipofectamine RNAiMax, according to manufacturer's instructions. Transfection medium was replaced 6 h post-transfection and cells cultured for three days.

2.9.4 TurboID proximity labeling

Stable Flp-In T-Rex cells were cultured in Dulbecco's modified Eagle's medium (DMEM) supplemented with 10% dialyzed FBS two days before experiment. Cells were seeded into a 10 cm plate (Sarstedt) and induced by 0.25 µg/ml doxycycline to express the TurboID constructs for 24 h. For biotinylation, cells were labeled by supplementing media with 500 µM biotin for 10 min at 37°C. To stop the labeling reaction, cells were placed on ice and washed 5 times with ice-cold PBS. Cells were harvest and pellets were flash-frozen and stored in -80 °C until streptavidin pull down.[110]

2.10 Molecular biological methods

2.10.1 Immunofluorescence

Stable HeLa Flp-In T-Rex cells were seeded 10×10^4 on coverslips (VWR) in a 12-well plate (Sarstedt) and induced with 0.25 µg/ml doxycycline to express the GRSF1-EGFP construct for 24 h. Cells were treated with 5 µM IMT1, 3µM EtBr, 3µg/ml ActD, 300 µg/ml erythormycin, 300 µg/ml rifampicin, 50 µM menadione or 10 µM CCCP for appropriate time points. For bromouridine (BrU) labeling, cells were incubated in 5 mM for 1 h. Cells were fixed with 4% paraformaldehyde solution in PBS for 15 min at RT and washed 3 times with PBS. This was followed by permeabilization with 0.1% Triton X-100. Cells were washed 3 times with 0.01% Tween in PBS. Samples were blocked with 1% BSA in PBS for 2 h at RT and incubated 1:100 with primary antibodies anti-dsRNA J2, anti-ATP5A1, anti-Bromodeoxyuridine or anti-FLAG in 1% BSA in PBS. Cells were washed three times with PBS and incubated 1:1000 with secondary goat anti-mouse or rabbit IgG (H+L) conjugated with Alexa Fluor 405, 488 or 594 in 1% BSA in PBS for 1 h. Coverslips were washed 3 times with PBS and fixed with ProLong Diamond Antifade Mountant with DAPI on a glass slide (Engelbrecht). All images were obtained with a 60 × objective on a Leica TCS-SP8 inverted spectral confocal microscope (Leica Microsystems).

2.10.2 Western blotting

Proteins were boiled in 6x SDS loading dye at 90°C for 5 min and separated with 4-12% Bolt Bis-Tris Gels. Gels were run in 20x Bolt MES SDS Running Buffer with Chameleon Duo Pre-stained Protein Ladder at 200 V for 20 min. Semi-dry western blotting was performed using the Trans-Blot Turbo Transfer System (Bio-Rad). Protein samples were transferred onto a 0.2 µM nitrocellulose membranes and blocked in 5% BSA in PBS for 30 min at RT. The blotting membrane was incubated with a specific primary antibody, appropriately diluted in 5% BSA in PBS, for 2 h at RT. The blotting membrane was washed three times with PBST (PBS containing 0.1% Tween) and incubated with a secondary antibody conjugated with IRDye (1:15,000) in 5% BSA in PBS, for 1 h at RT. The blotting membrane was washed three times with PBST and dried. Proteins were detected by using the Odyssey CLx imager (LI-COR), which detected the fluorescent signal emitted by the labeled secondary antibody.

2.10.3 RNA quantification

RNA was extracted using the NucleoSpin RNA Kit for RNA purification, according to manufacturer's instructions. During all procedures, RNA was kept cool and free from RNases. Final RNA concentration was determined with NanoDrop ND-100 *Spektralphotometer* (Thermo Fisher). Reverse transcription of 1 ug RNA to cDNA was performed with the ProFelx PCR System (Thermo Scientific) using the thermal cycling conditions according to the High Capacity cDNA RT Kit. Samples were mixed with 2x qPCR SYBR Green Master Mix, no ROX and measured with the LightCycler 480 System (Roche).

2.10.4 Gene amplification

DNA was amplified by polymerase chain reaction (PCR) using NEBNext High-Fidelity 2x PCR Master Mix. The thermal cycler parameters were set according to manufacturer's instructions. PCR products and GeneRuler 100 bp DNA-Ladder were mixed with 1 µl of MIDORI green direct and loaded on a 1% agarose peqGOLD in TAE buffer (40 mM Tris-HCl pH 8, 40 mM aceticacid and 1 mM EDTA).

2.10.5 Plasmid DNA purification

Bacterial culture was grown in 5 ml of lysogeny broth (LB) medium (10 g/l NaCl, 10 g/ml trypton, 5 g/ml yeast extract) supplemented with carbenicillin (50 µg/ml) shaking O/N at 37°C. On the next day, plasmid DNA was purified using the GeneJET Plasmid Miniprep Kit according to manufacturer's protocol.

2.10.6 Gibson assembly cloning

Cloning for all constructs was done according to the Gibson NEBuilder Hifi DNA Assembly Kit. The online tool NEBuilder was used for primer design to generate PCR fragments with 25 bp overlaps complementary to the vector pcDNA^{TM}5/FRT/TO. For restriction enzyme digestion, 1 µg of vector DNA was incubated with 10 units of *Bam*HI-HF and 10 units of *Not*I-HF at 37°C for 2 h. All Turbo fragments were amplified from plasmid V5-TurboID-NES_pcDNA3. The linearized backbone and fragments were purified with the QIAquick PCR Purification Kit and concentration was determined with NanoDrop ND-100 *Spektralphotometer* (Thermo Fisher). For assembly reaction, the vector and two inserts (ratio 1:3 vector/insert) were assembled at 50°C for 1 h. Transformation of

assembled product in competent *E. coli* (*Escherichia coli*) TOP10 cells (Thermo Fisher) was done according to manufacturer's protocol. Cells were plated on a LB-agar plate (LB medium, 1.5% (w/v) agar) containing 50 µg/ml carbenicillin and incubated at 37°C O/N. On the next day, single colonies were picked and inoculated into LB-medium and cultured at 37°C O/N (see section 2.10.5).

2.10.7 Streptavidin pull down

All buffers were prepared freshly on the day of streptavidin pull-down experiments. Frozen cell pellets were thawed on ice and lysed with lysis buffer (8 M Urea, 100 mM sodium phosphate pH 8, 100 mM ammonium bicarbonate, 1% (w/v) SDS, 10 mM TCEP, 40 mM chloroacetamide and cOmplete, Mini, EDTA-free Protease Inhibitor Cocktail for 15 min. Lysates were sonicated on ice with three cycles for 30 s bursts with 2 s rest in between at 40% amplitude. For trichloroacetic acid (TCA) precipitation, an equal volume of 40% ice cold TCA was added and incubated for 1 h on ice. Precipitated proteins were centrifuged at 20.000 x g at 4°C for 10 min. Pellets were washed three times with 90% ice-cold acetone and air-dried. Afterwards, pellets were dissolved in resuspension buffer (8 M Urea, 100 mM sodium phosphate pH 8, 100 mM ammonium bicarbonate and 1% SDS) by shaking for 1 h at room temperature. Protein concentrations were quantified using the BCA Protein Assay Kit to adjust equal amounts of lysates. Per sample 15 µl of streptavidin-coupled dynabeads were washed three times with washing buffer (4M urea, 0.5 % (w/v) and 100 mM sodium phosphate pH 8). Protein lysates were diluted 1:2, mixed with streptavidin beads and gently rotated O/N at 4°C. Beads were separated and washed 5 times with washing buffer with SDS and 10 times without SDS.[111]

2.11 Mass spectrometric methods

2.11.1 Sample preparation

Streptavidin beads were resuspended in elution buffer (2 M urea, 200 mM EPPS pH 8.2, 8% (v/v) ACN). For on-bead digestion, 1 µg of LysC was added and incubated 2-3 h at 37°C. Samples were dilute 1:2.5 with 200 mM EPPS pH 8.2 and further digested with 0.4 µg Trypsin O/N at 37°C. Beads were separated and supernatant was transferred into a fresh tube. The amount of ACN was adjusted to 20% and peptides were incubated with

20 µg of Tandem Mass Tag (TMT) reagents for 1 h at room temperature. TMT-labeling reaction was quenched with addition of hydroxylamine to a final concentration of 0.5% (v/v) for 15 min at room temperature. Samples were pooled and dried using vacuum centrifugation (Thermo Fisher).

2.11.2 Sample purification

All buffers used for purification were LC-MS grade. Dry peptides were resuspended in 3% acetonitrile (ACN) and 5% formic acid (FA) and acidified with 50% FA. For purification, peptide samples were desalted using Empore C-18 Disk resin material. Material was activated by incubation with Methanol for 5 min, followed by one wash each with 50% ACN/5% formic acid (FA) and 3% ACN/5% FA. Samples were resuspended in 3% ACN/5% FA and loaded to resin material. Peptides were washed with 3% ACN/5% FA, eluted with 75% ACN/5% FA and dried. Samples were resuspendet in 80% isopropanol with 0.8% TFA and further purified using SDB-RPS clean-up.[112] Peptides were directly load onto membrane, followed by one wash with 1% TFA in isopropanol and a second wash with 0.2% TFA in water. Peptides were eluted with 80% ACN and 5% ammonia, dried and resuspended in 0.1% FA for LC-MS analysis.

2.11.3 Mass spectrometry (Q Exactive HF – Orbitrap)

Dried peptides were resuspended in 0.1% FA and separated on an easy nLC 1200 (Thermo Fisher) and a 22 cm long, 75 µm ID fused-silica column, which has been packed in house with 1.9 µm C18 particles (ReproSil-Pur, Dr. Maisch), and kept at 45°C using an integrated column oven (Sonation). Peptides were eluted by a non-linear gradient from 5-38% ACN over 120 minutes and directly sprayed into a QExactive HF mass-spectrometer equipped with a nanoFlex ion source (Thermo Fisher) at a spray voltage of 2.3 kV. Full scan MS spectra (350-1400 m/z) were acquired at a resolution of 120,000 at m/z 200, a maximum injection time of 100 ms and an AGC target value of 3×10^6. Up to 20 most intense peptides per full scan were isolated using a 1 Th window and fragmented using higher energy collisional dissociation (normalized collision energy of 35). MS/MS spectra were acquired with a resolution of 45,000 at m/z 200, a maximum injection time of 80 ms and an AGC target value of 1×10^5. Ions with charge states of 1 and > 6 as well as ions with unassigned charge states were not considered for

fragmentation. Dynamic exclusion was set to 20 s to minimize repeated sequencing of already acquired precursors.[113]

2.12 Computational analysis

2.12.1 Processing of raw files

Raw files were analyzed using Proteome Discoverer (PD) v2.4 software and database searches were run against trypsin-digested Homo sapiens SwissProt database (TaxID:9606, version 2020-03-12) and FASTA files of common contaminants (`contaminants.fasta` provided with MaxQuant) for quality control. Spectra were selected using default settings and database searches performed using SequestHT node. Static modifications were set as TMT6/11 (+229.1629) or TMTpro (+304.207) at the N-terminus as well as lysines and carbamidomethyl (+57.021464) at cysteine residues. Dynamic modifications were set as methionine oxidation (+15.995) and acetylation (+42.0106) at the N-terminus. Posterior error probabilities were calculated and PSMs filtered using Percolator default settings. The consensus workflow for reporter ion quantification was performed with default settings. Results were then exported to Microsoft Excel 2016 and proteins annotated based on MitoCarta3.0.[114] Statistical data analysis was performed using the peptide-based linear mixed models tool PBLMM-v2.2.0.[108]

2.12.2 Network analysis

Network analysis and visualization was performed with Cytoscape v3.7.1.[105] Functional enrichment analysis was carried out by Omics Visualizer[115] and ReactomeFI[116] cytoscape plugins. To generate a STRING based network, a high confidence score of 0.8 was chosen. The layout algorithm edge weighted spring embedded was applied on networks.[117] GO enrichment analysis of interactome data was performed by using DAVID. GO enrichments were visualized with the EnrichmentMap plug-in.[116]

2.12.3 Data analysis

Raw data were filtered and cutoffs were set for significantly (q value ≤ 0.01) and enriched ($\log_2 \geq 0.5$) hits. Data were uploaded on prohits-viz.org to generate correlation maps and dot plots.[109] For analysing GTBPB6 interactome data, z-score transformation was applied and clustering was performed using Mfuzz package for RStudio v3.6.2.[118]

The number of clusters was set to 3 and proteins were assigned based on cluster memebership 0.5. Circos plot was visualized with the circos table viewer v0.63-10.[104]

2.12.4 Statistical analysis

Protein quantifications were restricted to unique peptides and resulting p values were corrected using Benjamini-Hochberg FDR procedure.[119] Adjusted p values ≤ 0.01 were considered as significant.

2.12.5 Microscopy quantification

ImageJ v2.3.0 software was used to open and process microscopy images.[106] For the quantification analysis of MRG disassembly and reassembly dynamics, images were randomized and foci of about 50 cells per condition were counted using the custom-made in-house package for Python v3.9. The random Image labeler package is freely accessible via Github under (https://github.com/science64/Random-Image-Labeler). To measure RNA fluorescence intensities, I selected mitochondria and calculated the corrected total fluorescence intensity (CTFI).[18] Quantification of BrU intensities was performed for about 50 cells per condition and quantification of J2 intensities for about 100 cells per condition.

3 Results

3.1 The comprehensive MRG proteome at high-depth

MRGs have been emerged as crucial regulators of the mitochondrial gene expression. Dysregulation of mitochondrial RNA metabolism has been associated with various human diseases, including neurodegenerative and metabolic disorders as well as certain types of cancer.[120,54] However, our understanding of their composition, structure and dynamics as well as the identity of most proteins carrying out the required reactions within the MRGs remain elusive. Therefore, it is critical to expand our knowledge of MRGs and their role in mitochondrial biology. One important objective is to elucidate the MRG protein-protein network under homeostatic conditions. For this purpose, I used enzyme-catalyzed proximity labeling, coupled to quantitative, multiplexed proteomics. Proximity labeling is a cutting-edge technique and powerful approach to create comprehensive protein-protein interaction (PPI) maps. This technique is based on a biotin ligase tagged to the protein of interest to identify interacting proteins in close proximity. In this study, I employed the previously developed proximity labeling tool TurboID.[110]

TurboID is an engineered version of the *E. coli* biotin ligase BirA and was specifically designed to have a faster and higher labeling efficiency compared to other biotin ligases like BioID.[110] Additionally, unlike APEX, TurboID does not require the use of additional hydrogen peroxide and is thus less harmful to cells.[121] The labeling radius of TurboID has been estimated to 10 nm, allowing the identification of highly specific and local interactions. The enhanced efficiency and reduced background of TurboID makes it an excellent tool for studying spatial and temporal profiles of PPIs under biological conditions.[110]

To express human proteins associated with MRGs, I employed inducible HeLa FLp-In T-Rex cells as a cellular model. This cell model provides a controlled system that enables inducible gene expression of MRG-related proteins fused to the C-terminal TurboID tag at nearly endogenous levels. MRG proteins, utilized for PPI profiling in this study, are nuclear-encoded, translated within the cytosol and therefore have to be imported into mitochondria by a mitochondrial targeting sequence (MTS). To ensure accurate

mitochondrial import of the TurboID tagged constructs, I chose the longest isoform of the MRG fusion proteins, that includes an N-terminal MTS. Moreover, I incorporated an integrated FLAG tag to facilitate the identification and analysis of these constructs (Figure 9 A).

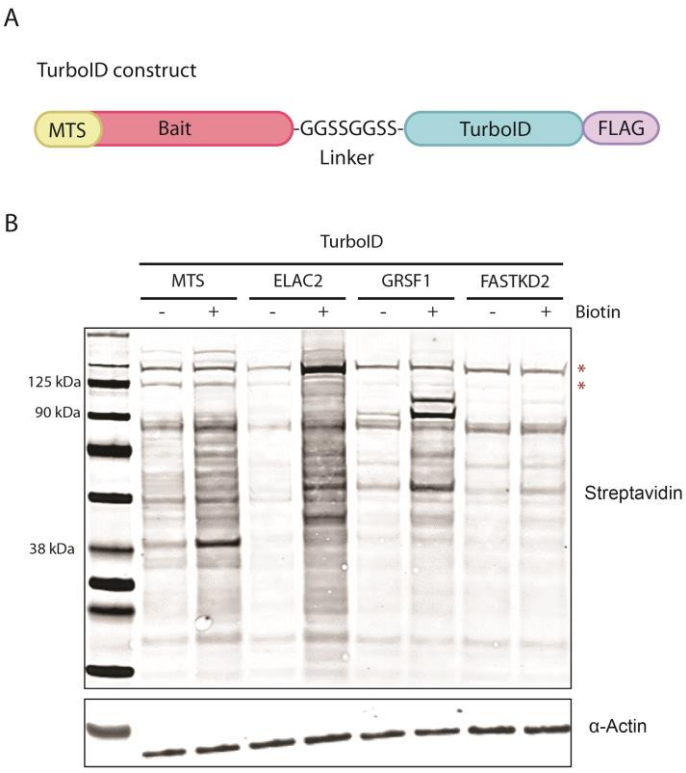

Figure 9: Biotinylation patterns of TurboID fusion proteins. (A) Schematic representation of the TurboID construct used in this study. Cloning was done with the longest isoform of the protein of interest (bait), including the mitochondrial targeting sequence (MTS). A glycine-serine linker was incorporated between the bait and the biotin ligase TurboID to ensure proper protein folding. A FLAG tag at the C-terminus allows the detection of TurboID constructs using an anti-FLAG antibody **(B)** Representative streptavidin western blot of TurboID fusion proteins. Inducible HeLa Flp-In T-Rex stably expressing TurboID constructs were cultured either without (-) or with 500 µM biotin (+) for 10 min at 37°C. Cell lysates were collected and biotinylation detected with streptavidin conjugated to IRDye fluorophore. Asterisks indicate naturally biotinylated carboxylases.

Each TurboID construct's expression was induced with doxycycline for 24 h prior to proximity labeling. To initiate the biotinylation reaction, cells were incubated in growth medium supplemented with biotin for 10 minutes at 37°C (Figure 10). Cells that were not treated with biotin were used as control. The efficiency and specificity of TurboID-mediated biotinylation were both tested by western blotting (Figure 9 B). Endogenous proteins in a close proximity (prey) to the protein of interest fused to TurboID (bait) were covalently biotinylated and thus selectively isolated by a streptavidin pulldown. The high

affinity between biotin and streptavidin enables capturing of even dynamic and transient interactions. Moreover, due to harsh and denaturing washing conditions during pulldown, unspecific binding was reduced. Subsequently, on beads-digestion with trypsin was performed and peptides were labeled with unique isobaric tandem mass tags (TMT), a quantitative method that allows simultaneous analysis of multiple samples. In this study, three biological replicates per condition were used for each TurboID bait, resulting in a total of 120 samples analyzed by quantitative multiplexed mass spectrometry, creating a comprehensive network of more than 1,700 PPIs (Figure 10).

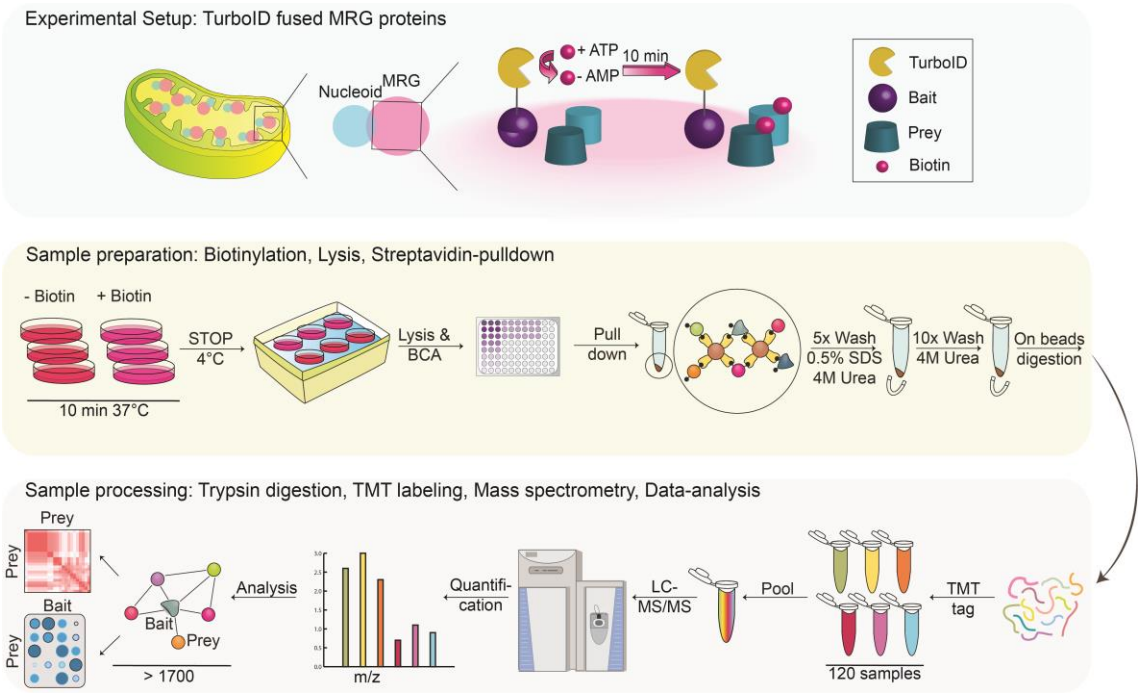

Figure 10: Experimental scheme of TurboID interaction proteomics. Proteins related to mitochondrial RNA granules (MRGs) were fused to a C-terminal TurboID tag in FLp-In T-Rex HeLa cells. Expression of the construct was induced by doxycycline for 24 h. Cell culture medium was supplemented either with or without biotin for 10 min at 37°C. Proteins in a close proximity (prey) to the protein of interest (bait) were covalently tagged with biotin. The reaction was stopped on ice and total protein concentrations of cell lysates were adjusted using a protein assay (BCA). Biotinylated proteins were captured by streptavidin pulldown and washed under harsh conditions with urea and SDS. On-beads digested peptides were multiplexed with tandem mass tag (TMT) reagents and subjected to LC-MS/MS. In total, 120 samples were quantified and over 1,700 protein-protein interactions were identified, creating a comprehensive network map of MRGs.

To conduct the initial TurboID experiments, I selected five candidates that had already been defined as *bona fide* MRG proteins. One of these well-studied MRG proteins is the RNA binding protein GRSF1, a key regulator of RNA metabolism and an excellent marker of MRGs for microscopy.[82] In addition, I analyzed two RNAse P subunits (MRPP1 and MRPP3) and two proteins of the FASTK family (FASTKD2 and FASTKD5) that are known to localize within MRGs, where they interact with GRSF1 to process mitochondrial precursor RNA.[82,88]

Among all five baits, (GRSF1, MRPP1, MRPP3, FASTKD2 and FASTKD5), GRSF1 was identified as a top interactor. Conversely, these candidates were cross-validated as highly ranked preys, demonstrating the sensitivity of this pulldown method. To expand the MRG protein network, I selected additional five proteins for PPI profiling based on the first interactome data. Among these five proteins, I chose RNMTL1, a methyltransferase, that has been found to accumulate in discrete foci adjacent to nucleoids.[61] In addition, I included MTPAP, an enzyme known for its role in mRNA polyadenylation and thus a relevant player in MRG biology, as previously documented.[86]

Interestingly, the PPI profiling data of the first 10 MRG candidates identified proteins associated with the mitochondrial DNA replication and transcription machinery. In particular, the well-established nucleoid components POLDIP2, SSBP1 and TWNK were detected. This observation is also in line with new findings that reported a strong interplay and active exchange between nucleoid and MRG proteins.[38,93]

An additional class of proteins, the GTPases GTPBP5,[75] GTPBP6[78] and GTPBP10[76,77] were strongly represented in the MRG proteome of this study. All three proteins have been characterized as mitochondrial ribosome assembly factors in humans.[75-78] GTPBP10 was reported to be part of the MRGs, where it facilitates proper maturation of the mtLSU.[76,77] However, it had not been shown by now whether GTPBP6 and GTPBP5 are part of MRGs. Later in this study, interactome profiling coupled with additional confocal microscopy analyses, confirmed GTPBP6 for the first time as a novel MRG protein (Figure 20, 21).

Building upon these preliminary insights into the MRG proteome from 10 distinct PPI datasets, I expanded the list of candidates for proximity labeling and included the

nucleoid proteins POLDIP2 and SSBP1, as well as proteins involved in mitochondrial ribosome assembly such as DDX28, ERAL1 and GTPBP10. This approach allowed me to create a more comprehensive and expansive MRG network. In total, I analyzed PPIs of 20 diverse MRG-related proteins tagged to TurboID, providing an understanding of how different aspects of gene expression are interconnected within the mitochondrial RNA metabolism system.

To create a network based on interaction data from STRING database, I conducted functional enrichment analyses of the 20 selected MRG baits.[115] The annotation based on known or predicted PPIs, resulted in a bait-bait network, that was subdivided into five, manually assigned functional categories as follows: 1. RNA processing, 2. RNA modification, 3. ribosome assembly (including the novel GTPases), 4. translation and 5. DNA replication (Figure 11 A).

Next, to gain a better understanding of the individual PPIs between MRG baits analyzed in this study, I employed a comprehensive circus plot (Figure 11 B). This circular layout provides an overall visual representation of the interactions among all 20 baits. Hereby, I was able to distinguish between outgoing interactions that represent connections from one bait to other proteins and incoming interactions that represent connections from other proteins to the bait. In this visualization, each interaction is depicted as a ribbon, with the width reflecting the strength between the baits. To enhance clarity, each bait obtained a unique filled color, while the outer unfilled segment was color-coded to indicate the five functional groups defined before (Figure 11 A).

By comparing the STRING based network, that displayed baits in clearly delimited sections (Figure 11 A), the circus plot based on my PPI profiling data (Figure 11 B) emphasized the complexity and high connectivity between these 20 MRG-related baits across diverse functional categories. Furthermore, this illustration led me differentiate between strong and weak baits. For instance, GRSF1 and MRPP1 were identified as strong baits, exhibiting a high number of outgoing interactions. Conversely, FASTK and IARS2 revealed fewer outgoing interactions, suggesting differences in affinities towards their respective interacting partners (Figure 11 B).

I further elaborated the functional association among selected MRG candidates and analyzed their interaction patterns to identify groups of baits that display similar interaction profiles. To represent the statistical relationships between baits in a correlation map, the Pearson correlation coefficient was calculated (Figure 11 C). The positive correlation between two baits indicates whether they tend to interact and show a similar pattern of interactions. Each row and column in the correlation matrix represents a specific bait and colors indicate the strengths of the relationship between baits. A high correlation coefficient near +1 indicates a strong positive relationship, suggesting that these baits capture similar sets of interacting proteins. On the contrary, a low correlation coefficient near -1 suggests a strong negative relationship, indicating that these baits capture distinct or non-overlapping protein sets.

I identified prominent patterns showing a strong correlation between the clusters of baits associated with RNA processing/modification and baits involved in the DNA replication machinery (Figure 11 C). This observation further supports the notion of a close proximity between MRGs and nucleoids, likely driven by their functional connection.[92] Furthermore, I found a partial off-diagonal correlation pattern between proteins involved in RNA metabolism and those participating in ribosome assembly (Figure 11 C). This correlation highlights distinct biological roles for certain MRG proteins within diverse functional categories.

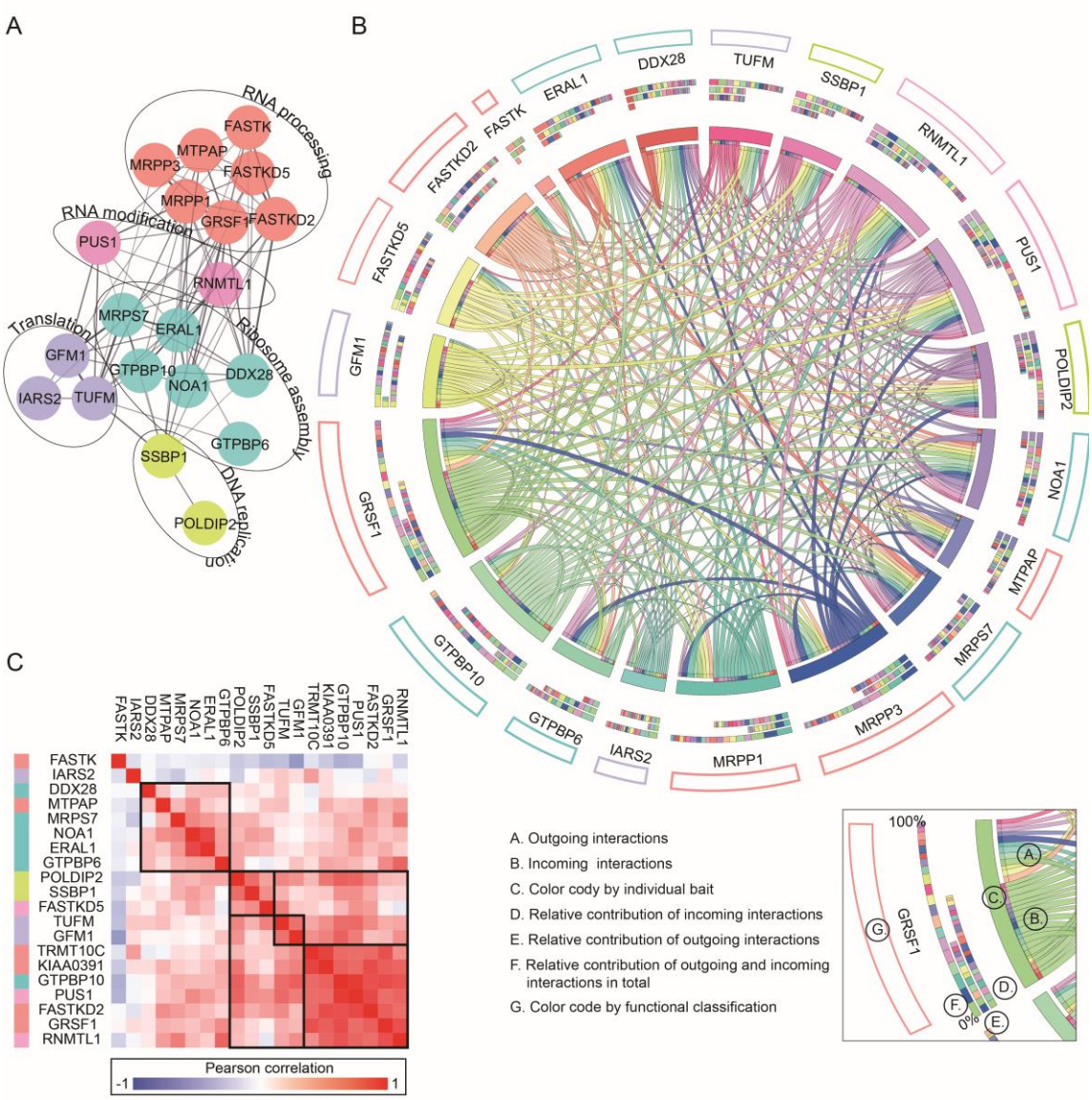

Figure 11: Establishment of a high-depth MRGs' protein network using proximity labeling mass spectrometry. (A) STRING based network analysis of 20 well selected MRG baits used in this study. Clusters were manually annotated to five different categories: RNA processing (red), RNA modification (pink), ribosome assembly (cyan), translation (violet) and DNA replication (green). **(B)** Circos plot of unidirectional connections between baits from section (A) based on TurboID profiling. Each bait obtained an individual filled color segment. Log_2 fold changes are displayed as ribbons, illustrating unidirectional connections between baits. Outer unfilled segments were color-coded by functional groups according to (A). **(C)** Hierarchically clustered correlation map of baits described in (A). Pearson correlation coefficient represents similarities of proteins. Red indicates high and blue low correlation. The color-coding of baits on the left corresponds to their functional groups, as shown in (A).

3.2 The complexity of MRGs' protein network architecture

To reveal the spatial organization of MRGs, I characterized the MRG proteome obtained from 20 TurboID baits. In total, the PPI profiling identified more than 1,700 cross validated and high-confidence interactions (FDR ≤ 1%, $\log_2$ fold change ≥ 0.5), resulting in a protein network characterized by high-depth and accuracy. For statistical analysis of the multi-bait PPI profiling data, the human MitoCarta3.0[114] was used for annotation of mitochondrial proteins and the peptide-based linear mixed model[108] for quantification.

Firstly, I performed a comparative analysis by integrating high-confidence PPIs with the STRING database,[115] considering interactions with a confidence score of 0.8. Secondly, I arranged these data by the spring embedded drawing algorithm[117] to create a more spatial and two-dimensional protein network. Thirdly, I applied a gene ontology (GO) term enrichment analysis to identify biological processes associated with these protein clusters (Figure 12 A).

This encompassing analysis revealed distinct functional groups, including RNA metabolism, translation and OXPHOS proteins, providing further evidence for the close proximity of the transcription and translation machinery to the inner mitochondrial membrane (Figure 12 A, B).[100] Strikingly, the majority of all connections were assigned to the GO term "translation", encompassing more than 40 different mitoribosomal subunits and their assembly factors (Figure 12 B). Interestingly, a considerable portion (~20%) of the identified connections was associated with the GO term "mitochondrial RNA metabolic processes" (Figure 12 B). These connections were enriched with genes involved in RNA processing, RNA modification, and DNA replication.

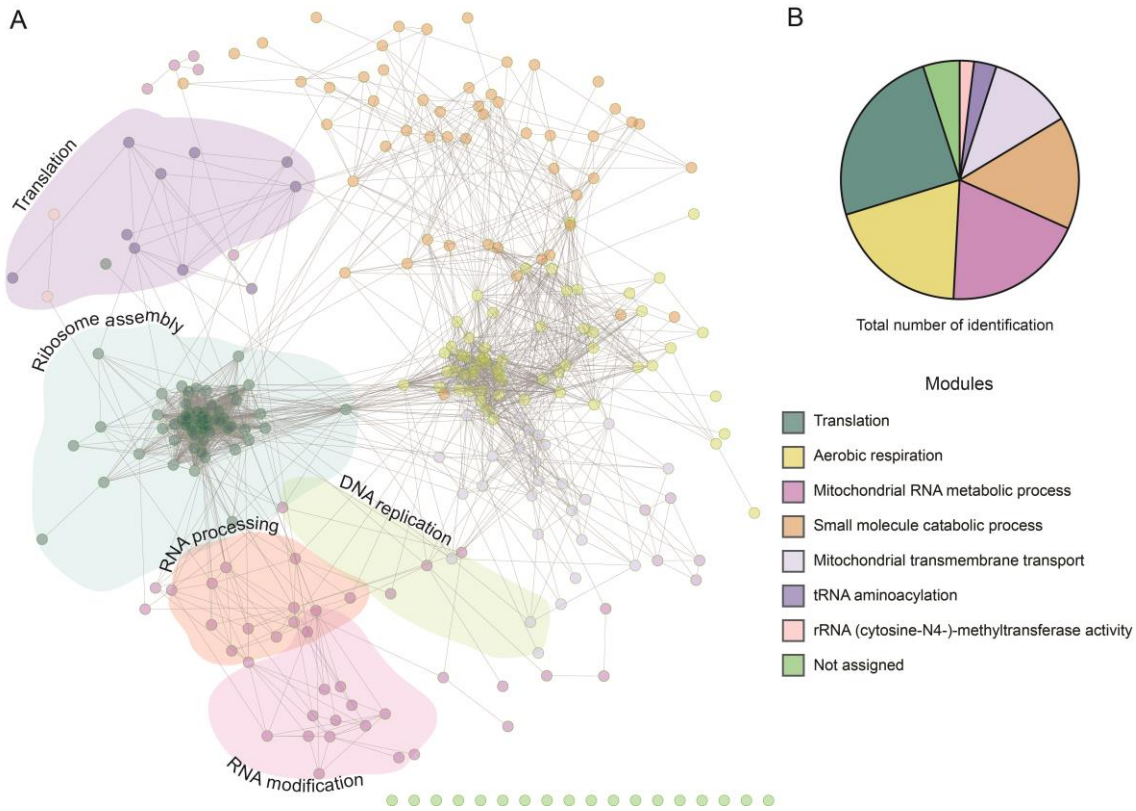

Figure 12: Functional network analysis of the MRG proteome. (A) Spatial network of TurboID profiling. Network is based on STRING database (confidence score 0.8) and arranged by the spring embedded drawing algorithm. GO term analysis showing clusters of significantly enriched proteins (log_2 fold change ≥ 2; FDR ≤ 0.01) identified by TurboID profiling. Preys are indicated as nodes and color-coded according to FI module function database. Clusters are color-coded according to functional categories (see Fig. 11 A). **(B)** Pie chart of modules based on the number of interactions found in (A).

To gain a comprehensive understanding of the MRG composition, I analyzed the correlation among all identified interactions (Figure 13). The pairwise comparison of high-confidence interactions across all MRG baits in a prey-prey matrix revealed four main clusters. Within the correlation map, I further investigated clusters of proteins with the same biotinylation pattern. Proteins sharing similar interaction patterns are likely to function together and co-localize. Cluster II displayed a striking pattern of highly correlated preys interacting with the same subset of baits (Figure 13). The GO term analysis of cluster II revealed a significant enrichment of proteins associated with "mitochondrial gene expression" ($P = 3.56 \times 10^{-68}$).

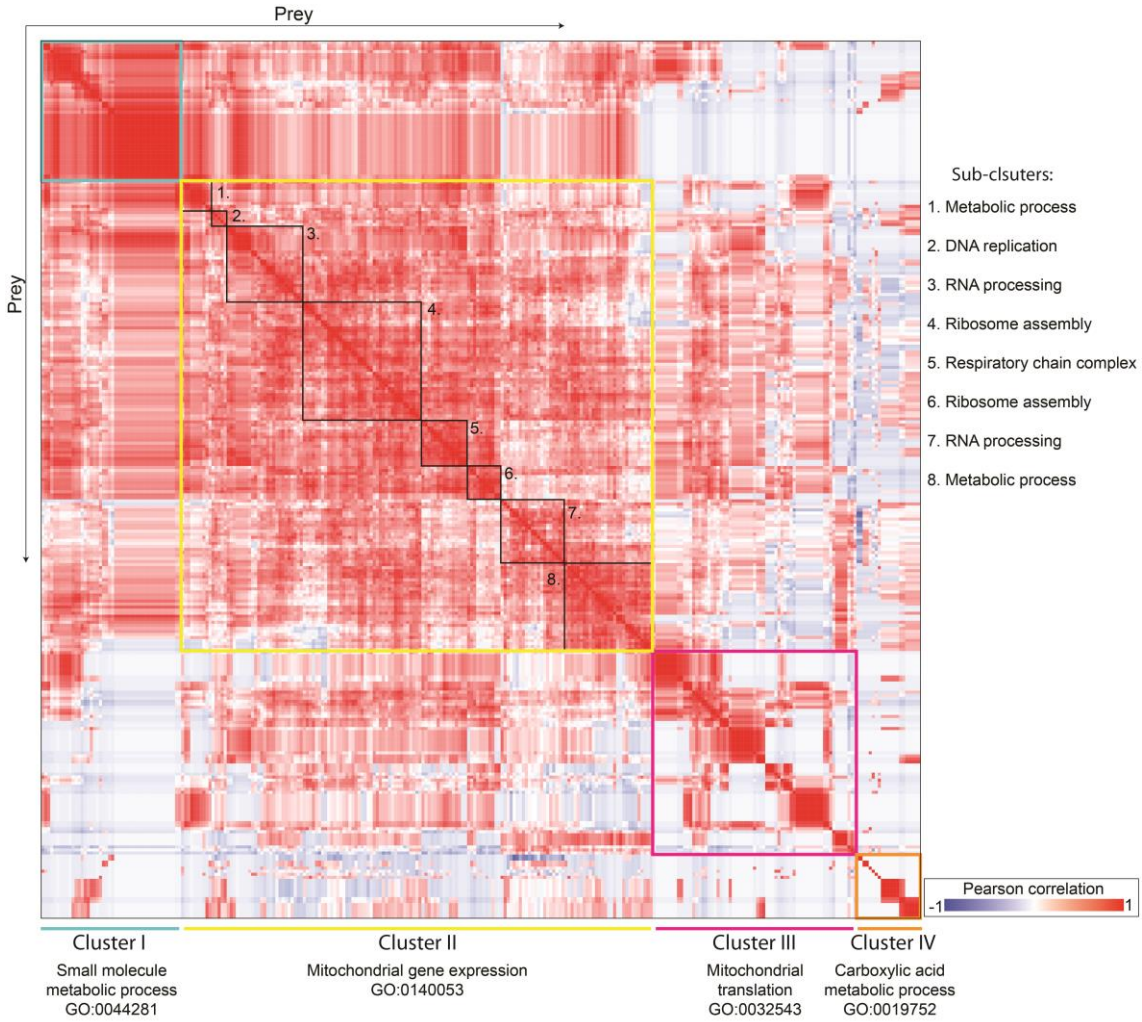

Figure 13: Interaction proteomics display the complex architecture of MRGs. Hierarchically clustered correlation map of all high-confidence hits (log_2 fold change ≥ 2; FDR ≤ 0.01) identified by TurboID profiling. Clusters are highlighted by colored boxes and annotated by gene ontology (GO) terms. Sub-clusters are highlighted by black rectangle and manually annotated according to functional categories. Pearson correlation coefficient represents similarities between proteins. Red indicates high and blue low similarities.

In a next step, proteins of cluster II were divided into different sub-clusters based on their functions, such as metabolic processes, RNA metabolism and ribosome assembly (Figure 13). For instance, sub-cluster 3. comprised well-known MRG proteins, such as GRSF1, MRPP3, and FASTKD2, that play significant roles in RNA processing within MRGs. Moreover, sub-cluster 3. included proteins involved in RNA modification, such as the methyltransferases NSUN3 and RNMTL1, emphasizing that proteins found in the MRG proteome have diverse functions related to multiple aspects of the RNA metabolism (Figure 14 A).

Interestingly, sub-cluster 4. and 6. of cluster II contained several subunits of the mitochondrial ribosome, alongside the two GTPases GTPBP10 and GTPBP5 (Figure 14 B). Notably, various other parts of the mitochondrial ribosome and numerous ribosome assembly factors including ERAL1, NOA1, DDX28, DHX30 and GTPBP6 were identified within cluster III (GO term "mitochondrial translation", $P = 3.759 \times 10^{-43}$; Figure 15). Although the mitochondrial protein translation has been found to clearly occur separately from MRGs at the cristae membrane, it still remains unclear whether only certain components of the ribosome assembly or the entire assembly machinery takes place within MRGs or in a separate entity adjacent to MRGs.[122]

The correlation between cluster II and III indicated a putative association of some proteins for different structures, emphasizing the sub-structural complexity of MRGs (Figure 13). The dual localization of proteins from cluster II and III suggests a potential compartmentalization or functional specialization in mitochondrial ribosome maturation within MRGs. To conclude, the in-depth examination of the MRG network showed additional evidence that certain parts of the mitochondrial ribosome are localized within MRGs, while other components of the ribosome assembly machinery appear to be distinctly separated. Further investigations are needed to determine the extent to which part of mitochondrial ribosome maturation takes place within MRGs.

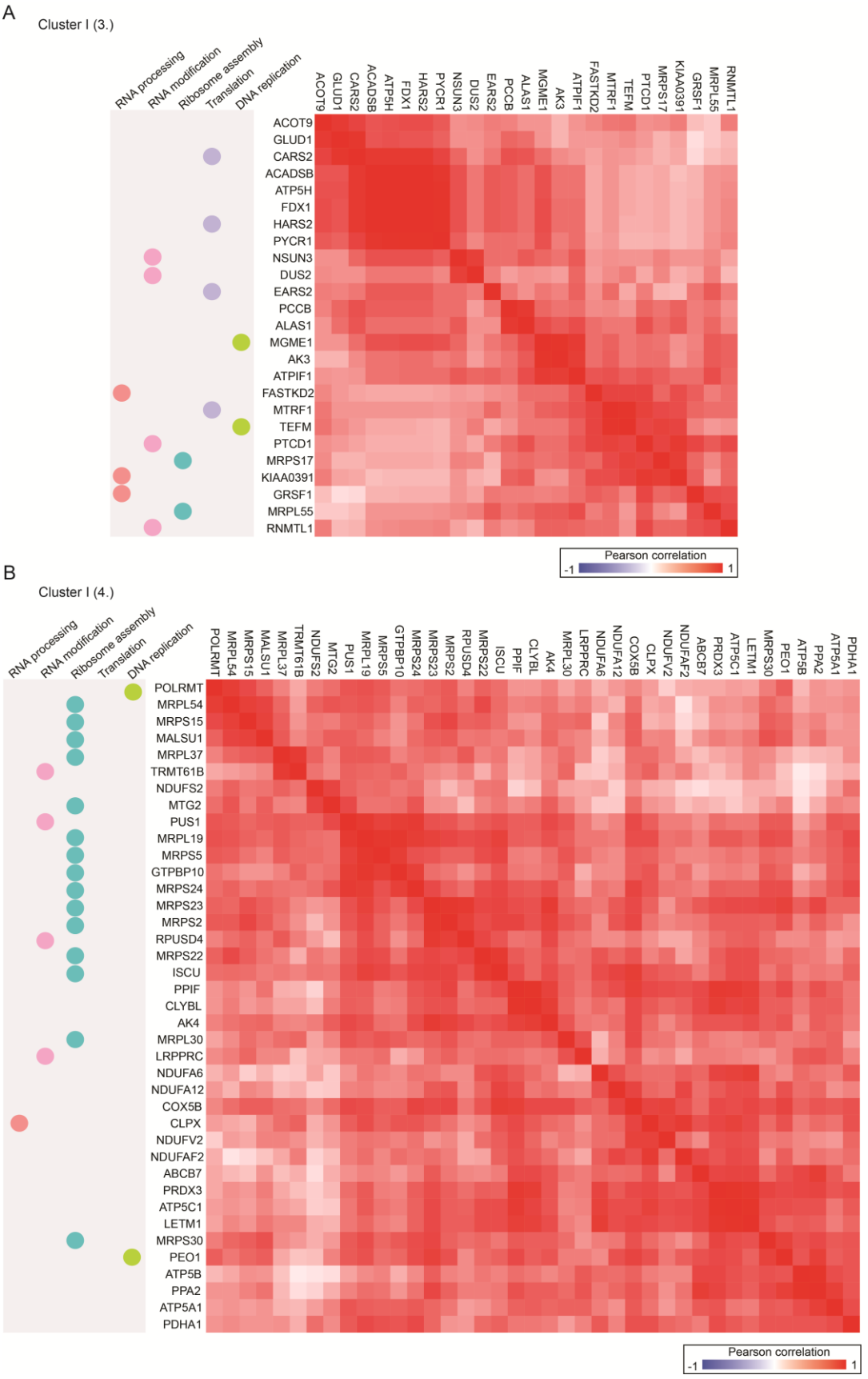

Figure 14: Hierarchically clustered correlation map of MRG proteome sub-clusters II 3. and 4. Enlarged view of **(A)** Sub-cluster 3. RNA processing and **(B)** sub-cluster 4. ribosome assembly (see. Figure 13). Nodes are color-coded based on functional categories. Pearson correlation coefficient represents similarities between proteins. Red indicates high and blue low similarities.

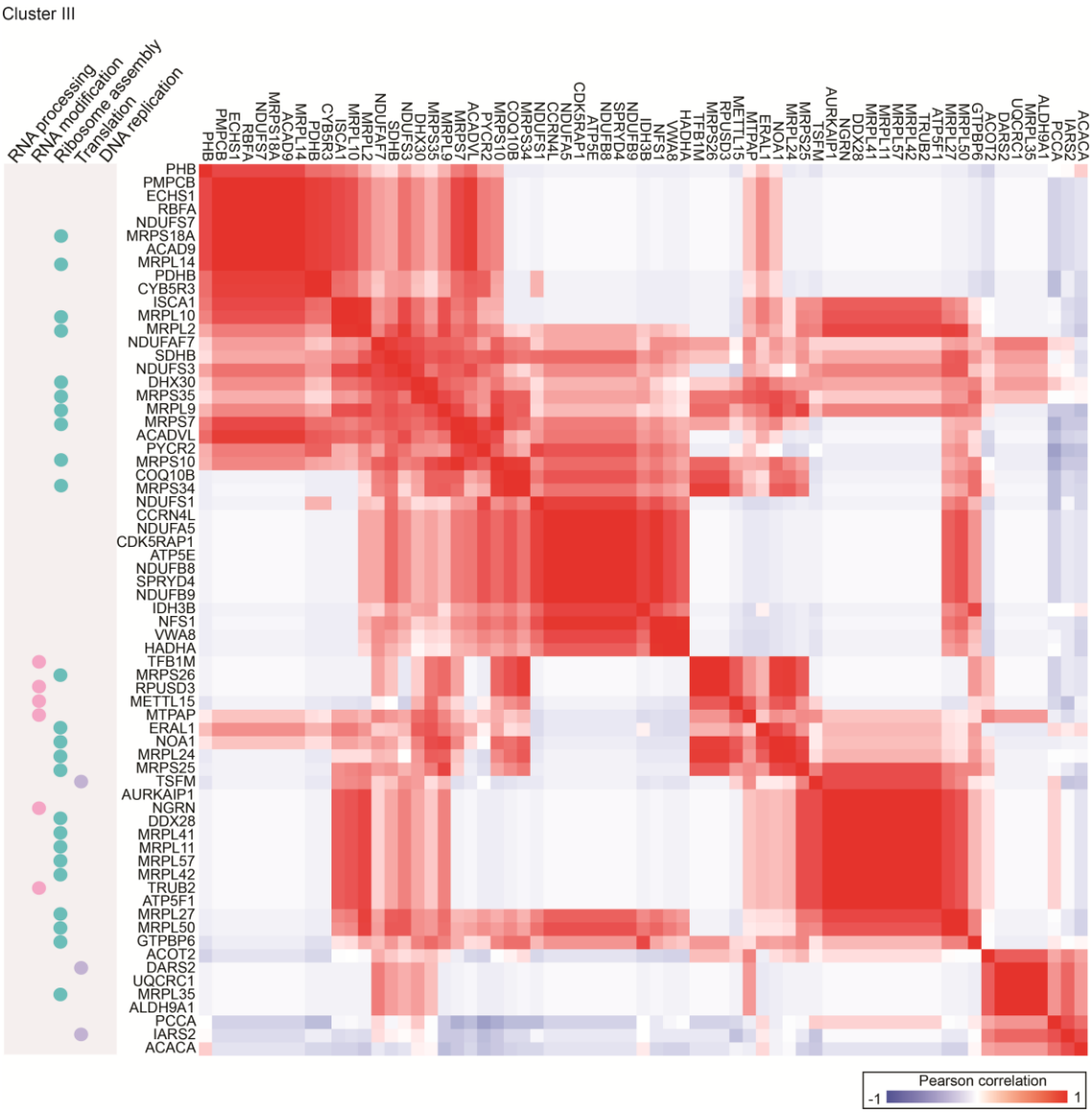

Figure 15: Hierarchically clustered correlation map of MRG proteome cluster III. Enlarged view of cluster III "mitochondrial translation" (see. Figure 13). Nodes are color-coded based on functional categories. Pearson correlation coefficient represents similarities between proteins. Red indicates high and blue low similarities.

3.3 The MRG core reveals a dense network comprised of RNA metabolism proteins

Following these extensive overall network analyses, I sought to define proteins of the MRG core structure. Therefore, I examined highly connected proteins derived from the comprehensive STRING based analysis (Figure 12 A) to identify essential components and gain a deeper understanding of the MRG architecture. I thus focused on the substantial proportion of interactions that was attributed to proteins involved in "RNA

metabolic processes" that included well-known MRG components (*e.g.,* GRSF1, MRPP3 and FASTKD2). This cluster comprised proteins manually assigned into four functional categories: 1. RNA processing, 2. RNA modification, 3. ribosome assembly and 4. DNA replication (Figure 16 A). Notably, the functional category "translation" was not found in this cluster. These findings were in keeping with the idea that MRGs' RNA metabolism is tightly connected with the replication machinery on one side and the ribosome maturation machinery on the other side.

In the next step, my primary objective was to pinpoint hub proteins within the MRG network, to define the MRG protein core. Therefore, I conducted a prey-bait network analysis, illustrated as a dot plot (Figure 16 B). Each dot on this plot displays one high-confidence prey per bait, with the position and size of the dots representing the abundance. The larger dots found in the top quadrant represent highly abundant and specific interactors, implying strong functional relationships between these MRG candidates. An enlarged and more detailed overview along with an ordered summary of the identified functional categories from this dot plot, are provided in the supplement (Figure S 2, S 3).

I observed a subset of highly cross-validated preys, that were identified by 11 or more baits, revealing a dense section of MRG proteins (Figure 16). To further elaborate PPIs found within this dense core, I created an interaction network limited to the top preys (Figure 16 C). This network comprised multiple proteins involved in RNA processing, including GRSF1, MRPP1, MRPP2 and FATSKD2, as well as proteins associated with RNA modification such as PUS1 and PTCD1. Interestingly, within the core network, there was only one ribosome assembly factor (GTPBP10) and a few mitoribosomal subunits, indicating that ribosome maturation does not occur in the MRG core. Furthermore, proteins directly participating in mitoribosome maturation, like MALSU1, DHX30 and DDX28 appeared in a separate section on the dot plot (Figure S 2).

In conclusion, these systematic proteome profiling data provided novel insights into the MRGs structure and complexity of MRGs at high-depth. While many steps of the mitoribosome maturation seems to be tightly connected with RNA processing, most ribosome assembly factors were not found to be part of the MRG protein core.

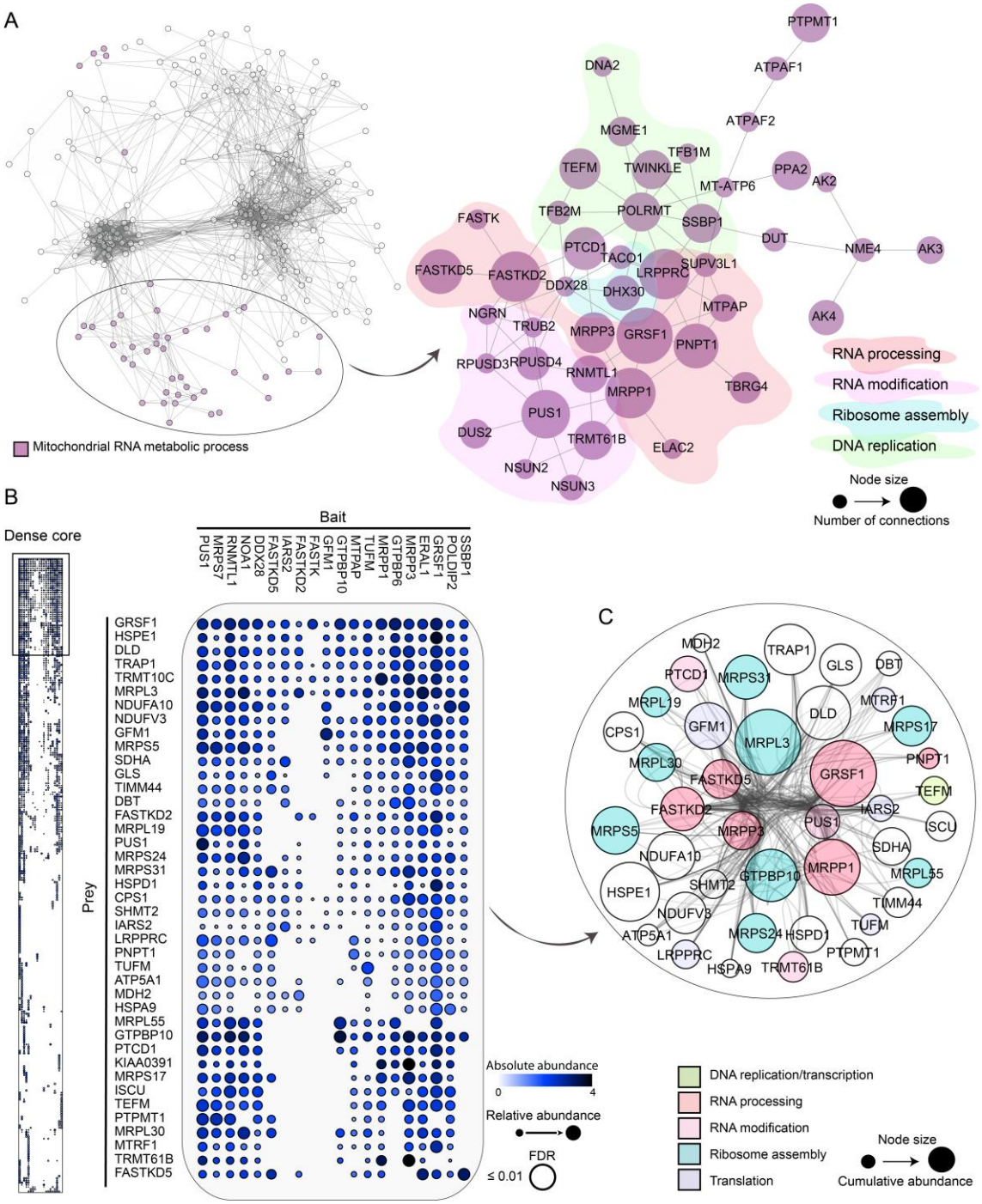

Figure 16: Characterization of the MRG core reveals a dense network comprising proteins of RNA metabolism. (A) Enlarged view of the GO term "mitochondrial RNA metabolic process" derived from STRING network (see Figure 12 A). Clusters are color-coded according to functional categories. **(B)** Dot plot visualization of all significantly enriched (log_2 fold change ≥ 2; FDR ≤ 0.01) preys across 20 TurboID baits (left). Node size represents relative enrichment, light blue indicates low and dark blue high log_2 values. The upper dense part restricted to the top quarter is enlarged on the right, displaying the top hits. **(C)** Interaction sub-network restricted to the top hits (B) showing the MRG core. Node size corresponds to total log_2 fold changes across all baits. Proteins are color-coded according to functional categories.

3.4 MRGs are highly dynamic during stress

After elucidating the MRG (sub)architecture at basal conditions, my next focus was to investigate the impact of mitochondrial stresses on MRGs and characterize their dynamics upon disassembly and reassembly. To study these physical properties of MRGs, I characterized different mitochondrial stresses and identified conditions upon which MRGs disassemble and subsequently recover. For this purpose, I generated a stable HeLa Flp-In T-Rex cell line expressing GRSF1 fused to EGFP to visualize and monitor MRGs' morphology using confocal fluorescence microscopy (Figure 17 A).

Pioneering work by Antonicka et al.[83] and Jordain et al.[123] has provided initial insights, demonstrating that stress induction with the well-known transcription inhibitors actinomycin D (ActD)[124] and ethidium bromide (EtBr),[124] resulted in complete loss of MRG foci within mitochondria. Both inhibitors are widely recognized for their ability to block RNA polymerases, leading to effective inhibition of transcription.[125] These promising results have prompted me to use ActD and EtBr and investigate these treatments more closely. I was able to observe the same effect and found completely dissolved MRGs within 1 h of stress induction (Figure 17 C)

Subsequently, I tested other stressors specifically targeting mitochondria. Interestingly, in contrast, mitochondrial depolarization induced by CCCP[126] or inhibition of mitochondrial DNA replication by vitamin K3[127] did not affect their integrity and MRGs remained intact (Figure 17 C). Similarly, erythromycin[128] and rifampicin,[129] that are known to promote bacterial ribosome stalling[128] and inhibit mitochondrial transcription,[129] respectively, showed no impact on the MRG morphology (Figure 17 C). These findings demonstrated MRGs' robustness towards a range of mitochondrial stresses (Figure 17 B).

Previous research has also reported that depletion of essential MRG proteins including GRSF1, DHX30, DDX28, FASTKD2 and FASTKD5 does not affect the morphology of MRGs.[87] These results, along with my observations, showed that MRGs are more stable than previously thought and only disassemble when RNA production is impaired, supporting the hypothesis that the integrity of MRGs is primarily driven by RNA-dependent, rather than protein-dependent, properties.[91]

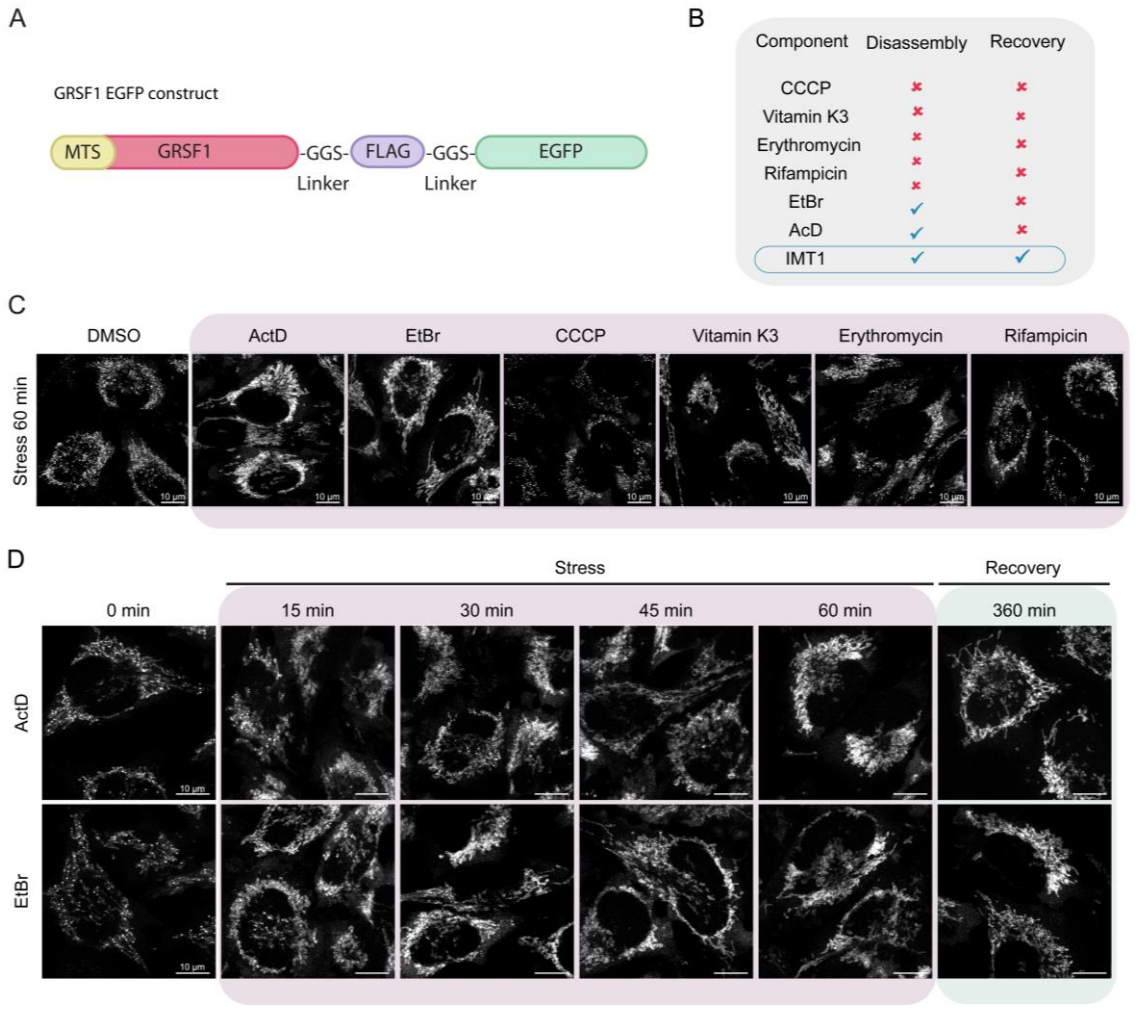

Figure 17: Characterization of MRGs' morphology upon diverse mitochondrial stresses. (**A**) Schematic representation of the GRSF1-EGFP fusion construct used in this study. Cloning was done with isoform 1 of GRSF1 including the mitochondrial targeting sequence (MTS). Glycine-serine linkers were incorporated to ensure proper protein folding. A FLAG tag enables its detection with an anti-FLAG antibody, facilitating the identification and analysis of the construct. (**B**) Summary table of components tested in this study to induce mitochondrial stress. MRGs disassembly and reassembly is indicated with a tick for successful or a cross for not successful. (**C**) Representative confocal images of MRGs upon different mitochondrial stresses. HeLa Flp-In T-Rex stably expressing GRSF1-EGFP were treated with ActD (3 mM), EtBr (3 mg/ml), CCCP (10 µM), vitamin K3 (50 µM), erythromycin (300 µg/ml) or rifampicin (300 µg/ml) for 60 min. Cells were fixed with 4% paraformaldehyde solution in PBS and imaged on a Leica TCS-SP8 inverted spectral confocal microscope. Lens x60; scale bar 10 µM. (**D**) Representative confocal images showing MRG time-dependent dynamics. Experiment was conducted as in (C) and cells were treated with of ActD (3 mM) or EtBr (3 mg/ml). Treatments were removed after 1 h and recovery was tested for 6 h. Cells were fixed with 4% paraformaldehyde solution in PBS and imaged on a Leica TCS-SP8 inverted spectral confocal microscope. Lens x60; scale bar 10 µM.

In a next step, I tested whether MRGs have sufficient recovery capacity and can reassemble when stress exposure was stopped. Thus, cells were treated either with ActD or EtBr for 1 h to ensure complete disassembly of MRGs and further cultured for up to 6 h in fresh medium without inhibitors to facilitate their recovery. However, even after 6 h of recovery, I could not observe any reassembly of MRGs (Figure 17 D). Notably, ActD has a weak reversibility[125] and both components intercalate into the DNA double helix, disrupting its structure and function, thereby causing side effects on the cell.[125,130]

These initial findings showed that transcription, particularly the production of RNAs, plays a central role in MRG formation. To further investigate this hypothesis, I therefore tested IMT1, the first-in-class-specific inhibitor of the mitochondrial transcription that was discovered in 2020.[131] In contrast to the previously used general DNA intercalating reagents ActD and EtBr,[125] IMT1 was identified as being a non-competitive inhibitor that selectively targets the mitochondrial DNA-directed RNA polymerase POLRMT1, resulting in a specific and fast reduction of mitochondrial transcript levels ranging from 37 min to 321 min.[132] I tested this effect of IMT1 on a selection of mitochondrial mature and precursor RNAs, using quantitative real-time polymerase chain reaction (RT-qPCR). To ensure accurate detection of precursor RNAs and differentiation from processed and mature RNA transcripts, I utilized custom-designed primers spanning junction regions[103] (Figure 18 A).

Depending on the RNA half-life,[131] transcripts displayed different degrees of reduction, with pre-RNA transcripts showing a faster decrease (Figure 18 B). As reported before,[131] treatments with IMT1 also led to reduced levels of mitoribosomal proteins, indicating its impact on mitochondrial protein synthesis. However, IMT1 did not affect the cytosolic ribosomal proteins even after 24 h.[131] This selective effect of IMT1 allowed me to study the role of RNAs in MRGs' assembly without affecting the cytosolic protein synthesis of MRG proteins.

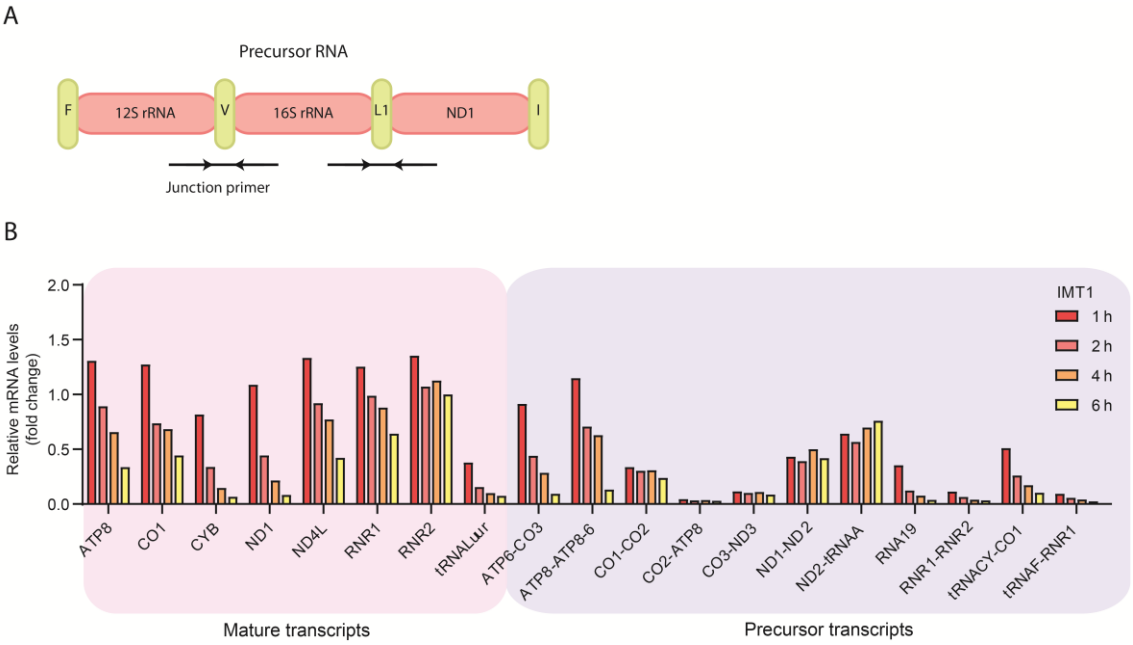

Figure 18: IMT1 treatment leads to reduced mitochondrial transcript levels. (A) Schematic representation of junction primer design to detect mitochondrial precursor transcripts. Transcription of the mitochondrial genome produces long polycistronic precursor RNAs that contain genes encoding for rRNAs and mRNAs (red). These genes are flanked by tRNAs (yellow) that facilitate subsequent processing events to generate mature RNA. **(B)** Mitochondrial transcript levels upon IMT1-induced stress. Cells were treated with IMT1 (5 µM) at indicated time points, followed by RNA isolation. Transcript levels were measured with RT–qPCR and normalized to GAPDH. N = 1 biological replicate.

In order to demonstrate that MRGs are highly dependent on mitochondrial pre-RNA, I aimed to investigate the correlation between MRG proteins and RNA during IMT1-induced stress. To achieve this, I employed labeling of newly synthesized RNA with the uridine analogue 5-bromouridine (BrU). BrU labeling is a well-established approach[81,82,83] that has been previously used to study mitochondrial transcription rates.[81] To co-stain MRGs with RNA, cells expressing GRSF1-EGFP were cultured in medium supplemented with BrU for 1 h prior to IMT1 treatments for indicated time points (Figure 19 A). Subsequently, the labeled nascent RNA was detected using immunostaining with an anti-BrU antibody, resulting in fluorescent signals that manifest as distinct foci within mitochondria.

In absence of stress, GRSF1 typically forms an average of approximately 130 distinct foci per cell. Yet, when compared to the DMSO control, cells treated with IMT1, here referred to as MRG stress, showed a significant reduction in the number of MRG foci and RNA intensities within just 15 min (Figure 19 B, D). Similar to treatments with ActD

and EtBr, transcription inhibition with IMT1 resulted in rapid disassembly of MRGs. The majority of MRGs were completely dissolved within an interval of 45 min and 60 min (Figure 19 B, D). Complete loss of GRSF1 foci was accompanied by significantly reduced RNA signals. (Figure 19 B, E)

These results encouraged me to investigate the dynamic properties of MRGs and their ability to recover from stress-induced disassembly, when transcription is restored. To address this, I removed IMT1 after 1 h of treatment and monitored MRGs during a recovery period of 2 h, 4 h or 6 h (Figure 19 A). Long-time intervals were chosen to ensure full recovery of RNA transcription. After 2 h of recovery, a small population of cells was capable to reform MRGs and only a weak BrU-RNA signal was detected (Figure 19 C-E). However, the majority of cells showed no distinct MRGs. Over time, the number of cells with intact MRGs increased and reached basal levels after 4 h of recovery (Figure 19 C, D). Consistent with the hypothesis that RNA forms a scaffold for MRGs, similar kinetics between MRGs and mitochondrial pre-RNA upon IMT1 treatment were observed.

Interestingly, after 6 h of recovery, I quantified significantly higher MRG numbers and increased RNA intensities compared to the DMSO control, suggesting an overcompensation of transcriptional feedback (Figure 19 C-E). These findings highlight the fast response of MRGs to mitochondrial transcription inhibition with IMT1, further emphasizing the critical role of pre-RNA production for their assembly.

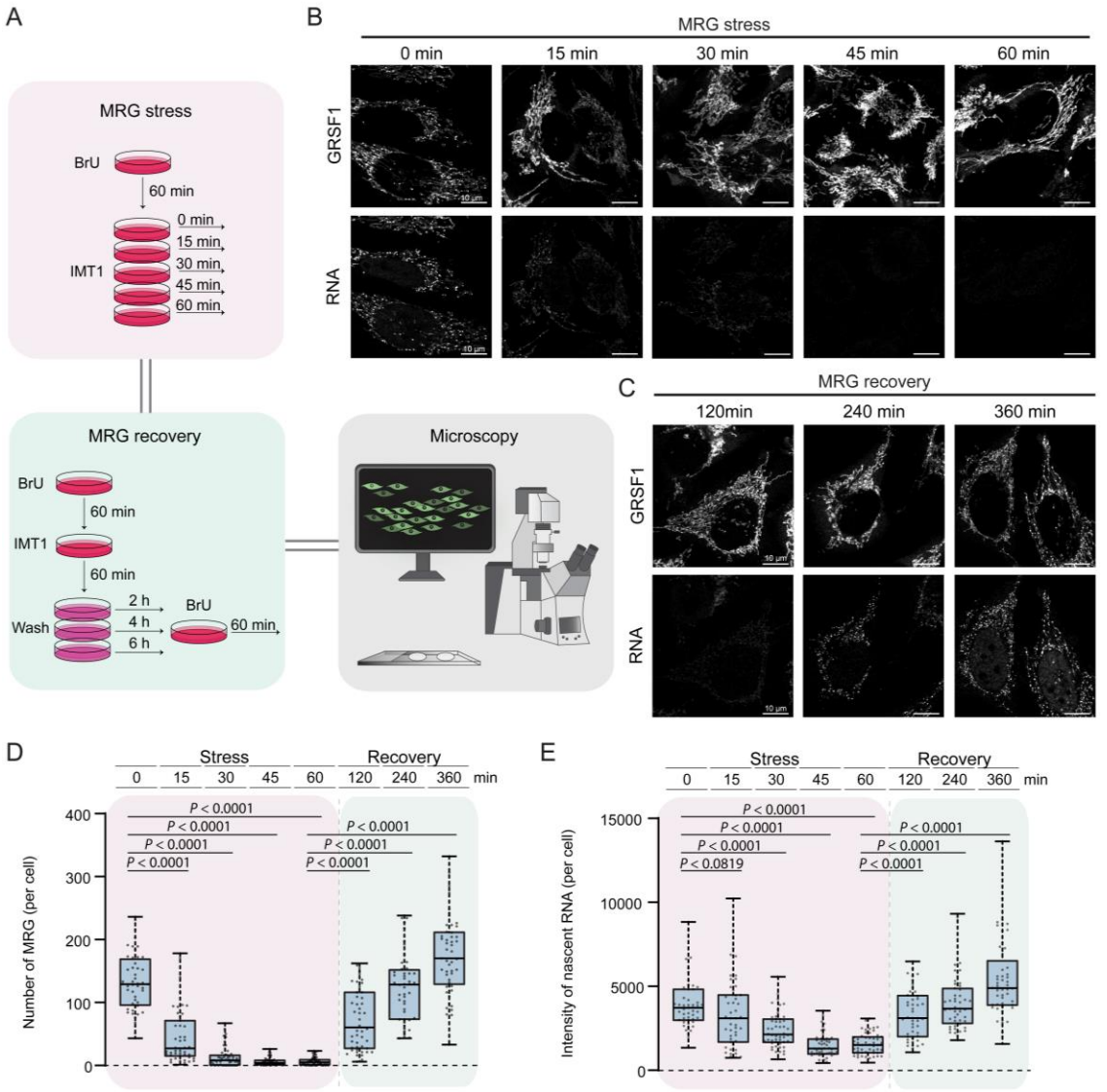

Figure 19: Time-resolved analysis upon stress demonstrates that MRGs are highly dynamic entities. (A) Schematic overview of the experimental design. MRG stress (pink box) induction is depicted at the top, followed by recovery (green box) at the bottom. Both experiments were analyzed using confocal fluorescence microscopy (grey box). **(B)** Representative confocal images showing MRGs (top) and RNA (bottom) during MRG stress. Cells were labeled with BrU for 1 h and treated with IMT1 (5 µM) for indicated time points. Cells were fixed with 4% paraformaldehyde solution in PBS. Nascent RNA was immunostained with anti-BrU antibody and imaged on a Leica TCS-SP8 inverted spectral confocal microscope. Lens x60; scale bar 10 µM. **(C)** Representative confocal images showing MRGs (top) and RNA (bottom) during MRG recovery. Experiment was conducted as in (B) and cells recovered for indicated time points. Cells were prepared as in (B) and imaged on a Leica TCS-SP8 inverted spectral confocal microscope. Lens x60; scale bar 10 µM. Box plots showing quantification of about 50 cells per condition from (B) and (C) displaying **(D)** MRG numbers and **(E)** RNA intensities. For significance a two-tailed unpaired t-test was applied.

This time-resolved microscopy demonstrated that recovery of granule formation occurred when mitochondrial RNA transcription was restored. Both MRGs and nascent RNA showed the same dynamics, highlighting their functional interplay. These results provide compelling evidence of MRGs' functional dependence on mitochondrial pre-RNA transcripts, emphasizing their critical role in MRG formation.

Next, I was interested to acquire a deeper understanding of MRG compositional changes upon disassembly and reassembly. Previous proximity profiling conducted in this study revealed GTPBP6 as a novel MRG protein forming distinct foci within mitochondria (Figure 20). Notably, GTPBP6 has recently been described as a mitochondrial protein with a dual function in ribosome assembly and ribosome recycling under stress conditions.[78] Here, I used interaction proteomics of this novel MRG protein GTPBP6 to study spatio-temporal effects on MRGs upon IMT1 treatment and subsequent recovery.

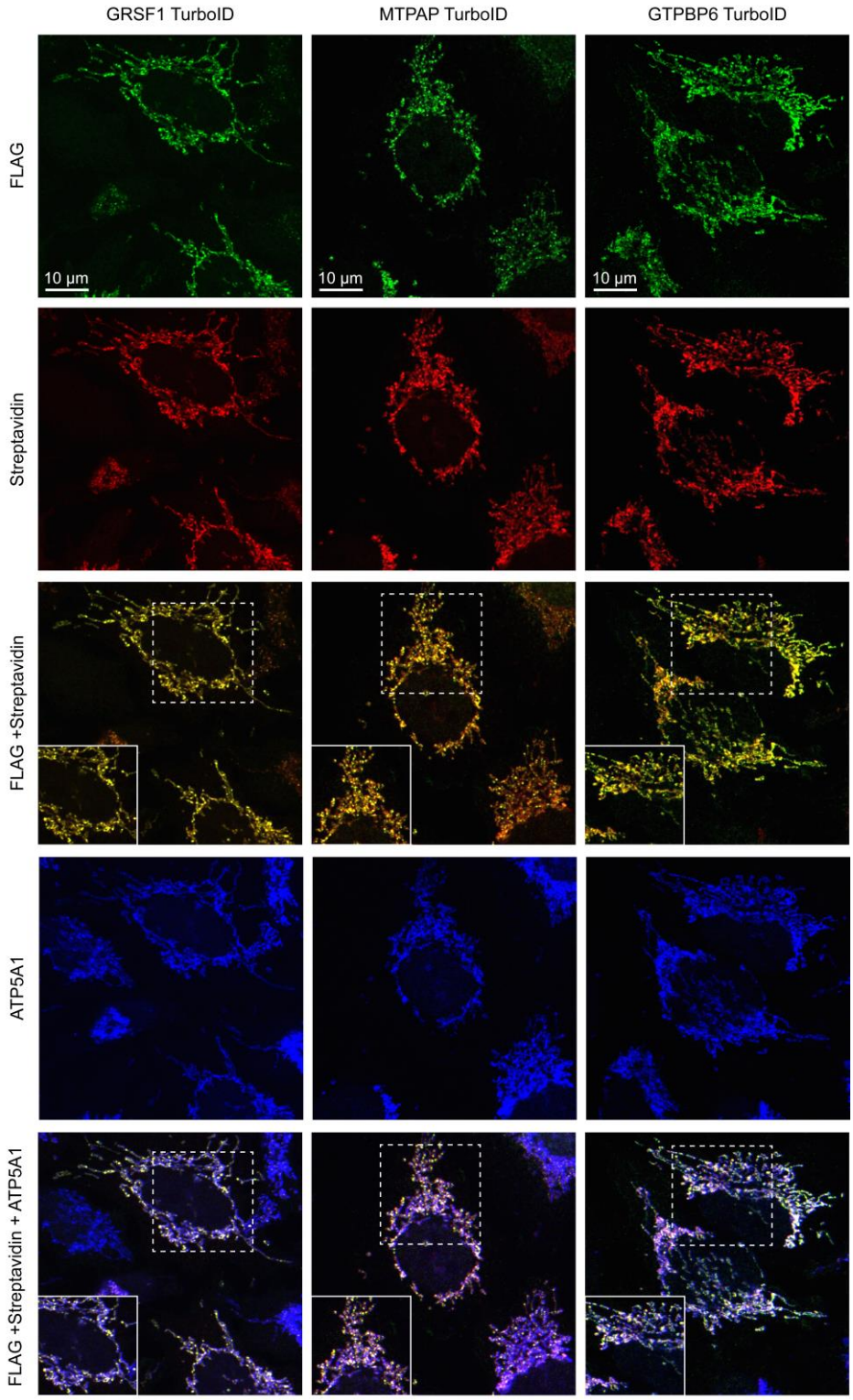

Figure 20: TurboID fusion proteins accumulate in discrete foci within mitochondria. Confocal images of HeLa Flp-In T-Rex cells stably expressing FLAG tagged TurboID fusion GRSF1, MTPAP or GTPBP6, cultured with biotin (500µM). Constructs were detected with anti-FLAG antibody (green). Streptavidin conjugated to Alexa 594 was used to visualize biotinylation (red) and anti-ATP5A1 antibody for mitochondrial (blue) co-staining. Images were obtained on a Leica TCS-SP8 inverted spectral confocal microscope. Lens x60; scale bar 10 µM.

To ensure complete disassembly of the MRG PPI network, I increased the IMT1 treatment time up to 6 h (Figure 21 A). After 6 h stress induction, GTPBP6 displayed significantly reduced PPIs with most MRG components, such as the RNA processing factors GRSF1, FASTKD2, FASTKD5 and MRPP1. Conversely, interactions with the ribosome assembly and translation machinery, including DDX28, ERAL1 and TUFM, increased (Figure 21 B).

During the recovery phase, diminished interactions with the MRG proteins (GRSF1, FASTKD2, FASTKD5 and MRPP1) were gradually restored (Figure 21 C, D). To group proteins with similar interaction kinetics, I employed the fuzzy c-means algorithm (MFuzz), a variation of the classical k-means clustering.[118] MFuzz allows greater flexibility and enables proteins to be assigned not only exclusively to one cluster but also to multiple clusters simultaneously, leading to more biological and accurate results. By utilizing this algorithm, the time-resolved PPI profiling data of GTPBP6 revealed three distinct clusters (Figure 21 C, D).

Cluster I displayed slightly different kinetics during recovery phase compared to cluster II, yet both demonstrated recovery of MRGs from stress after 6 h (Figure 21 C, D). Strikingly, cluster I showed a rapid recovery of MRG core proteins, including GRSF1, FASTKD2, MRPP1, and GTPBP10, that were the first to interact with GTPBP6 again, within 2 h of recovery (Figure 21 D, S 6). Interestingly, several proteins assigned to cluster III are involved in ribosome assembly and translation, including ERAL1, LRPPRC, TUFM and GFM1, demonstrating a reverse trend, as their interactions with GTPBP6 increased after 6 h of stress (Figure 21 C, D). For a more detailed and precise view, GTPBP6 PPIs were represented as a protein network, where only the high-confidence interactions are depicted to draw a direct comparison of compositional changes between these three conditions: basal, stress and recovery (Figure 22).

Overall, these findings are in keeping with the idea that certain MRG components have the ability to translocate to another substructure or entity when RNA transcription is paused, being part of a dynamic and adaptive response to stress.

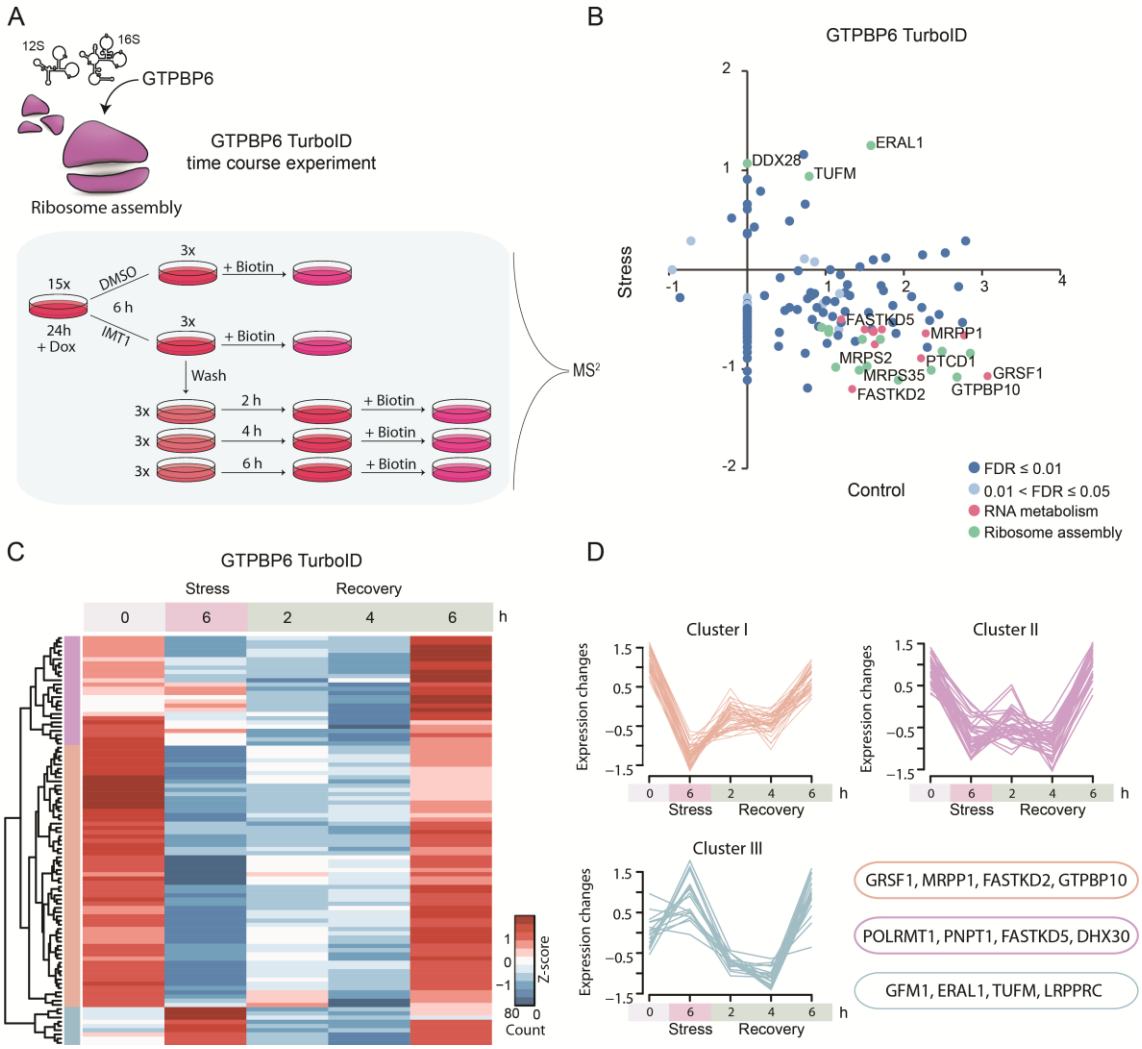

Figure 21: Spatio-temporal analysis of GTPBP6 TurboID reveals compositional changes of MRGs during disassembly and reassembly. (A) Schematic overview of the experimental design. HeLa Flp-In T-Rex cells stably expressing GTPBP6 fused to TurboID were treated with IMT1 (5 µM) for 6 h and recovered for indicated time points before biotinylation. Sample preparation was conducted as in (Fig. 10). **(B)** Scatterplot of GTPBP6 TurboID showing high-confidence preys upon 6 h MRG stress. Preys assigned to RNA processing/modification are displayed in pink and preys assigned to ribosome assembly are shown in green. Interactions with FDR between 0.01 and 0.05 are indicated in light blue and FDR ≤ 0.01 are indicated in dark blue. **(C)** Heatmap of GTPBP6 interactions upon MRG stress and recovery at indicated time points. Protein interactions are represented as z-scores. Only proteins that were previously found in the interactome data of GTPBP6 are shown. **(D)** MFuzz clustering analysis of GTPBP6 TurboID data reveals three distinct gene clusters sharing the same dynamics upon stress and recovery. Cluster I is associated with MRG core proteins and shows a fast recovery. Cluster II is associated with MRG proteins involved in multiple aspects of RNA metabolism and ribosome assembly and show different recovery dynamics. Cluster III is associated with proteins involved in mitochondrial translation, displaying contrasting trends in dynamics.

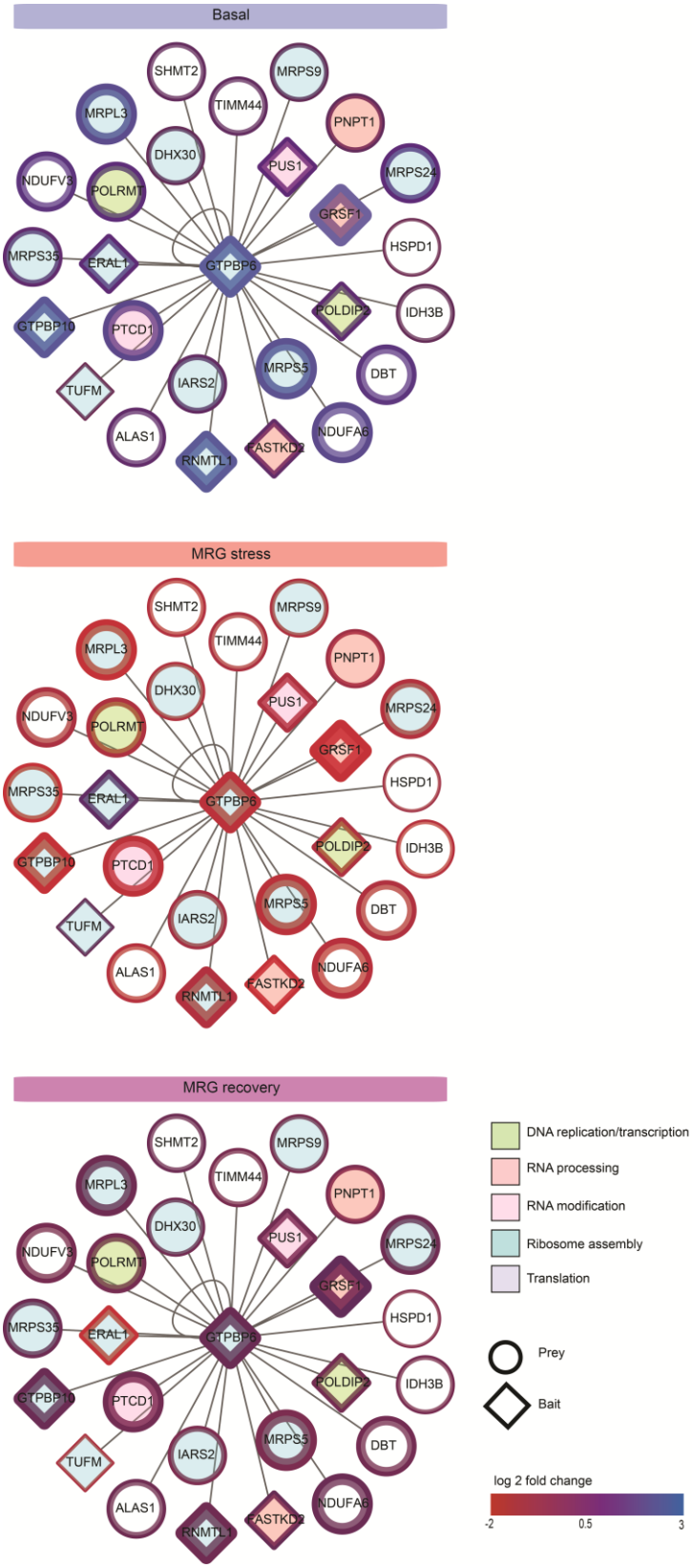

Figure 22: Time-resolved TurboID profiling reveals network dynamics of GTPBP6 upon stress and recovery. Baits used in this study are represented as diamonds, while preys are represented as circles. Gene functions were manually annotated to five different categories: DNA replication (green) RNA processing (red), RNA modification (pink), ribosome assembly (cyan) and translation (violet). The color intensity gradient, ranging from red to blue, indicates a proportional representation of enrichments. Only the top high-confidence interactions of GTPBP6 found in all three conditions were used for this analysis.

3.5 MRGs' integrity is dependent on RNA turnover and their assembly can be stabilized by dsRNA

The spatio-temporal analysis of MRG dynamics, demonstrated that pre-RNA serves as a scaffold for their assembly. Building on these observations, I hypothesized that increased RNA levels enhance the stability of MRGs and prevent their disassembly upon stress conditions. The mitochondrial genome encodes various RNA species, processed from the polycistronic precursor into functional tRNAs, rRNAs and mRNAs.[133] Besides these classic RNA species, a recent discovery has unveiled a new category of mitochondrial RNAs known as double-stranded RNA (dsRNA), with a remarkable 99% deriving from the mitochondrial genome.[18]

In particular, latest research[17,18,95,134] has increasingly focused on mitochondrial dsRNA, revealing its regulation by the RNA degradation machinery (mtEXO). The mtEXO complex, composed of PNPT1 and SUPV3L1, degrades mitochondrial RNA in distinct foci (D-foci) within mitochondria.[95] These D-foci were found to partially co-localize with MRGs in the mitochondrial matrix.[85,95] Moreover, loss of either PNPT1 or SUPV3L1 has been shown to result in elevated levels of dsRNA descended from the mitochondrial genome.[18] Remarkably, one-fifth of the total mtRNA consists of dsRNA, forming distinct punctae within the mitochondrial matrix that can be visualized with the anti-dsRNA J2 antibody.[17,18,135] The discovery of dsRNA foci has added another layer of complexity to the compartmentalization of mitochondrial gene expression. However, the spatial organization of these dsRNA foci and their relationship to MRGs remain largely unknown.

To address this question, I employed the inducible HeLa Flp-In T-Rex cell system expressing GRSF1-EGFP to image MRGs utilizing confocal fluorescence microscopy. To detect dsRNA, I performed immunofluorescence using the anti-dsRNA J2 antibody and co-stained with an anti-ATP5A1 antibody to visualize mitochondria (Figure 23 A). The microscopy analysis revealed diverse phenotypes of co-localizations between J2 foci and GRSF1 positive granules (Figure 23 B, C). Interestingly, dsRNA foci were found to be associated with, but also occasionally separated from MRGs, scattered along the mitochondrial network. Based on these arrangements of co-localizations between MRGs and dsRNA punctae, four different categories were defined as follows: 1. MRGs co-

localized with dsRNA foci, 2. MRGs adjacent to dsRNA foci, 3. MRGs without dsRNA foci and 4. dsRNA-foci without MRGs. An analogous microscopy analysis conducted by Borowski et al.[85] described diverse types of co-localizations between nascent RNA and the mtEXO complex, that both appear as granules in mitochondria[85]. Furthermore, when the mtEXO complex was inactive, the amount of GRSF1[95] or RNA[85]-positive D-foci significantly increased, providing additional evidence that granules can display a variation of co-localizations.

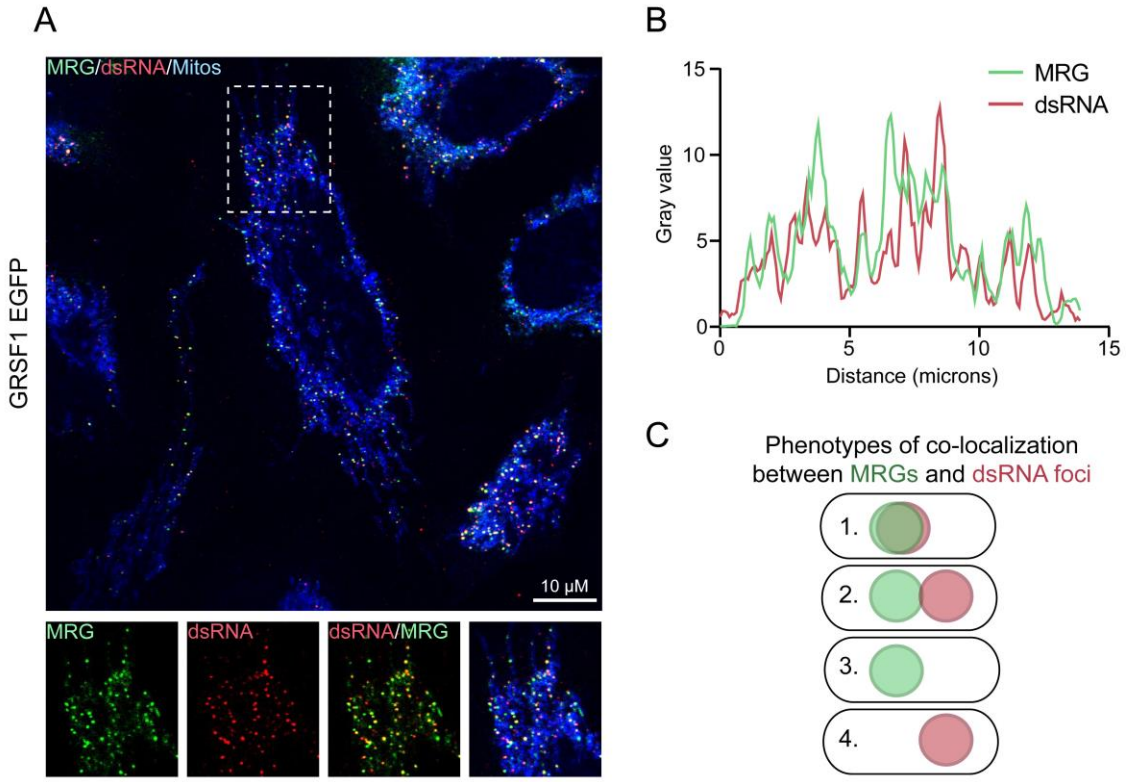

Figure 23: MRG and dsRNA foci indicate distinct patterns of co-localizations. (A) Representative confocal image showing MRGs and dsRNA foci in mitochondria. HeLa Flp-In T-Rex cells stably expressing GRSF1 fused to EGFP (green) were co-stained with dsRNA foci (J2 anti-dsRNA, red) and mitochondria (anti-ATP5A1, blue). Images were obtained on a Leica TCS-SP8 inverted spectral confocal microscope. The lower row shows magnified images of the section indicated by dashed box in the upper row. Lens x60; scale bar 10 µm. **(B)** Co-localization analysis of MRGs (green line) and dsRNA foci (red line). Fluorescent signals of the section indicated by a dashed box (A) were plotted into a histogram. **(C)** Schematic illustration presenting four different phenotypes of co-localizations between MRGs (green) and dsRNA foci (red): 1. MRGs co-localized with dsRNA foci, 2. MRGs adjacent to dsRNA foci, 3. MRGs without dsRNA foci and 4. dsRNA-foci without MRGs.

To test my hypothesis that elevated mitochondrial RNA levels enhance the stability of MRGs and thus prevent their disassembly upon stress conditions, I selectively depleted proteins involved in RNA turnover using siRNA mediated knockdowns (Figure 24 A, B). The efficiency of these knockdowns was confirmed with RT–qPCR, demonstrating a significant reduction in the transcript levels of the targeted genes (Figure 24 B). In total, four different proteins were individually depleted. One of the targeted proteins was FASTKD2, a well-established MRG component required for RNA processing of several mitochondrial transcripts, in particular of RNR2 and ND6.[52] Furthermore, I depleted the two RNA decay proteins PNPT1 and SUPV3L1, that have recently been shown to regulate dsRNA levels, as discussed before.[17,18] Additionally, I selected MTPAP, the mitochondrial poly(A) polymerase, as this protein is hypothesized to be involved in the RNA degradation pathway in humans.[136] A pooled non-targeting control (NTC) siRNA against firefly luciferase was used as control. Knockdown experiments were conducted for three days in HeLa Flp-In T-Rex cells. Expression of GRSF1-EGFP fusion protein was induced on the second day for 24 h. On the third day of knockdown, cells were treated with IMT1 and prepared for confocal microscopy to study time-resolved changes of MRGs' morphology.

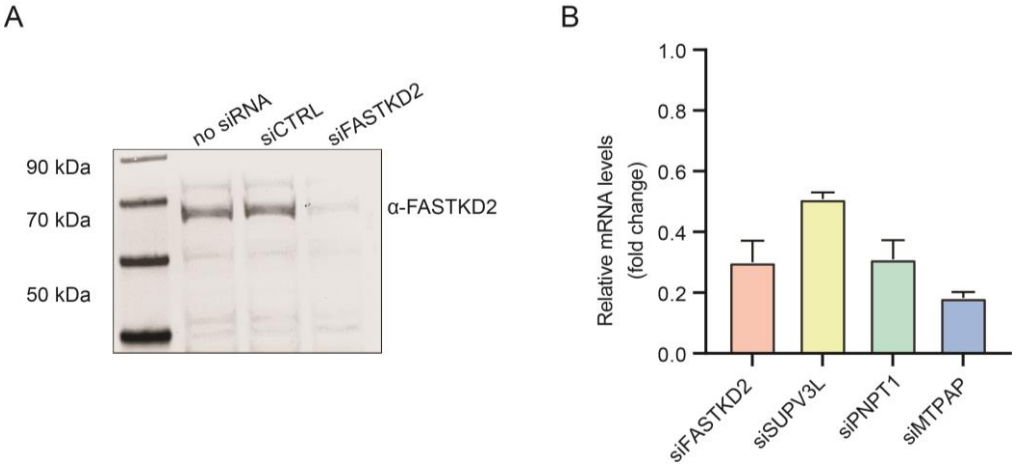

Figure 24: Validation of siRNA mediated knockdowns. Cells were transfected with 40 nM of stealth siRNAs targeting PNPT1, SUPV3L1, MTPAP, FASTKD2 or a pooled non-targeting control siRNA (CTRL) against firefly luciferase GL2 as control. Knockdowns were performed for 3 days, followed by cell harvesting. **(A)** Protein levels of FASTKD2 were analyzed with western blotting. **(B)** Transcript levels of siRNA targeted genes were measured with (qRT–PCR) and normalized to GAPDH. Error bars = SD; n = 3 biological replicates.

Consistent with previous reports,[17,18,95,134] siRNA-mediated depletion of either PNPT1 or SUPV3L1 led to significant accumulation of dsRNA (Figure 25). Interestingly, I observed the same effect in MTPAP depleted cells, showing an average of about 10-fold higher J2 intensities compared to control siRNA treated cells. Pajak et al.[137] reported dsRNA accumulation in MTPAP knockout larvae of *Drosophila melanogaster* (*dmmtpapKO*), leading to the hypothesis that poly(A) tail length could regulate degradation mediated by PNPT1 and SUPV3L1. However, this idea has not been investigated in humans yet.

In addition, to increased dsRNA levels, MRGs displayed enhanced stability upon stress conditions (Figure 26). The number of discrete MRG foci upon IMT1-induced stress was significantly higher when RNA decay was impaired by RNAi directed knockdown of PNPT1, SUPV3L1 or MTPAP (Figure 26). Specifically, downregulation of MTPAP led to an increased stability of MRGs. Even after 60 min of transcription inhibition, the average number of MRGs was over 140-fold higher compared to NTC treated cells (Figure 26). FASTKD2 knockdown resulted in only a minor increase in dsRNA intensities prior stress induction (Figure 25). However, in combination with MRG stress, FASTKD2 depleted cells showed significantly increased dsRNAs intensities and delayed MRG disassembly. These findings illustrate that integrity of MRGs can be maintained by dsRNA molecules when mitochondrial transcription is impaired.

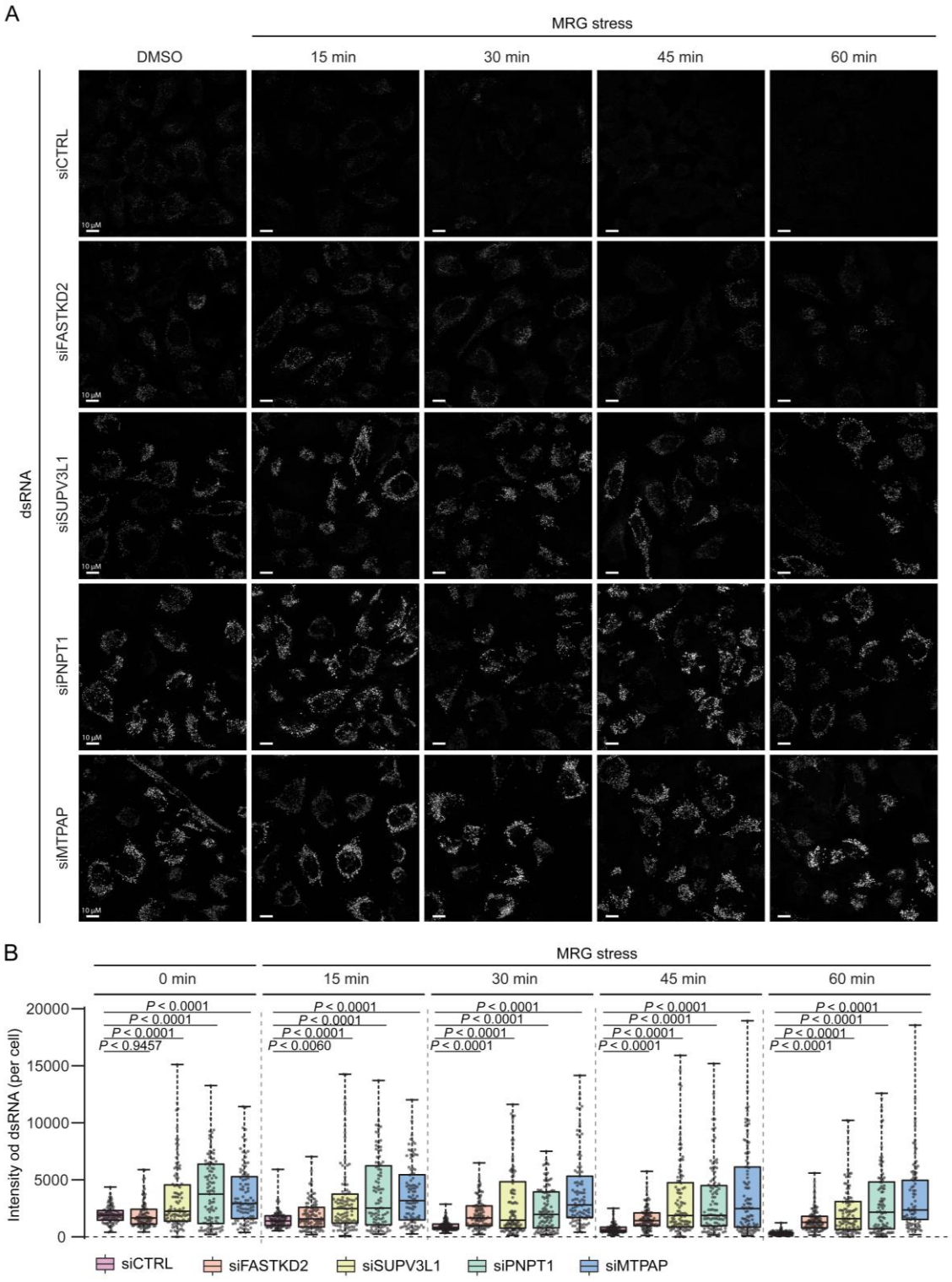

Figure 25: Depletion of mitochondrial RNA turnover factors lead to accumulation of dsRNA. (A) Representative confocal images showing MRGs dynamics under stress conditions when RNA degradation is impaired. HeLa Flp-In T-Rex cells stably expressing GRSF1 fused to EGFP were transfected with control, FASTKD2, SUPV3L1, PNPT1 or MTPAP siRNA for three days and treated with IMT1 (5 µM) for indicated time points. Double-stranded RNA (dsRNA) was immunostained with anti-dsRNA antibody. Lens x60; scale bar 10 µM. **(B)** Box plot presenting dsRNA intensities of about 100 cells per condition. For significance a two-tailed unpaired t-test was applied.

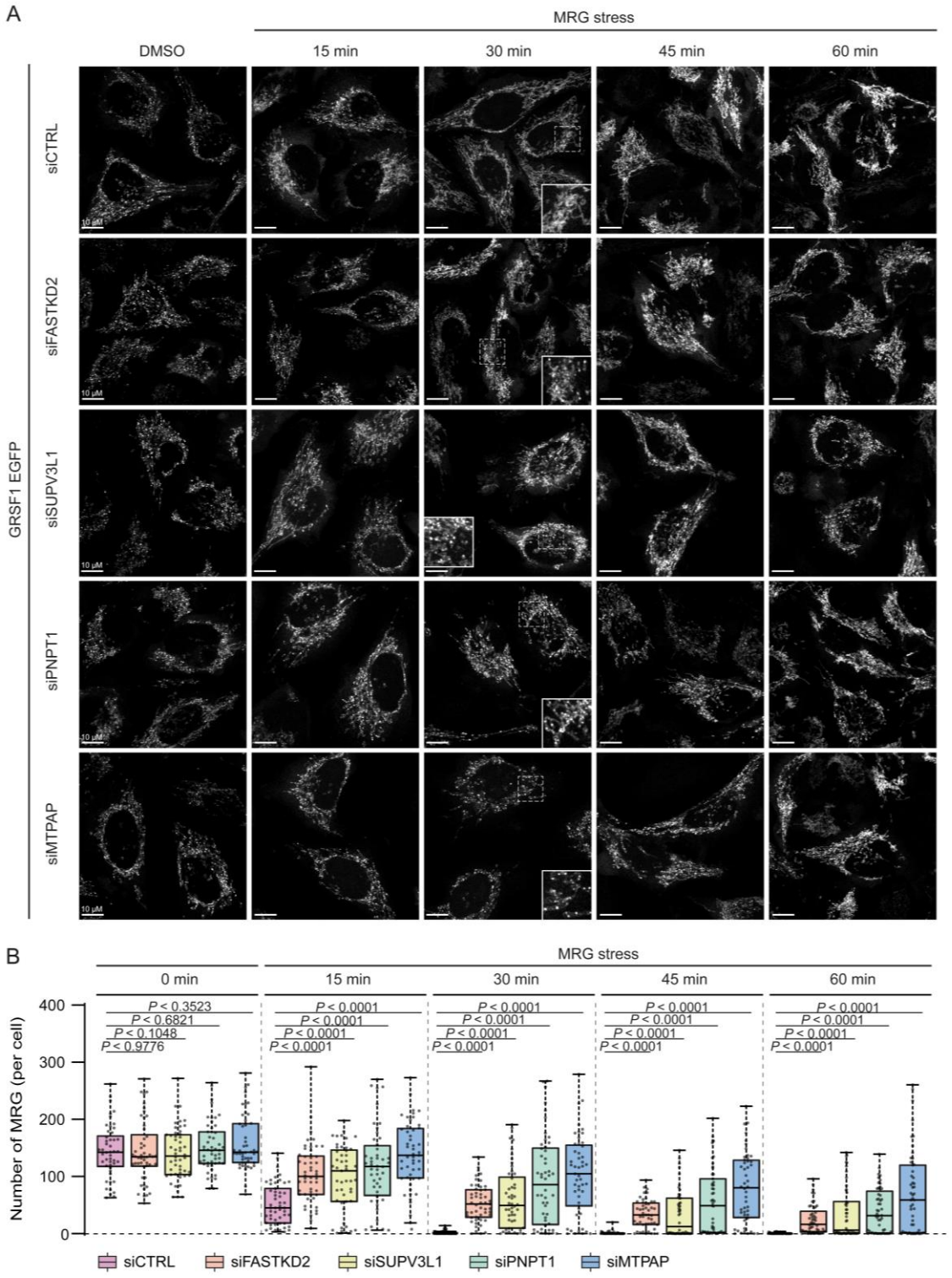

Figure 26: Formation of MRGs is highly dependent on RNA and can be stabilized by dsRNA. (A) Representative confocal images showing MRGs dynamics under stress conditions when RNA degradation is impaired. HeLa Flp-In T-Rex cells stably expressing GRSF1 fused to EGFP were transfected with control, FASTKD2, SUPV3L1, PNPT1 or MTPAP siRNA for three days and treated with IMT1 (5 µM) for indicated time points. White square at 30 min displays an enlarged view. Lens x60; scale bar 10 µM. **(B)** Box plot presenting MRG numbers of about 50 cells per condition. For significance a two-tailed unpaired t-test was applied.

I was curious about whether a specific RNA species or transcript, shows significant accumulation in MRG stress robust cells. To investigate this hypothesis, I measured mitochondrial mature and precursor RNA transcript levels of FASTKD2, SUPV3L1, PNPT1 or MTPAP depleted cells with RT-qPCR (Figure 27 A-D). In total, I measured more than 160 transcripts, including unprocessed and processed mRNAs, tRNAs and rRNAs. Among a few changes of individual transcript levels, the analysis of 33 different mitochondrial transcripts did not reveal a specific RNA species or pinpointed one transcript that was overall changed in all knockdown cell lines (Figure 27 A-D).

However, recent research by Zhu et al.[99] brought attention to the mitochondrial non-coding 7S RNA, located in the D-loop of the non-coding region, as a key regulator of the mitochondrial transcription initiation. Their study demonstrated the accumulation of 7S RNA when the mtEXO complex was impaired by knockdown of SUPV3L1 or PNPT1.[99] On the basis of these novel findings, I used RT-qPCR analysis to measure 7S RNA levels and found remarkably elevated levels in FASTKD2, SUPV3L1, PNPT1, and MTPAP depleted cells (Figure 28 A, B). Interestingly, already under unstressed conditions, the non-coding 7S RNA was significantly increased in all four knockdowns (Figure 28 B). Following 60 min of IMT1-induced stress, 7S RNA levels were highly elevated, with fold changes ranging from 50-200 times higher in comparison to NTC (Figure 28 B).

Consistent with the findings of Zhu et al.,[99] cells depleted of SUPV3L1 and PNPT1 showed significantly increased transcript levels of the non-coding 7S RNA. Notably, knockdown of MTPAP resulted in both, dsRNA accumulation and markedly elevated levels of 7S RNA (Figure 25, 28 B).

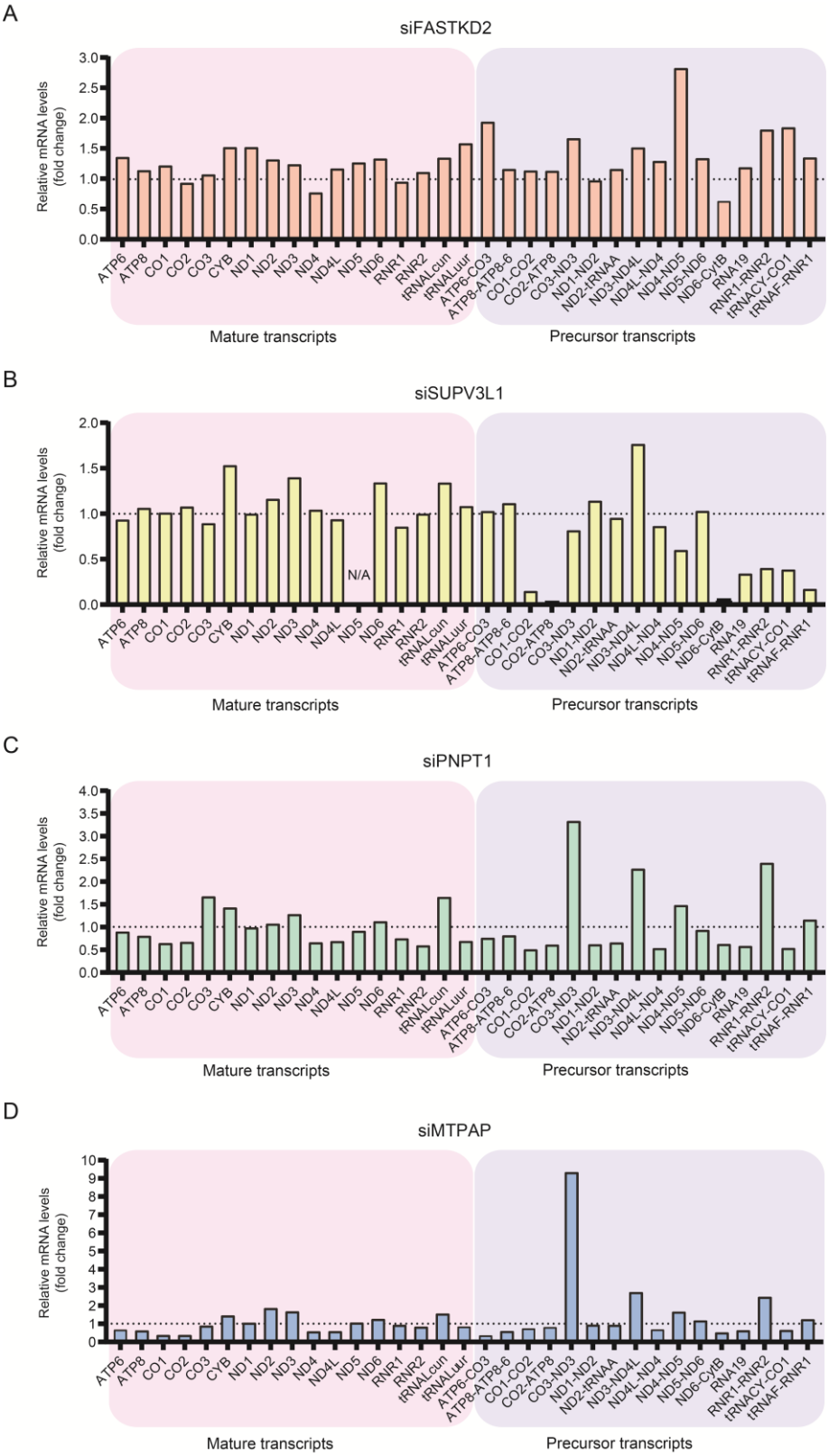

Figure 27: Depletion of MRG proteins involved in RNA processing and RNA degradation does not affect a specific mitochondrial RNA. Cells were transfected with 40 nM of stealth siRNAs targeting **(A)** FASTKD2, **(B)** SUPV3L1, **(C)** PNPT1 or **(D)** MTPAP knockdowns were performed for 3 days, followed by RNA isolation. Junction primers were used to detect precursor transcripts (see. Figure 18 A). Transcript levels were measured with qRT-PCR and normalized to GAPDH. N = 1 biological replicate.

My findings further provide evidence that MTPAP plays a role in regulating RNA levels through degradation, within the same pathway as SUPV3L1 and PNPT1 in human mitochondria. Furthermore, consistent with previous iCLIP data[52] confirming 7S RNA as a target of FASTKD2, I detected significantly higher 7S RNA levels in FASTKD2 depleted cells. However, dsRNA intensities were not significantly higher than those observed with control siRNA under unstressed conditions, suggesting a different pathway of 7S RNA accumulation. The precise mechanism underlying the regulation of the 7S RNA by FASTKD2 needs to be further investigated and could be subject of future studies.

These results demonstrate the critical role for dsRNA in supporting the stability and stress response of MRGs, highlighting the complex interplay between RNA turnover pathways and MRGs.

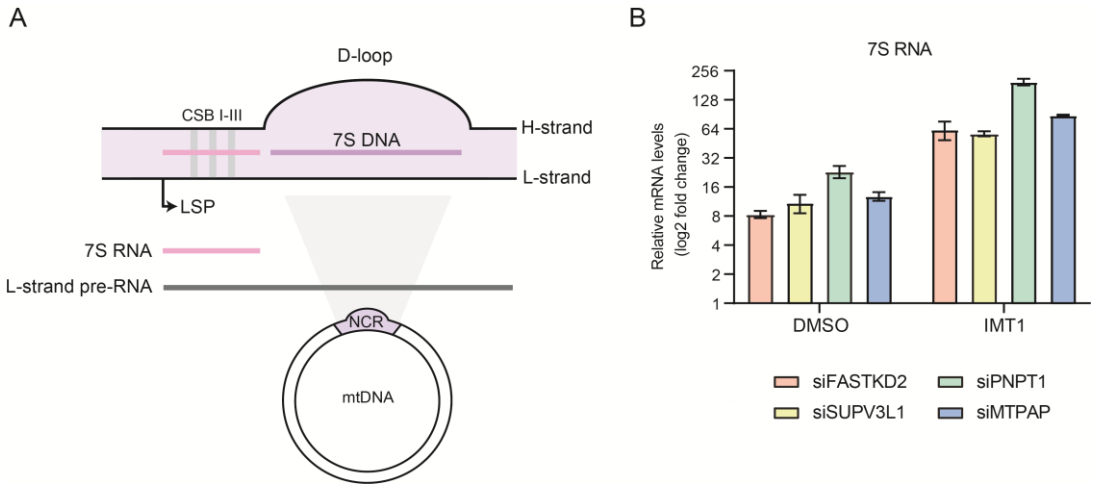

Figure 28: The non-coding 7S RNA accumulates in stress robust MRGs. (A) Schematic illustration of the non-coding region (NCR) in the mitochondrial genome. In association with the mitochondrial DNA (mtDNA), 7S DNA forms the triple stranded displacement loop (D-loop). In addition to full-length transcript from the light strand promoter (LSP), premature transcription termination at CSB1 generates the non-coding 7S RNA. **(B)** Quantification of 7S RNA transcript. Cells were transfected with control, FASTKD2, SUPV3L1, PNPT1 or MTPAP siRNA for three days and treated with IMT1 (5 µM) for 1 h. Total RNA was isolated and analyzed with RT–qPCR. Transcript levels were normalized to GAPDH. Relative mRNA levels are shown as $\log_2$ fold changes. Error bars = SD; n = 3 biological replicates.

To conclude, under basal conditions, transcription of the mitochondrial genome produces long precursor RNAs that are further processed into functional rRNA, tRNAs, and mRNAs. These RNA transcripts serve as a scaffold for MRG proteins, forming a membraneless ribonuclease protein complex. Notably, transcripts originated from the L-strand undergo degradation, a regulatory mechanism that prevents accumulation of dsRNA in mitochondria. However, under stress conditions, such as transcription inhibition induced by IMT1, loss of pre-RNA results in MRG disassembly. Remarkably, a simultaneous inhibition of RNA transcription and RNA decay alters RNA surveillance, leading to elevated levels of dsRNA and the non-coding 7S RNA. The accumulation of RNA molecules increases MRGs' stability and counteracts their disassembly upon stress conditions. These findings demonstrate that MRG integrity is highly dependent on pre-RNA turnover and their assembly can be reinforced by dsRNA (Figure 29).

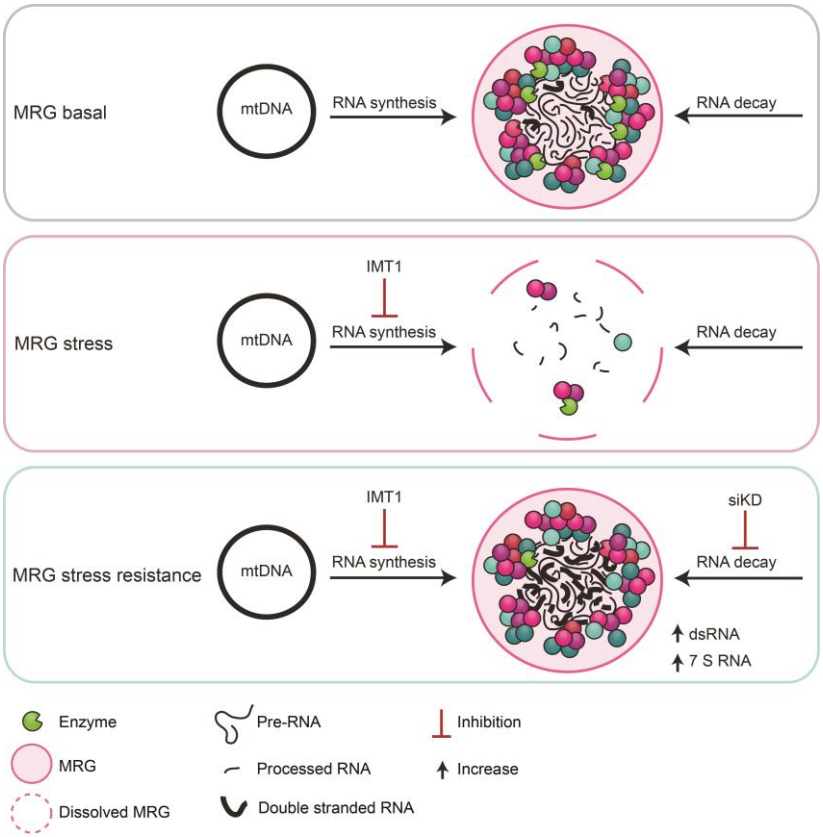

Figure 29: Depletion of MRG components associated with RNA degradation counteracts MRGs' disassembly under stress conditions. Schematic illustration of MRGs under basal conditions, where RNA transcripts levels are balanced by synthesis and decay processes. Upon IMT1-induced stress, RNA synthesis in inhibited and MRGs disassemble. Depletion of MRG components involved in degradation rescues MRG disassembly upon stress conditions causing elevated levels of double-stranded RNA and non-coding 7S RNA that contribute to enhance their stability.

4 Discussion

MRGs have emerged as crucial regulators of the mitochondrial gene expression, thus playing a critical role in cellular homeostasis.[138] Despite their significance, little is known about their (sub)architecture and characteristics, especially under stress conditions. Dysregulation of mitochondrial RNA metabolism has been associated with various human diseases, including neurodegenerative and metabolic disorders as well as certain types of cancer.[54,120] However, our understanding of their composition, structure and dynamics as well as the identity of most proteins carrying out the required reactions within the MRGs remain elusive.

The aim of this study was to investigate the MRG biology, focussing on fundamental characteristics of their composition, structure, regulation and dynamics. To systematically do this, a three step approach was used:

Firstly, defining the MRG proteome under physiological conditions. To identify essential components, a cutting-edge proximity labeling technique, TurboID combined with quantitative mass spectrometry was applied. The interactomes of 20 individual MRG-related proteins were analyzed and combined to obtain a comprehensive, MRG protein-protein network.

Secondly, investigating spatio-temporal dynamics of MRGs under stress conditions. Here, IMT1, a specific inhibitor for the mitochondrial transcription, was applied. Both time-dependent morphological alterations as well as compositional changes of MRGs were analyzed using fluorescent imaging with confocal microscopy and TurboID based interactomics, respectively.

Thirdly, elucidating the impact of mitochondrial RNAs on the integrity of MRGs. To achieve this, key players in RNA turnover were selectively depleted upon stress conditions. Simultaneously, stability of MRGs as well as levels of mitochondrial RNAs were examined using confocal fluorescence microscopy and quantitative real time PCR.

This comprehensive investigation has significantly expanded our knowledge and enhanced the overall understanding of MRGs. By identifying the molecular structure and dynamics, I gained a deeper understanding of the mitochondrial gene expression

facilitated by MRGs. This knowledge can be used for future studies to identify disease-related pathways and developing novel therapeutic approaches.

4.1 Revealing the MRG proteome: novel insights into their complex (sub)architecture

The systematic profiling of MRGs using proximity labeling combined with quantitative mass spectrometry revealed a comprehensive interaction map. The dataset obtained in this study comprised more than 1,700 high-confidence interactions across 20 selected MRG-related baits, elucidating the individual protein-protein interactions as well as the overall MRGs architecture at high-depth (Figure 10, 12-13).

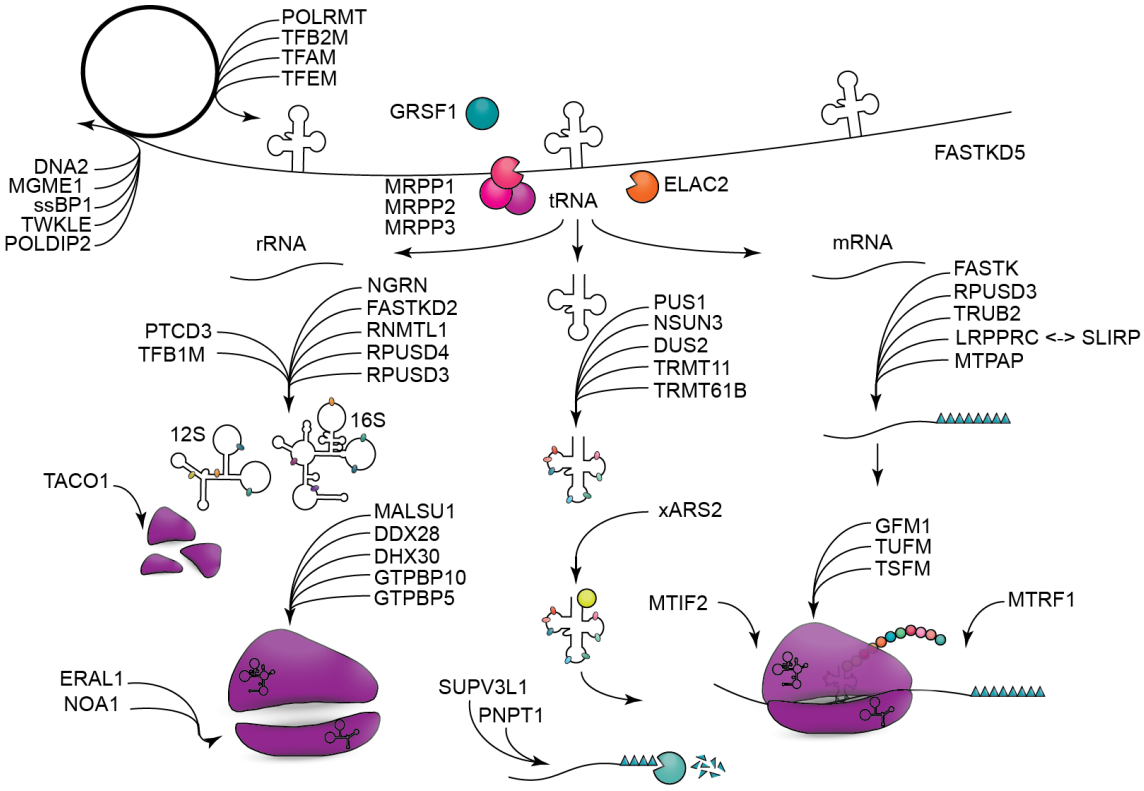

Figure 30: Functional assignment of the key proteins identified in this study within MRGs. MRGs are composed of mitochondrial RNAs (preRNA, mRNA, tRNA and rRNA) and a variety of nuclear encoded proteins essential for multiple steps of mitochondrial RNA metabolism. Proteins found in this study, encompass a wide range of functions, ranging from DNA replication and transcription, to RNA processing and modification and mitoribosome assembly and translation.

Based on the obtained PPI profiling data, the GTPases GTPBP10, GTPBP6 and GTPBP5 are components of the MRG network (Figure 30, S 2-3). These GTPases have recently been identified as proteins that coordinate ribosome maturation of 39S LSU in mitochondria.[75-78] In particular, GTPBP10 was strongly represented in my MRG proteome, indicating its prominent role in MRG-related processes (Figure 16 B, C). GTPBP10 is known to interact with 16S rRNA and is involved in the checkpoint for quality control to ensure proper ribosome biogenesis in mitochondria.[77,139] Consistent with previous immunoprecipitation data from Lavdovskaia et al.,[77] my study confirmed interactions between GTPBP10 and proteins associated with RNA processing and modification on one site (*e.g.,* FASTKD2, TRMT61B and RNMTL1) as well as ribosome assembly on the other site (*e.g.*, ERAL1 and DDX28). Furthermore, I found GTPBP10 significantly enriched in both nucleoid baits POLDIP2 and SSBP1, demonstrating its role in multiple aspects of mitochondrial gene expression (Figure 16). Accordingly, GTPBP10 emerged as a constituent of the MRG core network and key player in MRG biology. Interestingly, among ribosome assembly factors, GTPBP10 was the only GTPase found in the MRG core network, indicating that ribosome maturation does not take place in the granule core (Figure 16). This raises the question of whether GTPB10 fulfills further roles besides ribosome assembly and probably plays a multifunctional role in MRGs.

In my study, the GTPase, GTPBP6 was discovered as a novel MRG protein (Figure 20-21). Just recently in 2020,[78] GTPBP6 has been characterized for the first time as a mitochondrial protein that plays a dual role in both recycling and assembly of the mitoribosome. GTPBP6 is the human homolog of the bacterial ribosome splitting factor HflX, that is crucial for ribosome recue during heat shock stress.[78] A stalled LSU maturation and accumulation of assembly factors including GTPBP5, GTPBP10 could be observed during loss of GTPBP6.[78] In line with these findings, my PPI profiling data of GTPBP6 revealed significant interactions with multiple ribosomal subunits and assembly factors including GTPBP10 and GTPBP5. In addition, GRSF1 and MRPP3 were ranked among the top five high-confidence interactions in my data. Further validation with confocal fluorescence microscopy confirmed accumulation of GTPBP6 in discrete foci within mitochondria (Figure 20). Nonetheless, GTPBP6 foci were not as discrete as

GRSF1 foci. Moreover, compared to GTPBP10, GTPBP6 was less represented in my interactome data, showing a spatial separation from the MRG core (Figure 15-16).

Furthermore, my interactome data revealed several significant interactions between the well-established nucleoid proteins POLDIP2, TWNK and SSBP1 and the MRG components, providing further evidence for a dynamic exchange between both structures (Figure 30, S 2-3). This observation aligns with a previous study[92] that demonstrated the influence of two mitochondrial DNA replication factors, TWNK and SSBP1 on MRG biology. Previously, the TWNK interactome, analyzed by BioID, revealed reciprocal interactions with the MRG proteins GRSF1 and MRPP1.[92] Co-localization studies of TWNK confirmed its association with both MRGs and nucleoids,[92] highlighting potential roles of replication factors in mitochondrial RNA metabolism.[38]

Based on initial key studies conducted by Iborra et al.,[140] nucleoids and MRGs are considered as spatially separated structures within the mitochondrial matrix. This assumption is based on co-localization studies using immunolabeling techniques of DNA and nascent RNA molecules, which unlike proteins, display limited mobility and behave more static.[140] Given the tight coordination between DNA replication and transcription, along with my observations, it is evident that both processes are contagious and proteins can shuttle between both entities to facilitate an efficient regulation.

Moreover, the MRG proteome of this study identified several components of the respiratory chain and parts of the import complex (Figure 12, S 1), supporting previous findings showing[141] that MRGs are located next to the inner mitochondrial membrane. It is evident that MRGs are located near the IMM, as all MRG proteins need to be imported from the cytosol to mitochondria.[122] Additionally, translation of mitochondrial-encoded proteins occurs adjacent to the membrane, where also insertion of newly synthesized OXPHOS subunits into the IMM takes place.[122]

Through my correlation analysis of high-confidence PPIs across all 20 MRG-related baits, I identified distinct biotinylation patterns that revealed one major and prominent cluster assigned to the GO term “mitochondrial gene expression” (Figure 13). Interestingly, I found a correlation between this major cluster and a second cluster representing the GO term “mitochondrial translation”, indicating the association of certain MRG proteins

for different sub-structures (Figure 13). In-depth examination supports the notion of specific mitochondrial ribosome factors being localized within MRGs, while other components of the ribosome assembly and translation machinery appeared in a distinct structure.

An overall human mitochondrial proximity map, published by Antonicka et al.[142] obtained comparable results, indicating that MRGs are more structured than previously thought. Their correlation analysis disclosed that certain MRG proteins clustered with the mitochondrial ribosome while others were associated with the RNA processing machinery.[142] However, further studies are needed to determine whether part of the ribosome assembly machinery is clearly separated from MRGs or forms a specialized sub-domain within MRGs.

The high-resolution of my PPI screen, allowed me to identify RNA processing and modification factors as hub proteins, defining the MRG core (Figure 16 B). Bait-prey interactome data revealed a dense core composed of highly connected RNA binding proteins such as GRSF1, MRPP1, MRPP3, FASTKD2 (Figure 16 B, C) that were previously confirmed as established MRG components.[82,87] Recent super-resolution microscopy data from Rey et al.[100] have revealed that MRGs are organized by liquid-liquid phase separation, where both components, proteins and RNA, create a liquid-like structure. Their study[100] moreover indicates that MRGs are layered structures that are composed of multiple RNA binding proteins that surround mitochondrial RNAs. Other LLPS based granules such as stress granules or processing bodies are known to form a core that provides the structural stability of these membraneless condensates.[143]

Here, the identification of an MRG protein core (Figure 16 B, C) and their physical properties suggest a concept of an ordered assembly process, where RNA serves as a scaffold for essential RNA processing factors. It is tempting to speculate that in particular, MRG proteins that bind RNA transcripts might form an initial complex that recruits additional proteins involved in further processes like ribosome maturation. Such a model has been already proposed for stress granules where assembly occurs in distinct stages.[144] Initially, core proteins condense with mRNA to form a stable seed through strong interactions, before the assembly of a dynamic shell is triggered.[144]

4.2 Unveiling properties of MRGs under stress conditions: displaying their spatio-temporal dynamics

As previously discussed, MRGs undergo LLPS and behave like fluid condensates having a high level of flexibility.[100] My results characterized MRGs as highly dynamic structures, capable of rapid disassembly and reassembly in response to mitochondrial RNA availability.

Time-resolved microscopy analysis illustrated that MRG integrity is RNA driven and could confirm the idea that RNA transcripts form a scaffold for their formation (Figure 17, 19, 26). The assembly of MRGs is highly dependent on mitochondrial pre-RNA production (Figure 19) that also plays an essential role for their stability (Figure 26). Surprisingly, while complete loss of MRG foci was observed within 1 h of transcription inhibition with confocal microscopy (Figure 17, 19), I did not detect dramatic changes in PPI profiles of MRPP3, MTPAP and ERAL1 even after 6 h of IMT1-induced stress (Figure S 4-5). Therefore, I hypothesize that upon MRG disassembly, smaller sub-complexes stay connected that are below the detection limit of confocal microscope resolution. It is conceivable that a proportion of MRG proteins, in particular the core proteins, are still capable to form smaller complexes which can be directly recruited to nascent RNA during the recovery phase. This ability would allow MRGs to adapt fast to altered environmental conditions. However, the precise mechanism how mitochondrial RNA induces MRG assembly still remains unclear and requires further investigations. Moreover, studying the formation of sub-structures within MRGs and their possible guidance by different RNA species could be a crucial aspect in understanding the mechanism behind their assembly.

The spatio-temporal analysis of GTPBP6 provided initial insights into compositional changes upon stress, providing evidence that MRG proteins have diverse kinetics during assembly (Figure 21). Essential components within the MRG core showed rapid recovery, while other MRG proteins recover at later stages (Figure S 6). Interestingly, proteins associated with ribosome assembly and translation machinery behaved in the opposite way, displaying even stronger interactions with GTPBP6 upon stress-induced MRG disassembly (Figure 21). Conceivably, ribosome maturation factors relocate to a different fraction or entity when RNA transcription is paused.

Further findings of MRG proteome data upon EtBr treatment demonstrated a similar phenomenon (Figure 31). PPI profiling of GRSF1, GTPBP6, EARLA1, MTPAP, MRPS7 and MRPP3 upon 2 h EtBr revealed several significantly enriched interactions, particularly with subunits of the mitochondrial ribosome and ribosome assembly factors. This highlights the interplay between MRG proteins and the translation machinery in response to stress conditions. This observation, further implies that MRG proteins have the ability to localize and accumulate in other sub-structures or entities upon stress conditions. Taken together this suggests that MRG proteins have the flexibility to shift between complexes, potentially allowing them to respond rapidly and efficiently to cellular stress.

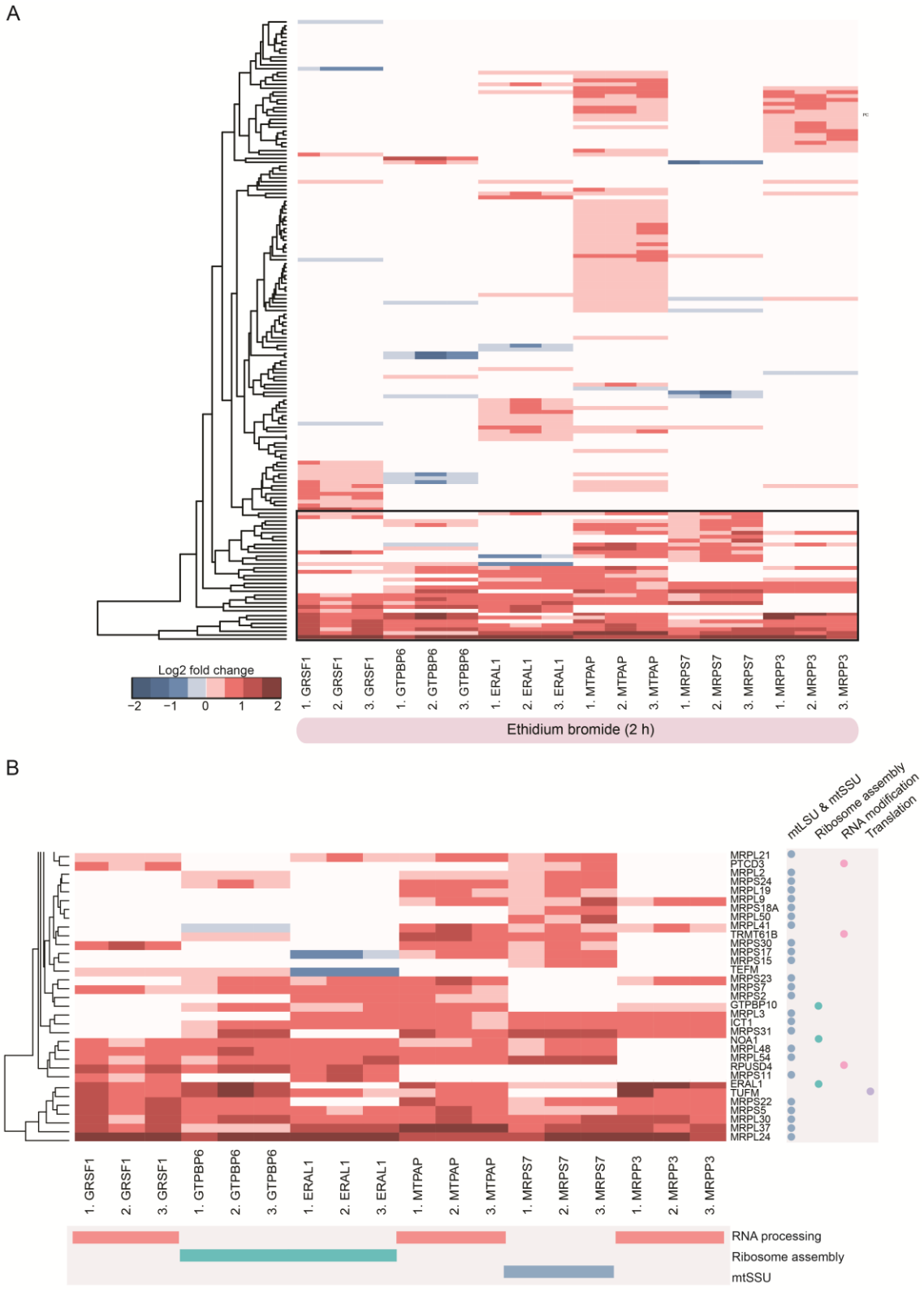

Figure 31: Mitochondrial ribosomes accumulate on MRGs in response to ethidium bromide-induced stress. HeLa Flp-In T-Rex cells stably expressing GRSF1, GTPBP6, ERAL1, MTPAP, MRPS7 or MRPP3 fused to TurboID were treated with 3 µg/ml EtBr for 2 h. **(A)** Heatmap displays the hierarchically clustering of proteins identified by TurboID interactome analysis **(B)** Enlarged view of cluster shown in (A). Nodes are color-coded based on functional categories, with subunits of the mitochondrial ribosome specifically highlighted in blue.

4.3 Elucidating the impact of mitochondrial RNAs on MRGs' integrity: impaired RNA turnover increases stability under stress conditions.

Recently, a specific form of mitochondrial RNA, the dsRNA has come into focus of current research. It has been shown that in particular the mtEXO complex comprising PNPT1 and SUPV3L1 is essential for the regulation of dsRNA levels.[17,18,95,134] Furthermore, confocal microscopy studies revealed dsRNA accumulation when GRSF1 or SSBP1 were impaired, giving the idea that dsRNA is regulated by MRG associated proteins.[18,145] However, the spatial arrangement of dsRNA foci and MRGs or their precise connections, remained largely uncharacterized.

My microscopy analysis, provided compelling evidence for a strong connection between dsRNA foci and MRGs (Figure 23). Further time-resolved monitoring of MRGs upon stress conditions, revealed delayed MRGs' disassembly when mitochondrial RNA turnover was impaired by knockdown of either FASTKD2, PNPT1, SUPV3L1 or MTPAP (Figure 26). During these investigations, it became evident that dsRNA accumulation is associated with an increased stability of MRGs upon transcription inhibition (Figure 25-26).

As mentioned before, in particular, PNPT1 and SUPV3L1 which form the D-foci,[95] were found to be highly critical for proper dsRNA degradation in mitochondria.[18] Despite the fact that these proteins were identified as top interactors of GRSF1 by immunoprecipitation,[87] both haven't been further validated as MRG proteins. Additionally, microscopy studies[85,95] showed only a partial co-localization of D-foci with MRGs, arguing for a separation between both structures. These observations suggest that D-foci and MRGs interact to some extent, but there are also distinct aspects or components of these structures that do not overlap. The PPI profiling in the present work, aligns with this idea and identified SUPV3L1 marginal in only three out of 20 baits (GRSF1, RNMTL1 and ERAL1; Figure S 2-3). Furthermore, another potential component of the D-foci, the exonuclease REXO2,[146] was not detected at all in the MRG proteome of this study. Interestingly, I identified the second key factor of the D-foci, PNPT1 as prey in multiple interactomes and thus defined as part of the MRG protein core (Figure 16 B, C). Therefore, it is more conceivable that PNPT1 has a dual function in MRGs, rather than RNA degradation occurs within MRGs. In line with this assumption, it has been shown

that PNPT1 is a multifunctional protein being required for translocation of RNAs into mitochondria in addition to RNA decay.[147]

Consistent with previous work,[17,18,134] I observed a strong accumulation of dsRNA molecules when the RNA degradosome was disrupted by PNPT1 or SUPV3L1 knockdown (Figure 25). Notably, I detected the same effect when the mitochondrial poly(A) polymerase MTPAP was impaired (Figure 25). This finding supports the idea that MTPAP is part of the SUPV3L1-PNPT1 mediated degradation pathway in humans as previously shown in *Drosophila melanogaster*.[137] Pajak et al.[137] proposed a model of post-transcriptional regulation of RNA in fly mitochondria, where MTPAP adds short poly(A) tails to both, antisense and sense RNA transcripts. On the one hand, the sense RNA is stabilized by the LRPPRC-SLIRP complex and subsequently undergoes further polyadenylation. On the other hand, the non-protected antisense RNA is degraded by the PNPT1-SUPV3L1 complex to prevent accumulation of dsRNA in mitochondria.[137] An additional study discovered that MTPAP forms a complex with PNPT1 and SUPV3L1 to regulate the poly(A) tail length in response to metabolic changes in Pi to ATP ratios.[148] My observations presented in this work, found dsRNA accumulation in MTPAP depleted cells (Figure 25), that along with previous findings, strongly suggests that MTPAP regulates stability of mitochondrial RNAs in collaboration with the PNPT1-SUPV3L1 complex. As recently discussed,[99] this mechanism may represent an adaptive response to metabolic changes, thereby playing a critical role in maintaining mitochondrial homeostasis.

On the contrary, when FASTKD2 was depleted, I did not observe highly elevated levels of dsRNA under unstressed conditions (Figure 25). However, when transcription was inhibited, I detected significantly higher dsRNA intensities, indicating the presence of precursor RNA transcripts that could still form RNA duplexes even when transcription was blocked (Figure 25). I presumed that depletion of FASTKD2 impacts RNA processing, resulting in extended half-lives of mitochondrial pre-RNA and thus enhances MRGs' stability. Given that mitochondria possesses complementary H- and L-strand transcripts, the annealing of these strands is the primary source of dsRNA.[15]

Therefore, it is plausible that in addition to RNA degradation, another mechanism exists to avoid accumulation of dsRNA. Probably certain MRG proteins directly intervene immediately after transcription to prevent dsRNA formation already at early stages.

Rackham et al.[15] discovered that long non-coding RNAs (lncRNAs) generated from the mitochondrial L-strand are capable of forming stable dsRNA with their respective complementary H-strand transcripts, adding another layer of gene regulation. One notable example is the stabilization of the ND6 transcript, which lacks polyadenylation.[15] In addition, Rackham et al.[15] investigations revealed that three lncRNAs, lncND5, lncND6, and lncCytB are processed by the well-known MRG RNase P protein MRPP1.[55] These investigations suggest that lncRNAs are another key player in mitochondrial gene expression and further studies could provide valuable insights into their role in the MRG biology.

Interestingly, latest sequencing techniques discovered a variety of mitochondrial encoded ncRNAs, including circular (circRNAs), small non-coding RNAs (sncRNA) and PIWI interacting RNAs (piRNA).[149] However, the majority of non-coding RNAs derived from the mitochondrial genome are still uncharacterized and their biogenesis and functions remain elusive.[149] Nevertheless, it has been demonstrated that ncRNAs originating from the nuclear DNA are imported into mitochondria and influence their gene expression.[149] One well studied example is the lncRNA RNA component of mitochondrial RNA-processing endoribonuclease (RMRP) that is imported into mitochondria where it is stabilized and guided by GRSF1.[150] This interplay between the lncRNAs and the MRG protein GRSF1 was identified as essential for mitochondrial DNA replication and RNA processing.[150] It can be hypothesized that mitochondrial-derived ncRNAs play analogous roles in mitochondrial gene expression, which makes it compelling to investigate their functions in association with MRGs.

In particular, one non-coding RNA, known as the 7S RNA, has been demonstrated to play a crucial role in transcription.[99] Very recently Zhu et al.[99] described that 7S RNA targets POLRMT and acts as an essential regulator of mitochondrial transcription. In line with their results, I detected elevated levels of 7S RNA when the decay complex was impaired by siRNA mediated knockdown of either PNPT1 or SUPV3L1 (Figure 28). Additionally,

depletion of two MRG proteins involved in RNA turnover, MTPAP or FASTKD2 resulted in the same strong increase of 7S RNA levels, indicating a putative compensatory mechanism driven by MRGs to counteract accumulation of mitochondrial RNA transcripts (Figure 28). These observations support the model that 7S RNA is part of a negative feedback loop that is activated in response to various metabolic stress conditions or pathological events,[99] emphasizing an important role of MRGs in maintaining cellular homeostasis.

Overall, my study reveals a clear correlation between MRG proteins involved in RNA turnover and the increase in dsRNA and 7S RNA levels, accompanied with enhanced stability of MRGs upon stress conditions. Nevertheless, the precise mechanism underlying the regulation of these mitochondrial encoded non-coding RNAs needs to be further investigated, making it a promising subject for future studies.

4.4 Concluding remarks

In conclusion, this study provides novel and fundamental insights into the composition, structure, regulation and dynamics of MRGs. The cutting-edge approach using TurboID based proximity labeling combined with quantitative mass spectrometry was successfully employed to define the overall MRG proteome. The in-depth of this PPI profiling unveiled a comprehensive protein network and facilitated the identification of essential MRG core components. Furthermore, this study validated GTPBP6 as a novel MRG protein, and provided evidence for the association of specific mitochondrial ribosome protein within MRGs. In sum, these observations offer new perspectives on the structural organization and functional regulation of MRGs.

Time-resolved investigations of MRGs' dynamics under stress conditions revealed their highly dynamic nature, with rapid disassembly and reassembly closely linked to mitochondrial RNA transcription. Additionally, these findings highlighted the importance of RNA turnover factors in maintaining MRG integrity as well as double-stranded RNA as an important factor that can stabilize MRGs.

The examination of various mitochondrial RNA species and their association with MRGs demonstrated the essential role of the non-coding 7S RNA. It appears that 7S RNA acts as a compensatory mechanism to counterbalance mitochondrial RNA accumulation when RNA turnover is impaired, highlighting its crucial role in maintaining cellular homeostasis under stress conditions. While this research has significantly expanded our understanding of MRGs, further studies about the regulation of specific mitochondrial-encoded non-coding RNAs and their precise roles within MRGs are required. Additionally, the formation of sub-structures within MRGs and their possible guidance by different RNA species would be an important aspect to understand how exactly they are assembled.

5 References

1. Sagan L. On the origin of mitosing cells. *J Theor Biol*. 1967;14(3):90079. doi:10.1016/0022-5193(67)90079-3

2. Dyall SD, Brown MT, Johnson PJ. Ancient Invasions : From Endosymbionts to Organelles Published by : American Association for the Advancement of Science Stable URL : https://www.jstor.org/stable/3836764 digitize , preserve and extend access to Science Ancient Invasions : From Endosymbion. 2020;304(5668):253-257.

3. Altmann R. *Elementarorganismen und ihre Beziehungen zu den Zellen*. *Verlag von Veit Comp*. 1894.

4. Ernster L, Schatz G. Mitochondria: A historical review. *J Cell Biol*. 1981;91(3 II). doi:10.1083/jcb.91.3.227s

5. Palade GE. The fine structure of mitochondria. *Anat Rec*. 1952;114(3):427-451.

6. Sjostrand FS. Electron microscopy of mitochondria and cytoplasmic double membranes. *Nature*. 1953:30-31.

7. Logan DC. The mitochondrial compartment. *J Exp Bot*. 2006;57(6):1225-1243. doi:10.1093/jxb/erj151

8. Ramaccini D, Montoya-Uribe V, Aan FJ, et al. Mitochondrial Function and Dysfunction in Dilated Cardiomyopathy. *Front Cell Dev Biol*. 2021;8(January):1-21. doi:10.3389/fcell.2020.624216

9. Kennedy EP, Lehninger AL. Oxidation of fatty acids and tricarboxylic acid cycle intermediates by isolated rat liver mitochondria. *J Biol Chem*. 1949;179(2):957-972. doi:10.1016/s0021-9258(19)51289-3

10. Fernandez-Vizarra E, Zeviani M. Mitochondrial disorders of the OXPHOS system. *FEBS Lett*. 2021;595(8):1062-1106. doi:10.1002/1873-3468.13995

11. Kehrein K, Bonnefoy N, Ott M. Mitochondrial protein synthesis: Efficiency and accuracy. *Antioxidants Redox Signal*. 2013;19(16):1928-1939.

doi:10.1089/ars.2012.4896

12. Larsson NG, Wang J, Wilhelmsson H, et al. Mitochondrial transcription factor A is necessary for mtDNA maintenance and embryogenesis in mice. *Nat Genet*. 1998;18(3):231-236. doi:10.1038/ng0398-231

13. Anderson S, Bankier AT, Barrell BG, de Bruijn MH, Coulson AR, Drouin J, Eperon IC, Nierlich DP, Roe BA, Sanger F, Schreier PH, Smith AJ, Staden R YI. Sequence and organization of the human mitochondrial genome. *Nature*. 1981;290(April):1-18.

14. Berk AJ, Clayton DA. Mechanism of mitochondrial DNA replication in mouse L-cells: Asynchronous replication of strands, segregation of circular daughter molecules, aspects of topology and turnover of an initiation sequence. *J Mol Biol*. 1974;86(4):801-824. doi:10.1016/0022-2836(74)90355-6

15. Rackham O, Shearwood AMJ, Mercer TR, Davies SMK, Mattick JS, Filipovska A. Long noncoding RNAs are generated from the mitochondrial genome and regulated by nuclear-encoded proteins. *Rna*. 2011;17(12):2085-2093. doi:10.1261/rna.029405.111

16. Wu Z, Sun H, Wang C, et al. Mitochondrial Genome-Derived circRNA mc-COX2 Functions as an Oncogene in Chronic Lymphocytic Leukemia. *Mol Ther - Nucleic Acids*. 2020;20(June):801-811. doi:10.1016/j.omtn.2020.04.017

17. Coomans de Brachène A, Castela A, Musuaya AE, Marselli L, Marchetti P, Eizirik DL. Endogenous mitochondrial double-stranded RNA is not an activator of the type I interferon response in human pancreatic beta cells. *Autoimmun Highlights*. 2021;12(1). doi:10.1186/s13317-021-00148-2

18. Dhir A, Dhir S, Borowski LS, et al. Mitochondrial double-stranded RNA triggers antiviral signalling in humans. *Nature*. 2018;560(7717):238-242. doi:10.1038/s41586-018-0363-0

19. Morgenstern M, Peikert CD, Lübbert P, et al. Quantitative high-confidence human mitochondrial proteome and its dynamics in cellular context. *Cell Metab*. 2021;33(12):2464-2483.e18. doi:10.1016/j.cmet.2021.11.001

20. Bogenhagen DF, Rousseau D, Burke S. The layered structure of human mitochondrial DNA nucleoids. *J Biol Chem*. 2008;283(6):3665-3675. doi:10.1074/jbc.M708444200

21. Satoh M, Kuroiwa T. Organization of multiple nucleoids and DNA molecules in mitochondria of a human cell. *Exp Cell Res*. 1991;196(1):137-140. doi:10.1016/0014-4827(91)90467-9

22. Kukat C, Wurm CA, Spåhr H, Falkenberg M, Larsson NG, Jakobs S. Super-resolution microscopy reveals that mammalian mitochondrial nucleoids have a uniform size and frequently contain a single copy of mtDNA. *Proc Natl Acad Sci U S A*. 2011;108(33):13534-13539. doi:10.1073/pnas.1109263108

23. Gustafsson CM, Falkenberg M, Larsson NG. Maintenance and Expression of Mammalian Mitochondrial DNA. *Annu Rev Biochem*. 2016;85:133-160. doi:10.1146/annurev-biochem-060815-014402

24. Wanrooij S, Fusté JM, Farge G, Shi Y, Gustafsson CM, Falkenberg M. Human mitochondrial RNA polymerase primes lagging-strand DNA synthesis in vitro. *Proc Natl Acad Sci U S A*. 2008;105(32):11122-11127. doi:10.1073/pnas.0805399105

25. Robberson DL, Kasamatsu H, Vinograd J. Replication of mitochondrial DNA. Circular replicative intermediates in mouse L cells. *Proc Natl Acad Sci U S A*. 1972;69(3):737-741. doi:10.1073/pnas.69.3.737

26. Clayton DA. Replication of animal mitochondrial DNA. *Cell*. 1982;28(4):693-705. doi:10.1016/0092-8674(82)90049-6

27. Falkenberg M. Mitochondrial DNA replication in mammalian cells: Overview of the pathway. *Essays Biochem*. 2018;62(3):287-296. doi:10.1042/EBC20170100

28. Jemt E, Farge G, Bäckström S, Holmlund T, Gustafsson CM, Falkenberg M. The mitochondrial DNA helicase TWINKLE can assemble on a closed circular template and support initiation of DNA synthesis. *Nucleic Acids Res*. 2011;39(21):9238-9249. doi:10.1093/nar/gkr653

29. Agaronyan K, Morozov YI, Anikin M, Temiakov D. Replication-transcription switch

in human mitochondria. *Science (80-)*. 2015;347(6221):548-551. doi:10.1126/science.aaa0986

30. Kühl I, Miranda M, Posse V, et al. POLRMT regulates the switch between replication primer formation and gene expression of mammalian mtDNA. *Sci Adv*. 2016;2(8):1-15. doi:10.1126/sciadv.1600963

31. Chang DD, Clayton DA. Precise identification of individual promoters for transcription of each strand of human mitochondrial DNA. *Cell*. 1984;36(3):635-643. doi:10.1016/0092-8674(84)90343-X

32. Posse V, Gustafsson CM. Human mitochondrial transcription factor B2 is required for promoter melting during initiation of transcription. *J Biol Chem*. 2017;292(7):2637-2645. doi:10.1074/jbc.M116.751008

33. Ramachandran A, Basu U, Sultana S, Nandakumar D, Patel SS. Human mitochondrial transcription factors TFAM and TFB2M work synergistically in promoter melting during transcription initiation. *Nucleic Acids Res*. 2017;45(2):861-874. doi:10.1093/nar/gkw1157

34. Ngo HB, GA Lovely, Phillips R CD. Distinct structural features of TFAM drive mitochondrial DNA packaging versus transcriptional activation Huu. *Nat Commun*. 2017;176(5):139-148. doi:10.1038/ncomms4077.Distinct

35. Posse V, Shahzad S, Falkenberg M, Hällberg BM, Gustafsson CM. TEFM is a potent stimulator of mitochondrial transcription elongation in vitro. *Nucleic Acids Res*. 2015;43(5):2615-2624. doi:10.1093/nar/gkv105

36. Minczuk M, He J, Duch AM, et al. TEFM (c17orf42) is necessary for transcription of human mtDNA. *Nucleic Acids Res*. 2011;39(10):4284-4299. doi:10.1093/nar/gkq1224

37. Hillen HS, Parshin A V., Agaronyan K, et al. Mechanism of transcription anti-termination in human mitochondria. *Cell*. 2017;171(5):1082-1093.e13. doi:10.1016/j.cell.2017.09.035

38. Jiang S, Koolmeister C, Misic J, et al. TEFM regulates both transcription elongation

and RNA processing in mitochondria. 2019:1-18. doi:10.15252/embr.201948101

39. Kruse B, Narasimhan N, Attardi G. Termination of transcription in human mitochondria: Identification and purification of a DNA binding protein factor that promotes termination. *Cell*. 1989;58(2):391-397. doi:10.1016/0092-8674(89)90853-2

40. Terzioglu M, Ruzzenente B, Harmel J, et al. MTERF1 binds mtDNA to prevent transcriptional interference at the light-strand promoter but is dispensable for rRNA gene transcription regulation. *Cell Metab*. 2013;17(4):618-626. doi:10.1016/j.cmet.2013.03.006

41. Rossmanith W, Karwan RM. Characterization of human mitochondrial RNase P: Novel aspects in tRNA processing. *Biochem Biophys Res Commun*. 1998;247(2):234-241. doi:10.1006/bbrc.1998.8766

42. Ojala D, Montoya J, Attardi G. tRNA punctuation model of RNA processing in human mitochondria. *Nature*. 1981:470-474.

43. Rackham O, Mercer TR, Filipovska A. The human mitochondrial transcriptome and the rna-binding proteins that regulate its expression. *Wiley Interdiscip Rev RNA*. 2012;3(5):675-695. doi:10.1002/wrna.1128

44. Holzmann J, Frank P, Löffler E, Bennett KL, Gerner C, Rossmanith W. RNase P without RNA: Identification and Functional Reconstitution of the Human Mitochondrial tRNA Processing Enzyme. *Cell*. 2008;135(3):462-474. doi:10.1016/j.cell.2008.09.013

45. Lopez Sanchez MIG, Mercer TR, Davies SMK, et al. RNA processing in human mitochondria. *Cell Cycle*. 2011;10(17):2904-2916. doi:10.4161/cc.10.17.17060

46. Reinhard L, Sridhara S, Hällberg BM. The MRPP1/MRPP2 complex is a tRNA-maturation platform in human mitochondria. *Nucleic Acids Res*. 2017;45(21):12469-12480. doi:10.1093/nar/gkx902

47. Münch C, Harper JW. Mitochondrial unfolded protein response controls matrix pre-RNA processing and translation. *Nature*. 2016;534(7609):710-713.

doi:10.1038/nature18302

48. Münch C. The different axes of the mammalian mitochondrial unfolded protein response. *BMC Biol*. 2018;16(1):1-9. doi:10.1186/s12915-018-0548-x

49. Marsh SE, Blurton-Jones M. Examining the mechanisms that link β-amyloid and α-synuclein pathologies. *Alzheimer's Res Ther*. 2012;4(2):1-8. doi:10.1186/alzrt109

50. Ohkubo A, van Haute L, Rudler DL, et al. The FASTK family proteins fine-tune mitochondrial RNA processing. *PLoS Genet*. 2021;17(11). doi:10.1371/journal.pgen.1009873

51. Jourdain AA, Popow J, De La Fuente MA, Martinou JC, Anderson P, Simarro M. Survey and summary: The FASTK family of proteins: Emerging regulators of mitochondrial RNA biology. *Nucleic Acids Res*. 2017;45(19):10941-10947. doi:10.1093/nar/gkx772

52. Popow J, Alleaume AM, Curk T, Schwarzl T, Sauer S, Hentze MW. FASTKD2 is an RNA-binding protein required for mitochondrial RNA processing and translation. *Rna*. 2015;21(11):1873-1884. doi:10.1261/rna.052365.115

53. Antonicka H, Choquet K, Lin Z, Gingras A, Kleinman CL, Shoubridge EA. A pseudouridine synthase module is essential for mitochondrial protein synthesis and cell viability. 2017;18(1):28-38. doi:10.15252/embr.201643391

54. Boughanem H, Böttcher Y, Tomé-Carneiro J, et al. The emergent role of mitochondrial RNA modifications in metabolic alterations. *Wiley Interdiscip Rev RNA*. 2022;(March):1-23. doi:10.1002/wrna.1753

55. Mercer TR, Neph S, Dinger ME, et al. The human mitochondrial transcriptome. *Cell*. 2011;146(4):645-658. doi:10.1016/j.cell.2011.06.051

56. Tomecki R, Dmochowska A, Gewartowski K, Dziembowski A, Stepien PP. Identification of a novel human nuclear-encoded mitochondrial poly(A) polymerase. *Nucleic Acids Res*. 2004;32(20):6001-6014. doi:10.1093/nar/gkh923

57. Rorbach J, Minczuk M. The post-transcriptional life of mammalian mitochondrial

RNA. *Biochem J*. 2012;444(3):357-373. doi:10.1042/BJ20112208

58. Ruzzenente B, Metodiev MD, Wredenberg A, et al. LRPPRC is necessary for polyadenylation and coordination of translation of mitochondrial mRNAs. *EMBO J*. 2012;31(2):443-456. doi:10.1038/emboj.2011.392

59. Han VX, Tan TS, Wang FS, Tay SK-H. Novel LRPPRC Mutation in a Boy With Mild Leigh Syndrome, French–Canadian Type Outside of Québec. *Child Neurol Open*. 2017;4:2329048X1773763. doi:10.1177/2329048x17737638

60. Safra M, Sas-Chen A, Nir R, et al. The m1A landscape on cytosolic and mitochondrial mRNA at single-base resolution. *Nature*. 2017;551(7679):251-255. doi:10.1038/nature24456

61. Lee KW, Okot-Kotber C, La Comb JF, Bogenhagen DF. Mitochondrial ribosomal RNA (rRNA) methyltransferase family members are positioned to modify nascent rRNA in foci near the mitochondrial DNA nucleoid. *J Biol Chem*. 2013;288(43):31386-31399. doi:10.1074/jbc.M113.515692

62. Jedynak-Slyvka M, Jabczynska A, Szczesny RJ. Human mitochondrial RNA processing and modifications: Overview. *Int J Mol Sci*. 2021;22(15). doi:10.3390/ijms22157999

63. Perks KL, Rossetti G, Kuznetsova I, et al. PTCD1 is required for 16S rRNA maturation complex stability and mitochondrial ribosome assembly. *Cell Rep*. 2018;23(1):127-142. doi:10.1016/j.celrep.2018.03.033

64. Rebelo-Guiomar P, Powell CA, Van Haute L, Minczuk M. The mammalian mitochondrial epitranscriptome. *Biochim Biophys Acta - Gene Regul Mech*. 2019;1862(3):429-446. doi:10.1016/j.bbagrm.2018.11.005

65. Suzuki T, Yashiro Y, Kikuchi I, et al. Complete chemical structures of human mitochondrial tRNAs. *Nat Commun*. 2020;11(1):1-15. doi:10.1038/s41467-020-18068-6

66. Sauter C, Lorber B, Gaudry A, et al. Neurodegenerative disease-associated mutants of a human mitochondrial aminoacyl-tRNA synthetase present individual

molecular signatures. *Sci Rep*. 2015;5(October):1-13. doi:10.1038/srep17332

67. González-Serrano LE, Chihade JW, Sissler M. When a common biological role does not imply common disease outcomes: Disparate pathology linked to human mitochondrial aminoacyl-tRNA synthetases. *J Biol Chem*. 2019;294(14):5309-5320. doi:10.1074/jbc.REV118.002953

68. O'Brien TW. The general occurrence of 55 S ribosomes in mammalian liver mitochondria. *J Biol Chem*. 1971;246(10):3409-3417. doi:10.1016/s0021-9258(18)62239-2

69. Tu YT, Barrientos A. The Human Mitochondrial DEAD-Box Protein DDX28 Resides in RNA Granules and Functions in Mitoribosome Assembly. *Cell Rep*. 2015;10(6):854-864. doi:10.1016/j.celrep.2015.01.033

70. Surovtseva Y V., Shutt TE, Cotney J, et al. Mitochondrial ribosomal protein L12 selectively associates with human mitochondrial RNA polymerase to activate transcription. *Proc Natl Acad Sci U S A*. 2011;108(44):17921-17926. doi:10.1073/pnas.1108852108

71. Rackham O, Busch JD, Matic S, et al. Hierarchical RNA processing is required for mitochondrial ribosome assembly. *Cell Rep*. 2016;16(7):1874-1890. doi:10.1016/j.celrep.2016.07.031

72. Silva D De, Tu Y, Amunts A, Fontanesi F, Barrientos A. Mitochondrial ribosome assembly in health and disease. 2015;14(14):2226-2250.

73. Antonicka H, Shoubridge EA. Mitochondrial RNA Granules Are Centers for Posttranscriptional RNA Processing and Ribosome Biogenesis. *Cell Rep*. 2015;10(6):920-932. doi:10.1016/j.celrep.2015.01.030

74. Dennerlein S, Rozanska A, Wydro M, Chrzanowska-Lightowlers ZMA, Lightowlers RN. Human ERAL1 is a mitochondrial RNA chaperone involved in the assembly of the 28S small mitochondrial ribosomal subunit. *Biochem J*. 2010;430(3):551-558. doi:10.1042/BJ20100757

75. Maiti P, Antonicka H, Gingras AC, Shoubridge EA, Barrientos A. Human GTPBP5

(MTG2) fuels mitoribosome large subunit maturation by facilitating 16S rRNA methylation. *Nucleic Acids Res*. 2020;48(14):7924-7943. doi:10.1093/nar/gkaa592

76. Maiti P, Kim HJ, Tu YT, Barrientos A. Human GTPBP10 is required for mitoribosome maturation. *Nucleic Acids Res*. 2018;46(21):11423-11437. doi:10.1093/nar/gky938

77. Lavdovskaia E, Kolander E, Steube E, Mai MMQ, Urlaub H, Richter-Dennerlein R. The human Obg protein GTPBP10 is involved in mitoribosomal biogenesis. *Nucleic Acids Res*. 2018;46(16):8471-8482. doi:10.1093/nar/gky701

78. Lavdovskaia E, Denks K, Nadler F, et al. Dual function of GTPBP6 in biogenesis and recycling of human mitochondrial ribosomes. *Nucleic Acids Res*. 2020;48(22):12929-12942. doi:10.1093/nar/gkaa1132

79. Lopez Sanchez MIG, Krüger A, Shiriaev DI, Liu Y, Rorbach J. Human mitoribosome biogenesis and its emerging links to disease. *Int J Mol Sci*. 2021;22(8). doi:10.3390/ijms22083827

80. Kim HJ, Barrientos A. MTG1 couples mitoribosome large subunit assembly with intersubunit bridge formation. *Nucleic Acids Res*. 2018;46(16):8435-8453. doi:10.1093/nar/gky672

81. Iborra FJ, Kimura H, Cook PR. The functional organization of mitochondrial genomes in human cells. *BMC Biol*. 2004;2(February). doi:10.1186/1741-7007-2-9

82. Jourdain AA, Koppen M, Wydro M, et al. GRSF1 regulates RNA processing in mitochondrial RNA granules. *Cell Metab*. 2013;17(3):399-410. doi:10.1016/j.cmet.2013.02.005

83. Antonicka H, Sasarman F, Nishimura T, Paupe V, Shoubridge EA. The mitochondrial RNA-binding protein GRSF1 localizes to RNA granules and is required for posttranscriptional mitochondrial gene expression. *Cell Metab*. 2013;17(3):386-398. doi:10.1016/j.cmet.2013.02.006

84. Qian Z, Wilusz J. GRSF-1: A poly(A)+ mRNA binding protein which interacts with a conserved G-rich element. *Nucleic Acids Res*. 1994;22(12):2334-2343. doi:10.1093/nar/22.12.2334

85. Borowski LS, Dziembowski A, Hejnowicz MS, Stepien PP, Szczesny RJ. Human mitochondrial RNA decay mediated by PNPase-hSuv3 complex takes place in distinct foci. *Nucleic Acids Res*. 2013;41(2):1223-1240. doi:10.1093/nar/gks1130

86. Wilson WC, Hornig-Do HT, Bruni F, et al. A human mitochondrial poly(A) polymerase mutation reveals the complexities of post-transcriptional mitochondrial gene expression. *Hum Mol Genet*. 2014;23(23):6345-6355. doi:10.1093/hmg/ddu352

87. Antonicka H, Shoubridge EA. Mitochondrial RNA granules are centers for posttranscriptional RNA processing and ribosome biogenesis. *Cell Rep*. 2015;10(6):920-932. doi:10.1016/j.celrep.2015.01.030

88. Jourdain AA, Koppen M, Rodley CD, et al. A Mitochondria-Specific Isoform of FASTK Is Present In Mitochondrial RNA Granules and Regulates Gene Expression and Function. *Cell Rep*. 2015;10(7):1110-1121. doi:10.1016/j.celrep.2015.01.063

89. Boehm E, Zaganelli S, Maundrell K, Jourdain AA, Thore S, Martinou JC. FASTKD1 and FASTKD4 have opposite effects on expression of specific mitochondrial RNAs, depending upon their endonuclease-like RAP domain. *Nucleic Acids Res*. 2017;45(10):6135-6146. doi:10.1093/nar/gkx164

90. Zaganelli S, Rebelo-Guiomar P, Maundrell K, et al. The pseudouridine synthase RPUSD4 is an essential component of mitochondrial RNA granules. *J Biol Chem*. 2017;292(11):4519-4532. doi:10.1074/jbc.M116.771105

91. Xavier VJ, Martinou J. RNA Granules in the Mitochondria and Their Organization under Mitochondrial Stresses. 2021:1-3.

92. Hensen F, Potter A, van Esveld SL, et al. Mitochondrial RNA granules are critically dependent on mtDNA replication factors Twinkle and mtSSB. *Nucleic Acids Res*. 2019:1-19. doi:10.1093/nar/gkz047

93. Hensen F, Potter A, Esveld SL Van, et al. Mitochondrial RNA granules are critically dependent on mtDNA replication factors Twinkle and mtSSB e. 2019;47(7):3680-3698. doi:10.1093/nar/gkz047

94. Szczesny RJ, Borowski LS, Brzezniak LK, et al. Human mitochondrial RNA turnover caught in flagranti: Involvement of hSuv3p helicase in RNA surveillance. *Nucleic Acids Res*. 2009;38(1):279-298. doi:10.1093/nar/gkp903

95. Pietras Z, Wojcik MA, Borowski LS, et al. Dedicated surveillance mechanism controls G-quadruplex forming non-coding RNAs in human mitochondria. *Nat Commun*. 2018;9(1). doi:10.1038/s41467-018-05007-9

96. Chujo T, Ohira T, Sakaguchi Y, et al. LRPPRC/SLIRP suppresses PNPase-mediated mRNA decay and promotes polyadenylation in human mitochondria. *Nucleic Acids Res*. 2012;40(16):8033-8047. doi:10.1093/nar/gks506

97. Aloni Y, Attardi G. Symmetrical in vivo transcription of mitochondrial DNA in HeLa cells. *Proc Natl Acad Sci U S A*. 1971;68(8):1757-1761. doi:10.1073/pnas.68.8.1757

98. Xavier VJ, Martinou JC. Rna granules in the mitochondria and their organization under mitochondrial stresses. *Int J Mol Sci*. 2021;22(17):1-3. doi:10.3390/ijms22179502

99. Zhu X, Xie X, Das H, et al. Non-coding 7S RNA inhibits transcription via mitochondrial RNA polymerase dimerization. *Cell*. 2022;185(13):2309-2323.e24. doi:10.1016/j.cell.2022.05.006

100. Rey T, Zaganelli S, Cuillery E, et al. Mitochondrial RNA granules are fluid condensates positioned by membrane dynamics. *Nat Cell Biol*. 2020;22(10):1180-1186. doi:10.1038/s41556-020-00584-8

101. King MP, Atrardi G. Human cells lacking mtDNA: repopulation with exogenous mitochondria by complementation. *Science (80-)*. 1989;820(1981):6-9.

102. Ullmann R, Chien CD, Avantaggiati ML, Muller S. An Acetylation Switch Regulates SUMO-Dependent Protein Interaction Networks. *Mol Cell*. 2012;46(6):759-770.

doi:10.1016/j.molcel.2012.04.006

103. Fleck D, Phu L, Verschueren E, et al. PTCD1IS required for mitochondrial oxidative-phosphorylation: Possible genetic association with Alzheimer's disease. *J Neurosci*. 2019;39(24):4636-4656. doi:10.1523/JNEUROSCI.0116-19.2019

104. Krzywinski M, Schein J, Birol I, et al. Circos: An information aesthetic for comparative genomics. *Genome Res*. 2009;19(9):1639-1645. doi:10.1101/gr.092759.109

105. Paul Shannon 1, Andrew Markiel 1, Owen Ozier, 2 Nitin S. Baliga, 1 Jonathan T. Wang, 2 Daniel Ramage 2, et al. Cytoscape: A Software Environment for Integrated Models. *Genome Res*. 1971;13(22):426. doi:10.1101/gr.1239303.metabolite

106. Schneider CA, Rasband WS, Eliceiri KW. NIH Image to ImageJ: 25 years of image analysis. *Nat Methods*. 2012;9(7):671-675. doi:10.1038/nmeth.2089

107. Cox J, Mann M. MaxQuant enables high peptide identification rates, individualized p.p.b.-range mass accuracies and proteome-wide protein quantification. *Nat Biotechnol*. 2008;26(12):1367-1372. doi:10.1038/nbt.1511

108. Klann K, Münch C. PBLMM: Peptide-based linear mixed models for differential expression analysis of shotgun proteomics data. *J Cell Biochem*. 2022;123(3):691-696. doi:10.1002/jcb.30225

109. Knight JDR, Choi H, Gupta GD, et al. ProHits-viz: A suite of web tools for visualizing interaction proteomics data. *Nat Methods*. 2017;14(7):645-646. doi:10.1038/nmeth.4330

110. Branon TC, Bosch JA, Sanchez AD, et al. Efficient proximity labeling in living cells and organisms with TurboID. *Nat Biotechnol*. 2018;36(9):880-898. doi:10.1038/nbt.4201

111. Michaelis JB, Brunstein ME, Bozkurt S, et al. Protein import motor complex reacts to mitochondrial misfolding by reducing protein import and activating mitophagy. *Nat Commun*. 2022;13(1). doi:10.1038/s41467-022-32564-x

112. Kulak NA, Pichler G, Paron I, Nagaraj N, Mann M. Minimal, encapsulated proteomic-sample processing applied to copy-number estimation in eukaryotic cells. *Nat Methods*. 2014;11(3):319-324. doi:10.1038/nmeth.2834

113. Klann K, Tascher G, Münch C. Functional translatome proteomics reveal converging and dose-dependent regulation by mTORC1 and eIF2α. *Mol Cell*. 2020;77(4):913-925.e4. doi:10.1016/j.molcel.2019.11.010

114. Rath S, Sharma R, Gupta R, et al. MitoCarta3.0: An updated mitochondrial proteome now with sub-organelle localization and pathway annotations. *Nucleic Acids Res*. 2021;49(D1):D1541-D1547. doi:10.1093/nar/gkaa1011

115. Legeay M, Doncheva NT, Morris JH, Jensen LJ. Visualize omics data on networks with Omics Visualizer, a Cytoscape App. *F1000Research*. 2020;9(June):157. doi:10.12688/f1000research.22280.2

116. Merico D, Isserlin R, Stueker O, Emili A, Bader GD. Enrichment map: A network-based method for gene-set enrichment visualization and interpretation. *PLoS One*. 2010;5(11). doi:10.1371/journal.pone.0013984

117. Kamada T, Kawai S. An algorithm for drawing general undirected graphs. *Information Process Lett*. 1989;31:7-15.

118. Futschik ME, Carlisle B. Noise-robust soft clustering of gene expression time-course data. *J Bioinform Comput Biol*. 2005;3(4):965-988. doi:10.1142/S0219720005001375

119. Benjamini Y, Hochberg Y. Controlling the false discovery rate: A practical and powerful approach to multiple testing. *J R Stat Soc Ser B*. 1995;57(1):289-300. doi:10.1111/j.2517-6161.1995.tb02031.x

120. Kotrys A V., Szczesny RJ. Mitochondrial gene expression and beyond—novel aspects of cellular physiology. *Cells*. 2020;9(1). doi:10.3390/cells9010017

121. Botulinum RI, Study R. HHS Public Access. 2014;4(1):139-148. doi:10.1038/nmeth.2839.A

122. Zorkau M, Albus CA, Berlinguer-Palmini R, Chrzanowska-Lightowlers ZMA,

Lightowlers RN. High-resolution imaging reveals compartmentalization of mitochondrial protein synthesis in cultured human cells. *Proc Natl Acad Sci U S A*. 2021;118(6). doi:10.1073/pnas.2008778118

123. Jourdain A a, Koppen M, Wydro M, et al. GRSF1 regulates RNA processing in mitochondrial RNA granules. *Cell Metab*. 2013;17(3):399-410. doi:10.1016/j.cmet.2013.02.005

124. Piechota J, Tomecki R, Gewartowski K, et al. Differential stability of mitochondrial mRNA in HeLa cells. *Acta Biochim Pol*. 2006;53(1):157-167. doi:10.18388/abp.2006_3374

125. Bensaude O. Inhibiting eukaryotic transcription: Which compound to choose? How to evaluate its activity? *Transcription*. 2011;2(3):103-108. doi:10.4161/trns.2.3.16172

126. Haeusler BYG, Richards JG, Thorens S. CH-4002 Basle, Switzerland. 1981:537-556.

127. Sasaki R, Suzuki Y, Yonezawa Y, et al. DNA polymerase γ inhibition by vitamin K3 induces mitochondria-mediated cytotoxicity in human cancer cells. *Cancer Sci*. 2008;99(5):1040-1048. doi:10.1111/j.1349-7006.2008.00771.x

128. Arenz S, Ramu H, Gupta P, et al. Molecular basis for erythromycin-dependent ribosome stalling during translation of the ErmBL leader peptide. *Nat Commun*. 2014;5. doi:10.1038/ncomms4501

129. Buss WC, Kun E. Effects of rifampicin on RNA and protein synthesis in isolated rat liver mitochondria. *Biochem Pharmacol*. 1978;27(17):2139-2145. doi:10.1016/0006-2952(78)90286-1

130. Courchesne CL, Bantle JA. Analysis of the activity of DNA, RNA, and protein synthesis inhibitors on Xenopus embryo development. *Teratog Carcinog Mutagen*. 1985;5(3):177-193. doi:10.1002/tcm.1770050306

131. Bonekamp NA, Peter B, Hillen HS, et al. Small-molecule inhibitors of human mitochondrial DNA transcription. *Nature*. 2020;588(December). doi:10.1038/s41586-020-03048-z

132. Mennuni M, Filograna R, Felser A, et al. Metabolic resistance to the inhibition of mitochondrial transcription revealed by CRISPR-Cas9 screen. *EMBO Rep*. 2022;23(1):1-18. doi:10.15252/embr.202153054

133. Ojala D, Montoya J, Attardi G. Wi Wj5 ~. 1981:470-474.

134. Silva S, Camino LP, Aguilera A. Human mitochondrial degradosome prevents harmful mitochondrial R loops and mitochondrial genome instability. *Proc Natl Acad Sci U S A*. 2018;115(43):11024-11029. doi:10.1073/pnas.1807258115

135. Schonborn J, Oberstraß J, Breyel E, Tittgen J, Schumacher J, Lukacs N. Monoclonal antibodies to double-stranded RNA as probes of RNA structure in crude nucleic acid extracts. *Nucleic Acids Res*. 1991;19(11):2993-3000. doi:10.1093/nar/19.11.2993

136. Slomovic S, Laufer D, Geiger D, Schuster G. Polyadenylation and degradation of human mitochondrial RNA: the prokaryotic past leaves its mark. *Mol Cell Biol*. 2005;25(15):6427-6435. doi:10.1128/mcb.25.15.6427-6435.2005

137. Pajak A, Laine I, Clemente P, et al. Defects of mitochondrial RNA turnover lead to the accumulation of double-stranded RNA in vivo. *PLoS Genet*. 2019;15(7):1-25. doi:10.1371/journal.pgen.1008240

138. Jourdain AA, Boehm E, Maundrell K, Martinou JC. Mitochondrial RNA granules: Compartmentalizing mitochondrial gene expression. *J Cell Biol*. 2016;212(6):611-614. doi:10.1083/jcb.201507125

139. Maiti P, Kim HJ, Tu YT, Barrientos A. Human GTPBP10 is required for mitoribosome maturation. *Nucleic Acids Res*. 2018;46(21):11423-11437. doi:10.1093/nar/gky938

140. Iborra FJ, Kimura H, Cook PR. cells. 2004;14:1-14.

141. Rey AT, Zaganelli S, Cuillery E, Martinou J. Title : Mitochondrial RNA granules are fluid condensates , positioned by membrane dynamics. 2019:1-25.

142. Antonicka H, Lin Z-Y, Janer A, Weraarpachai W, Gingras A-C, Shoubridge EA. A high-density human mitochondrial proximity interaction network. *SSRN Electron*

J. 2020;32(3):479-497.e9. doi:10.2139/ssrn.3583659

143. Fare CM, Villani A, Drake LE, Shorter J. Higher-order organization of biomolecular condensates. *Open Biol*. 2021;11(6). doi:10.1098/rsob.210137

144. Wheeler JR, Matheny T, Jain S, Abrisch R, Parker R. Distinct stages in stress granule assembly and disassembly. *Elife*. 2016;5(Se):1-25. doi:10.7554/eLife.18413

145. Hensen F, Potter A, Van Esveld SL, et al. Mitochondrial RNA granules are critically dependent on mtDNA replication factors Twinkle and mtSSB. *Nucleic Acids Res*. 2019;47(7):3680-3698. doi:10.1093/nar/gkz047

146. Szewczyk M, Malik D, Borowski LS, et al. Human REXO2 controls short mitochondrial RNAs generated by mtRNA processing and decay machinery to prevent accumulation of double-stranded RNA. *Nucleic Acids Res*. 2020;48(10):5572-5590. doi:10.1093/NAR/GKAA302

147. Wang G, Chen H, Oktay Y, et al. PNPASE regulates RNA import into mitochondria. *Cell*. 2011;142(3):456-467. doi:10.1016/j.cell.2010.06.035.PNPASE

148. Wang DDH, Guo XE, Modrek AS, Chen CF, Chen PL, Lee WH. Helicase SUV3, polynucleotide phosphorylase, and mitochondrial polyadenylation polymerase form a transient complex to modulate mitochondrial mRNA polyadenylated tail lengths in response to energetic changes. *J Biol Chem*. 2014;289(24):16727-16735. doi:10.1074/jbc.M113.536540

149. Gusic M, Prokisch H. ncRNAs: New players in mitochondrial health and disease? *Front Genet*. 2020;11(February):1-27. doi:10.3389/fgene.2020.00095

150. Noh JH, Kim KM, Abdelmohsen K, et al. HuR and GRSF1 modulate the nuclear export and mitochondrial localization of the lncRNA RMRP. *Genes Dev*. 2016;30(10):1224-1239. doi:10.1101/gad.276022.115

6 Supplement

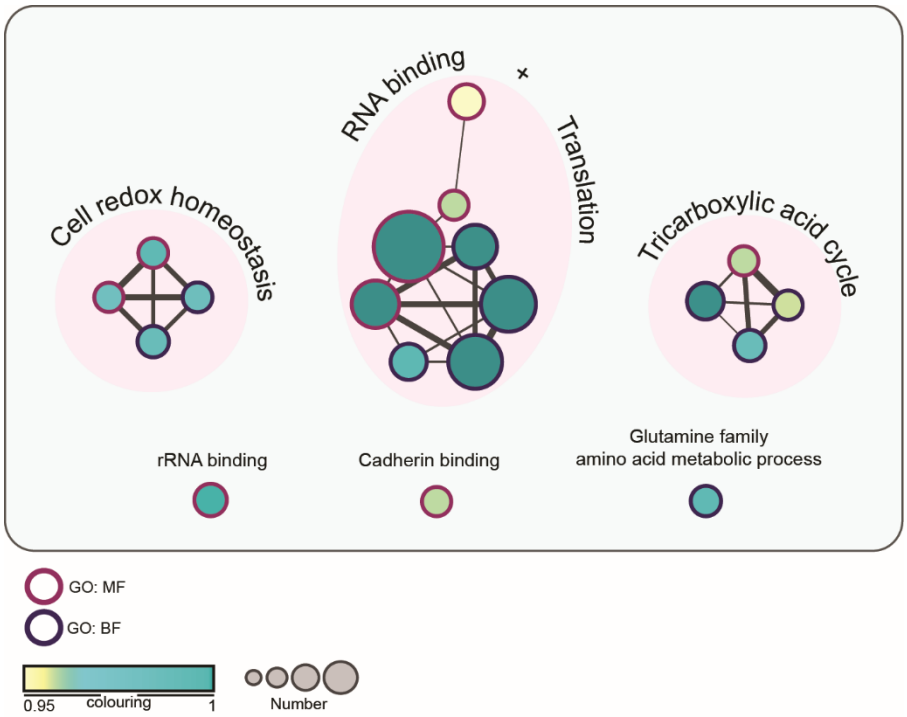

Figure S 1: GO term analysis of the MRG proteome. Enrichment map of GO Molecular Function (MF, magenta) and Biological Process (BF, purple) identified by TurboID profiling. Nodes represent gene-sets, while edges symbolize relations defined by Gene Ontology. The color intensity gradient, ranging from yellow to cyan, indicates a proportional representation of enrichment significance. Node sizes indicates number of genes assigned to a specific GO term.

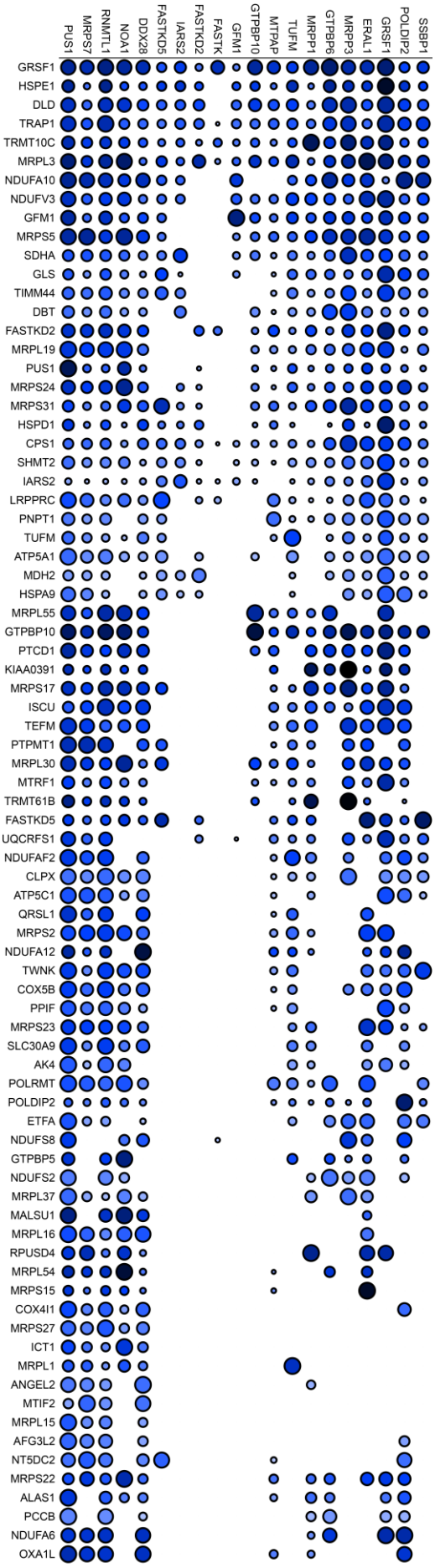
PUS1
MRPS7
RNMTL1
NOA1
DDX28
FASTKD5
IARS2
FASTKD2
FASTK
GFM1
GTPBP10
MTPAP
TUFM
MRPP1
GTPBP6
MRPP3
ERAL1
GRSF1
POLDIP2
SSBP1
GRSF1
HSPE1
DLD
TRAP1
TRMT10C
MRPL3
NDUFA10
NDUFV3
GFM1
MRPS5
SDHA
GLS
TIMM44
DBT
FASTKD2
MRPL19
PUS1
MRPS24
MRPS31
HSPD1
CPS1
SHMT2
IARS2
LRPPRC
PNPT1
TUFM
ATP5A1
MDH2
HSPA9
MRPL55
GTPBP10
PTCD1
KIAA0391
MRPS17
ISCU
TEFM
PTPMT1
MRPL30
MTRF1
TRMT61B
FASTKD5
UQCRFS1
NDUFAF2
CLPX
ATP5C1
QRSL1
MRPS2
NDUFA12
TWNK
COX5B
PPIF
MRPS23
SLC30A9
AK4
POLRMT
POLDIP2
ETFA
NDUFS8
GTPBP5
NDUFS2
MRPL37
MALSU1
MRPL16
RPUSD4
MRPL54
MRPS15
COX4I1
MRPS27
ICT1
MRPL1
ANGEL2
MTIF2
MRPL15
AFG3L2
NT5DC2
MRPS22
ALAS1
PCCB
NDUFA6
OXA1L

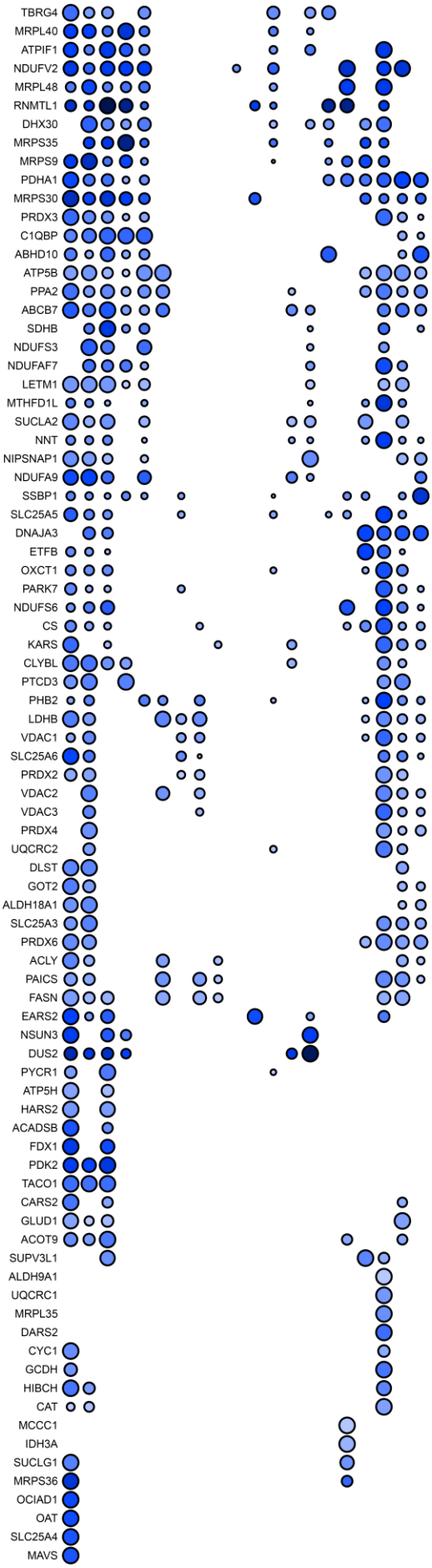
TBRG4
MRPL40
ATPIF1
NDUFV2
MRPL48
RNMTL1
DHX30
MRPS35
MRPS9
PDHA1
MRPS30
PRDX3
C1QBP
ABHD10
ATP5B
PPA2
ABCB7
SDHB
NDUFS3
NDUFAF7
LETM1
MTHFD1L
SUCLA2
NNT
NIPSNAP1
NDUFA9
SSBP1
SLC25A5
DNAJA3
ETFB
OXCT1
PARK7
NDUFS6
CS
KARS
CLYBL
PTCD3
PHB2
LDHB
VDAC1
SLC25A6
PRDX2
VDAC2
VDAC3
PRDX4
UQCRC2
DLST
GOT2
ALDH18A1
SLC25A3
PRDX6
ACLY
PAICS
FASN
EARS2
NSUN3
DUS2
PYCR1
ATP5H
HARS2
ACADSB
FDX1
PDK2
TACO1
CARS2
GLUD1
ACOT9
SUPV3L1
ALDH9A1
UQCRC1
MRPL35
DARS2
CYC1
GCDH
HIBCH
CAT
MCCC1
IDH3A
SUCLG1
MRPS36
OCIAD1
OAT
SLC25A4
MAVS


ME2
ECHDC1
AHCYL1
STOM
TRMT2B
MT-ATP6
BCAT2
HSD17B10
HINT2
MACROD1
AK2
OGDHL
SFXN1
UQCRQ
MYO19
OXSM
DNA2
FASTK
AKAP1
NUDT5
TFB2M
MRPL21
HSDL2
ALDH7A1
TIMM50
APEX1
HSD17B4
LYPLAL1
MRPL14
ACAD9
ECHS1
NDUFS7
PMPCB
MRPS18A
RBFA
PHB
SND1
MRPL10
ISCA1
ALDH4A1
COQ3
NDUFB3
PYCR2
MRPL9
MRPL2
ACADVL
MRPS7
MRPS10
ALDH1L2
IDH3B
ATP5E
SPRYD4
NDUFB9
NDUFB8
CCRN4L
CDK5RAP1
NDUFA5
GTPBP6
MRPL50
MRPL27
NME4
PREPL
TMLHE
RARS2
LDHAL6B
ATPAF2
GRHPR
VWA8
HADHA
NFS1
COQ10B
MRPS34
MRPS26
RPUSD3
TFB1M
PDHX
ELAC2
NDUFAF4
METTL15
ACO2
DLAT
ECH1
DUT
NDUFS1

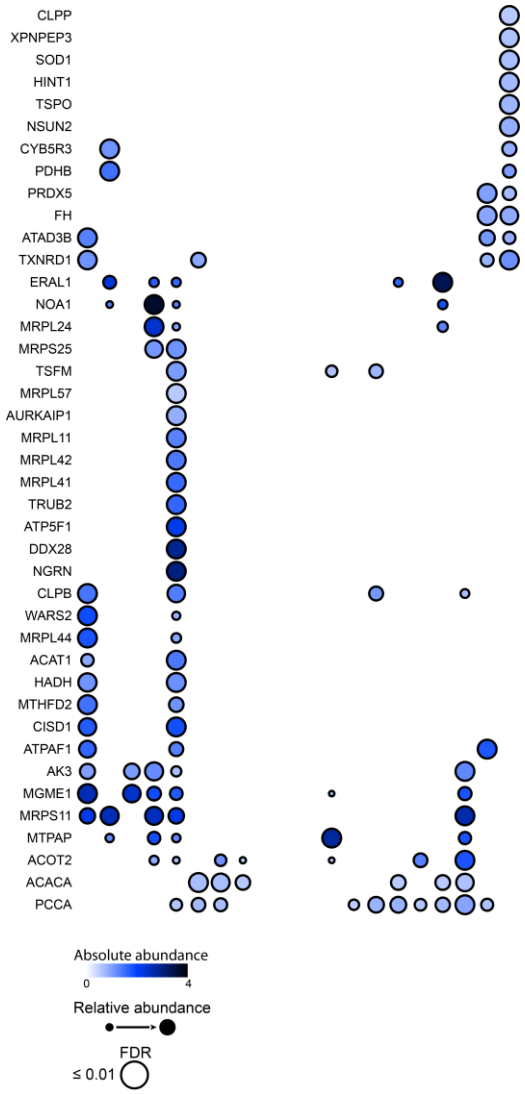

Figure S 2: Full dot plot of high-confidence preys identified by 20 MRG-related TurboID baits. This analysis includes only significantly enriched PPIs (log_2 fold change ≥ 2; FDR ≤ 0.01). Node size represents relative enrichment, light blue indicates low and dark blue high log_2 values. Preys are plotted on the y-axis, and the baits are shown on the x-axis.

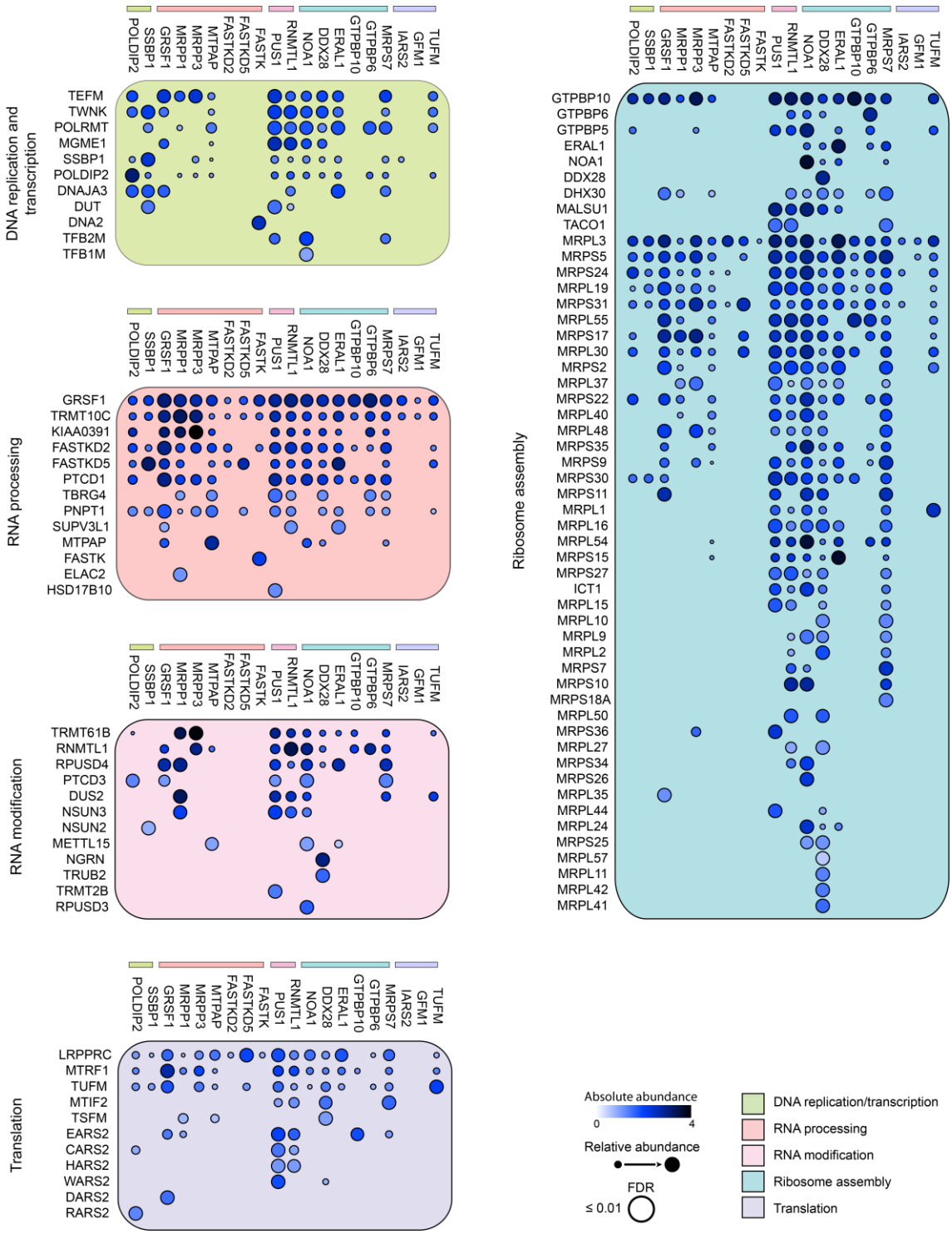

Figure S 3: Summarized dot plot of high-confidence preys identified by 20 MRG-related TurboID baits. This analysis includes only significantly enriched PPIs (log_2 fold change ≥ 2; FDR ≤ 0.01). Node size represents relative enrichment, light blue indicates low and dark blue high log_2 values. Preys are plotted on the y-axis, and the baits are shown on the x-axis. Preys and baits are grouped and colored according to their functional category.

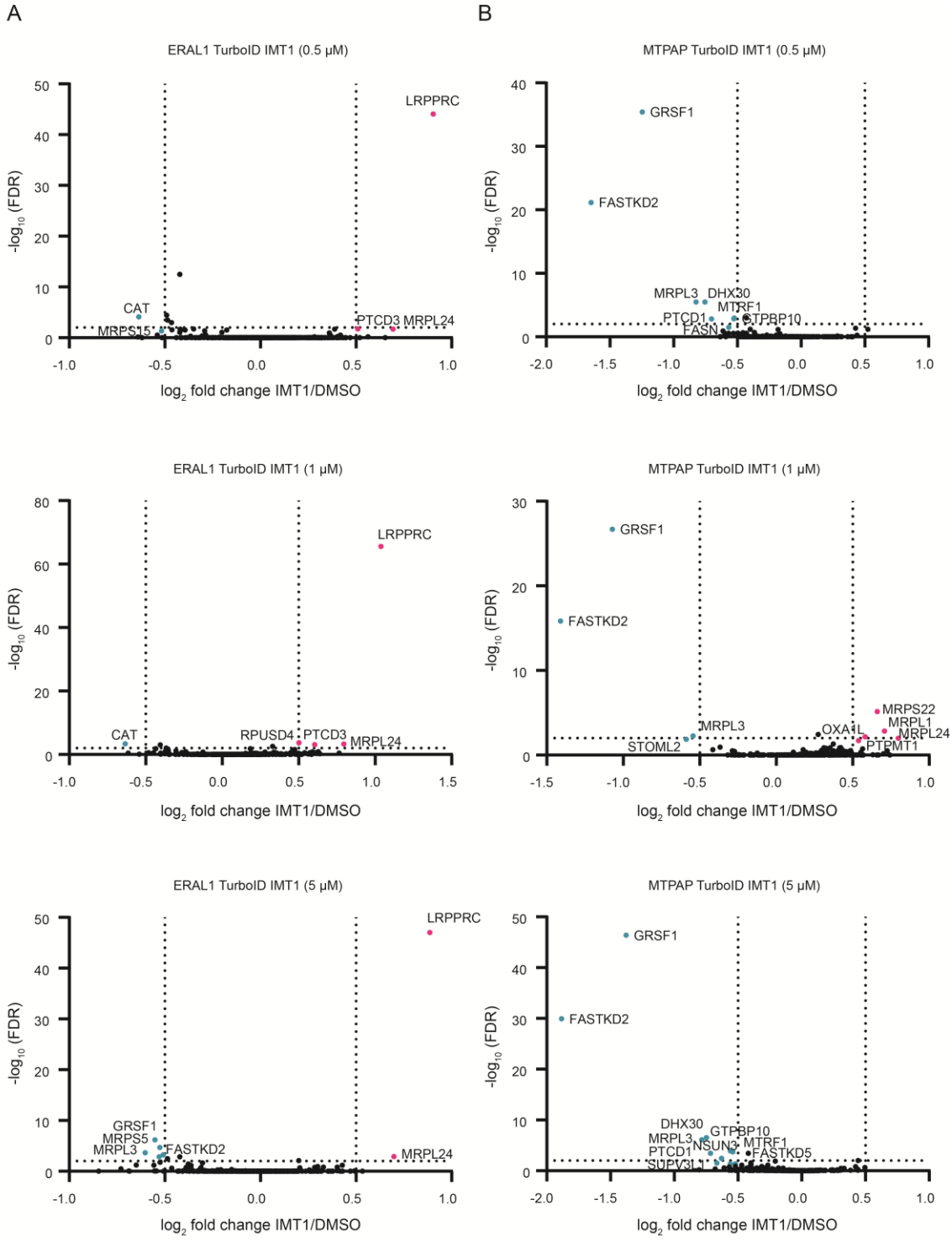

Figure S 4: Stress-induction with higher dosage of IMT1 leads to altered interactions of ERAL1 and MTPAP. Volcano plots of IMT1 dosage test experiments with the Turbo fusion proteins **(A)** ERAL1 and **(B)** MTPAP. Flp-In T-Rex cells were treated with indicated concentrations of IMT1 for 6 h and analyzed on MS_2 as shown in Figure 10.

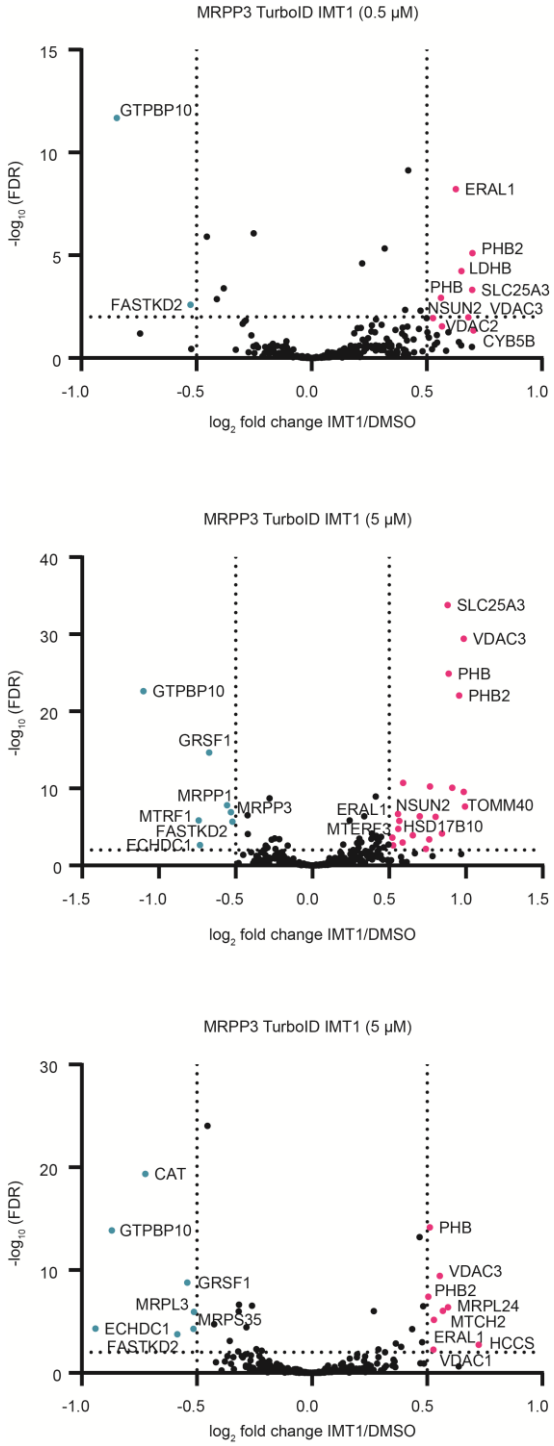

Figure S 5: Stress-induction with higher dosage of IMT1 leads to altered interactions of MRPP3. Volcano plots of IMT1 dosage test experiments with the Turbo fusion protein MRPP3. Flp-In T-Rex cells were treated with indicated concentrations of IMT1 for 6 h and analyzed on MS_2 as shown in Figure 10.

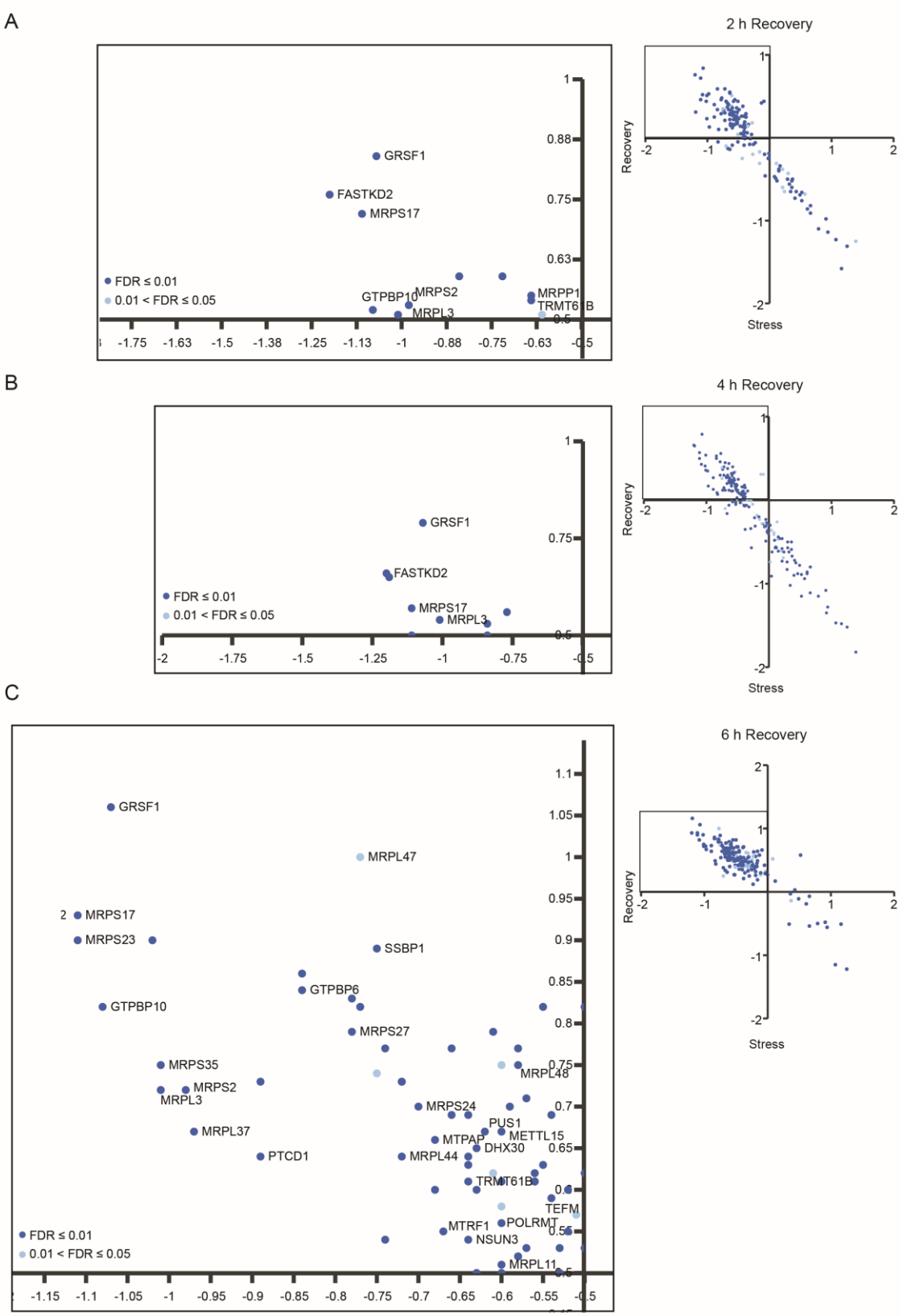

Figure S 6: Time-resolved TurboID profiling reveals recovery of GTPBP6 interactions after IMT1-induced stress. Scatter plots illustrate a pairwise comparison between the high-confidence interactions of GTPBP6 TurboID upon stress and recovery for **(A)** 2 h **(B)** 4 h and **(C)** 6 h. Enlarged section is depicted on the left. Interactions with an FDR between 0.01 and 0.05 are indicated in light blue and interactions with an FDR ≤ 0.01 are indicated in dark blue. Experiment was conducted as shown in Figure 21 A.

7 Schriftliche Erklärung

Ich erkläre ehrenwörtlich, dass ich die dem Fachbereich Medizin der Johann Wolfgang Goethe-Universität Frankfurt am Main zur Promotionsprüfung eingereichte Dissertation mit dem Titel

Interaction proteomics display the spatio-temporal complexity of mitochondrial RNA granules

in dem Zentrum der Biochemie, Institut für Biochemie II (Kardiovaskuläre Biochemie) unter Betreuung und Anleitung von Herrn Dr. Christian Münch ohne sonstige Hilfe selbst durchgeführt und bei der Abfassung der Arbeit keine anderen als die in der Dissertation angeführten Hilfsmittel benutzt habe. Darüber hinaus versichere ich, nicht die Hilfe einer kommerziellen Promotionsvermittlung in Anspruch genommen zu haben.

Ich habe bisher an keiner in- oder ausländischen Universität ein Gesuch um Zulassung zur Promotion eingereicht*. Die vorliegende Arbeit wurde bisher nicht als Dissertation eingereicht.

_____ _____

(Ort, Datum) (Unterschrift)

*) im Falle des Nichtzutreffens entfernen